Synthetic, kinetic and electrochemical studies on new osmocene-containing betadiketonato rhodium(I) complexes with biomedical applications.

A dissertation submitted in accordance with the requirements for the degree

Magister Scientiae

In the

Department of Chemistry

Faculty of Science

At the

University of the Free State

By

Zeldene Salomy Ambrose

Supervisor

Prof. J.C. Swarts

June 2006

Acknowledgements

To God all the praise, for He has carried me through it all. He gave me strength to carry on, dried my tears when all fell apart and never let me fall to hard.

I would like to thank my promoter, Prof. J.C. Swarts for all the guidance and time spent on this project. Also for all the words of wisdom that has stayed in my heart. I would also like to thank the Department Chemistry for laying the basic structure in my pre-graduate studies. To all the lectures and Professors, from Organic to Physical chemistry, thank you for making a difference in my life.

To my mother and family, thank you for making me laugh when I wanted to cry. God could not have given me a better family. I wish Dad was here, but I know he is very proud of me.

To all my crazy friends, words can not describe how much you mean to me. You guys cried with me, laughed with me and partied with me. You were my Dr. Phil, Oprah and Jerry Springer all in one. Aurelien Auger (bite me), Johan Barnard, Nicola Barnard (ZNN), Nicoline Cloete (sweetie-pie), Micheal Coetzee, Eleanor Fourie (E), Phillip Fullaway (Dr. Phil), Lizette Jordaan (Zet*), Christian Kemp (CK), Charlotte Kok (niemand), Inus Van Rensburg (Parakiet), Brent Grimsley, I truly love each one of you as my sister and brother. A special thanks to Lizette Erasmus (ou sus), words can not describe.

A special thanks to NPC-Natal Portland Cement, Giovanni Lodetti my boss, for accommodating me while I was writing up. Also thanks to the three amigo's and especially Manoel Revez.

God bless all those that has touched my heart and changed my live for the better.

Zeldene Salomy Ambrose
June 2006

I loving memory of the greatest man I will ever know, my father.
George Ambrose
1932-1999

Dad

Dad...so many images come to mind
whenever I speak your name;
It seems without you in my life
things have never been the same.

What happened to those lazy days
when I was just a child;
When my life was consumed in you
in your love, and in your smile.

What happened to all those times
when I always looked to you;
No matter what happened in my life
you could make my grey skies blue.

Dad, some days I hear your voice
and turn to see your face;
Yet in my turning...it seems
the sound has been erased.

A golden heart stopped beating,
Hard working hands to rest.
God broke our hearts to prove to us
He only takes the best

Oh, Dad, if I could turn back time
and once more hear your voice;
I'd tell you that out of all the dads
you would still be my choice.

Please always know I love you
and no one can take your place;
Years may come and go
but your memory will never be erased.

Today, Jesus, as You are listening
in Your home above;
Would You go and find my dad
and give him all my love.

Contents

List of Abbreviations **vii**

Chapter 1

Introduction and aim of study

1.1. Introduction **1**

1.2. Aims of the study **3**

Chapter 2

Literature survey

2.1. General chemistry of osmocene **5**

2.1.1. Osmocene synthesis 5

2.1.2. Stability and reactivity of osmocene and substituted osmocenes 6

2.1.3. General reactions of osmocene 8

2.2. Synthesis **9**

2.2.1. Synthesis of acetyl metallocenes 9

2.2.2. Synthesis of metallocene carboxylic acids 11

2.2.3. Synthesis of metallocene esters 12

2.2.4. Synthesis of β-diketones 13

2.2.5. Synthesis of metallocene β-diketones 15

2.3. Medicinal properties of metal complexes **18**

2.3.1. Transition metal complexes in chemotherapy 18

2.3.2. Rhodium and metallocenes in cancer therapy 20

2.4. Electrochemistry **21**

2.4.1. Introduction 21

2.4.2. Cyclic voltammetry 22

2.4.2.1. The basic cyclic voltammetry experiment 22

Contents

2.4.2.2. Important parameters of cyclic voltammetry 24

2.4.3. Electrochemistry of some metallocene complexes 27

2.4.3.1. Ferrocene 27

2.4.3.2. Ruthenocene 30

2.4.3.3. Osmocene 32

2.5. Acid dissociation constants 33

2.6. Electronegativities 35

2.7. Kinetics 38

2.7.1. Isomerization kinetics 38

2.7.2. Substitution kinetics 40

2.7.2.1. Introduction 40

2.7.2.2. Mechanism of substitution reactions 40

2.7.2.3. Factors influencing substitution reaction rates 44

2.7.2.4. Activation parameters 51

Chapter 3

Results and discussion

3.1. Introduction 59

3.2. Syntheses 60

3.2.1. Acetyl osmocene 60

3.2.2. β-diketones 61

3.2.3. Complexation reaction of β-diketones with rhodium 62

3.3. pK_a/ determinations 63

3.4. Isomerization kinetics between the keto-and enol-tautomers of the β-diketones

3.4.1. The observed solution phase equilibrium constant K_c 67

3.4.2. Kinetics of enol-keto conversion 72

3.4.3. Kinetics of keto-enol conversion 75

3.5. Kinetics of β-diketonato substitution in [Rh(β-diketonato)(cod)] 76

Contents

3.5.1. The Beer- Lambert Law 77

3.5.2. Substitution kinetics of [Rh(β-diketonato)(cod)] with 1,10-phenanthroline 79

3.6. Cyclic Voltammetry 87

3.6.1. Introduction 87

3.6.2. Osmocene-containing β-diketones 88

3.6.3. Rhodium complexes 95

Chapter 4

Experimental

4.1. Introduction 102

4.2. Materials 102

4.3. Techniques and apparatus 102

4.3.1. Chromatography 102

4.3.2. Melting point (m.p.) determination 102

4.3.3. Proton Nuclear Magnetic Resonance (^{1}H NMR) spectroscopy 102

4.3.4. Infrared (IR) spectroscopy 103

4.3.5. Electrochemistry 103

4.4. Synthesis 104

4.4.1. Synthesis of acetyl osmocene 104

4.4.2. Synthesis of metallocene methyl esters 104

4.4.2.1. Synthesis of methyl ferrocenoate 104

(i) Synthesis of 2-chlorobenzoyl ferrocene 104

(ii) Synthesis of ferrocenecarboxylic acid 105

(iii) Synthesis of methyl ferrocenoate 105

4.4.2.2. Synthesis of methyl ruthenocenoate 106

(i) Synthesis of 2-chlorobenzoyl ruthenocene 106

(ii) Synthesis of ruthenocenoic acid 106

(iii) Synthesis of methyl ruthenocenonoate 107

4.4.3. Synthesis of β-diketones 107

Contents

4.4.3.1. Synthesis of 1-osmocenyl-4,4,4-trifluorobutan-1,3-dione(Hoctfa) 107

4.4.3.2. Synthesis of 1-osmocenyl-3-phenylpropano-1,3-dione (Hbocm) 108

4.4.3.3. Synthesis of 1-osmocenylbutane-1,3-dione (Hoca) 109

4.4.3.4. Synthesis of 1-ferrocenyl-3-osmocenylpropane-1,3-dione (Hocfcm) 109

4.4.3.5. Synthesis of 1-osmocenyl-3-ruthenocenylpropane-1,3-dione (Hocrcm) 110

4.4.3.6. Synthesis of 1-osmocenyl-1,3-propanedione (Hoch) 111

4.4.4. Synthesis of rhodium complexes 112

4.4.4.1.Synthesis of di-μ-chloro-bis[(1,2,5,6-η)1,5-cyclooctadiene]rhodium 112

4.4.4.2. Synthesis of [Rh(octfa)(cod)] 112

4.4.4.3. Synthesis of [Rh(oca)(cod)] 113

4.4.4.4. Synthesis of [Rh(bocm)(cod)] 113

4.4.4.5. Synthesis of [Rh(ocfcm)(cod)] 114

4.4.4.6. Synthesis of [Rh(och)(cod)] 114

4.4.5. Electrolyte synthesis 114

4.5. Observed acid dissociation constant, $pK_a^{/}$, determination 115

4.6. Isomerization kinetics study 116

4.6.1. Monitoring of the conversion of enol to keto isomer 116

4.6.2. Monitoring of the conversion of keto to enol isomer 117

4.7. Substitution kinetics 118

Chapter 5

Summary and future perspective

5.1. Summary 119

5.2. Future perspectives 120

Contents

Appendix

^{1}H NMR spectra	I
Abstract	A
Opsomming	C

List of Abbreviations

A	Absorbance
Å	Angstrom
Bu_3P	Tributyl phosphine
$CDCl_3$	Deuterated chloroform
CH_3CN	Acetonitrile
CH_3OH	Methanol
Cisplatin	Cis-diamminedichloroplatinum(II)
CO	Carbon monoxide or carbonyl
cod	1,8-cyclooctadiene
Cp	Cyclopentadienyl $(C_5H_5)^-$
CV	Cyclic voltammetry
δ	Chemical shift
DCM	Dichloromethane
DMF	Dimethylformamide
DMSO	Dimethyl sulfoxide
ε	Molar absorptivity (previously molecular extinction coefficient)
E	Applied potential
$E^{o/}$	Formal reduction potential
E_a	Energy of activation
E_{pa}	Peak anodic potential
E_{pc}	Peak cathodic potential
ΔE_p	Separation of peak anodic and peak cathodic potentials
Et	Ethyl
F	Faraday constant (96485.3 C mol^{-1})
Fc	Ferrocene or ferrocenyl (Note: Strictly ferrocene should be Hfc and fc ferrocenyl, but it is customary in electrochemistry to abbreviate the ferrocene/ferrocenium couple as Fc/Fc^+. In this document this notation will be accepted as the current form.)
ΔG^*	Gibbs energy of activation
h	Planck's constant (6.626 x 10^{-34} J s)
ΔH^*	Enthalpy of activation
HMPT	Hexamethylphosphoric triamide
Hbocm	1-osmocenyl-3-phenylpropane-1,3-dione
Hoca	1-osmocenylbutane-1,3-dione
Hocfcm	3-ferrocenyl-1-osmocenylpropane-1,3-dione
Hoch	1-osmocenyl-1,3-propanedione
Hocrcm	1-osmocenyl-3-ruthenocenylpropane-1,3-dione
Hoctfa	1-osmocenyl-4,4,4-trifluorobutan-1,3-dione
i_{pa}	Peak anodic current
i_{pc}	Peak cathodic current
k_1	Forward rate constant
k_{-1}	Backward rate constant
k_2	Second-order rate constant
K-*t*-OC_4H_9	Potassium *tertiary*-butoxide
k_{obs}	Observed rate constant
k_s	Rate constant of solvation
L	Ligand
LDA	Lithium diisopropylamide
LiBu	*n*-butyl lithium
λ_{exp}	Wavelength at maximum absorbance

List of Abbreviations

M	Central metal atom
Me	Methyl
MeI	Methyliodide
n	Number of electrons
^{1}H NMR	Proton nuclear magnetic resonance spectroscopy
o	Ortho
Oc	Osmocene
Ph	Phenyl (C_6H_5)
Phen	1,10-phenanthroline
pK_a	-log K_a, K_a = acid dissociation constant
ppm	Parts per million
R	Gas constant (8.134 J K^{-1} mol^{-1})
Rc	Ruthenocene
$RhCl_3$	Rhodium trichloride
[Rh (cod)$_2$Cl$_2$]	di-μ-chloro-*bis*[1,2,5,6-η)1,5-cyclooctadiene]rhodium
[Rh (bocm)(cod)]	Rhodium 1-osmocenyl-3-phenylpropane-1,3-dionato 1,8-cyclooctadiene
[Rh (oca)(cod)]	Rhodium 1-osmocenylbutane-1,3-dionato 1,8-cyclooctadiene
[Rh (ocfcm)(cod)]	Rhodium 3-ferrocenyl-1-osmocenylpropane-1,3-dionato 1,8-cyclooctadiene
[Rh (och)(cod)]	Rhodium 1-osmocenyl-1,3-propanedionato 1,8-cyclooctadiene
[Rh (octfa)(cod)]	Rhodium 1-osmocenyl-4,4,4-trifluorobutan-1,3-dionato1,8-cyclooctadiene
S	Solvent
ΔS*	Entropy of activation
SCE	Standard calomel electrode
SHE	Standard hydrogen electrode
T	Temperature
THF	Tetrahydrofuran
UV/Vis	Ultraviolet/visible spectroscopy
ΔV*	Volume of activation
$\nu_{(C=O)}$	Infrared carbonyl stretching wave number
X	Halogen
χ_R	Group electronegativity (Gordy scale) of R-group

Chapter 1
Introduction and aim of the study

1.1. Introduction

The first characterized example of a sandwich cyclopentadienyl metal complex was ferrocene, $Fe(C_5H_5)_2$. Ferrocene has an iron(II) cation "sandwiched" between two planar C_5H_5 rings. The discovery of ferrocene and its structural elucidation led to a revolutionary advance in organometallic chemistry and the Nobel Prize in Chemistry were awarded jointly to Sir Geoffrey Wilkinson and Emile Fischer in 1973 for this work. Various sandwich metallocenes have since been synthesized and studied including ruthenocene, $Ru(C_5H_5)_2$, osmocene, $Os(C_5H_5)_2$, cobaltocenium salts, $[Co(C_5H_5)_2]^+$ and nickelocene, $Ni(C_5H_5)_2$.

Metallocenes have had an enormous impact on both industrial and biomedical chemistry.

In the medical field, metallocenes contribute in various biomedical applications varying from enzyme inhibitors, [1] anti-tumor properties, [2] and agents to modify antibiotics. [3] Radioactive metallocenes have played an important role in diagnostic nuclear medicine.[4,5] Ferrocene, for example, acts as a mediator in the biosensing of glucose.[6] Ruthenocene-containing chloroquine exhibits anti-malarial activity,[7] while titanocene dichloride has pronounced antiviral and anti-inflammatory activity.[8,9]

Uses of metallocenes in industrial chemistry include zirconocene and titanocene complexes as polymerization catalysts,[10,11,12] ferrocene derivatives as flame retardants [13] and as starting materials for the preparation of various organometallic compounds. [14,15]

Even though the group 8 metallocenes, ferrocene, ruthenocene and osmocene, are important in many facets of chemistry, there is a notable lack of studies on osmocene chemistry. The reasons for this range from the high cost of osmocene, low yields in derivatisation reactions, and to the high kinetic stability of osmocene.

Chapter 1
Introduction and aim of the study

A need has arisen in this research laboratory not only to synthesize and characterize new osmocene derivatives with biomedical applications, but also to develop osmocene derivates as ligands in coordination chemistry. With respect to this study, rhodium(I) has been chosen as the central metal to which osmocene-containing ligands must coordinate.

Rhodium coordination complexes were made famous by the use of $[Rh(CO)_2I_2]^-$ as catalyst in the Monsanto process (Scheme 1.1) where methanol is converted to acetic acid.[16,17] Rhodium(I) β-diketonato complexes have been used as catalysts in the hydrogenation of unhindered alkenes at low temperatures.[18] The reaction mechanism of the catalytic process usually involves oxidative addition to the metal by a suitable substrate followed by migration and insertion of a suitable ligand between metal moiety and coordinated ligand followed by reductive elimination of the final product.[19]

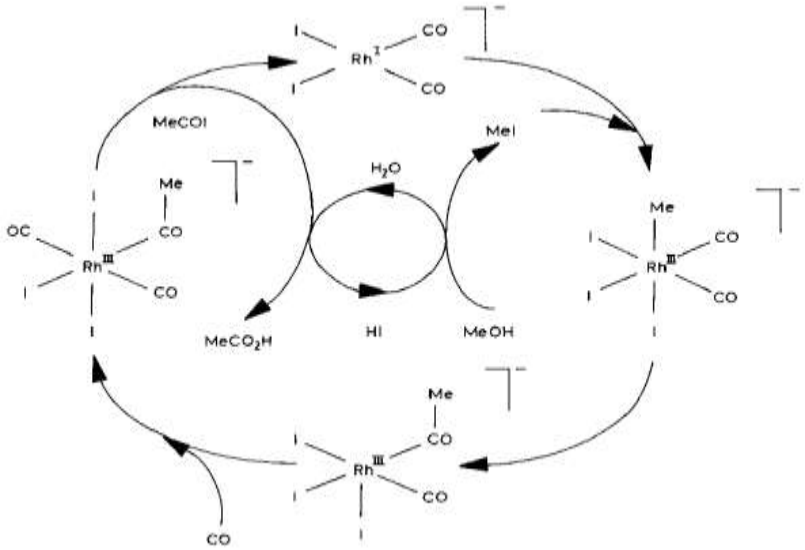

Scheme 1.1. Catalytic cycle for the rhodium-catalyzed carbonylation of methanol to acetic acid.

A systematic study of different ligands coordinated to the rhodium center showed that more electron-donating ligands induce faster oxidative addition to the metallic core, while electron-withdrawing groups decelerate the rate of oxidative addition.[20] In terms of

substitution reactions which are important in terms of the anticancer activity of the platinum group metal complexes, exactly the opposite trend has been observed.

No information is available how mixed metal complexes containing both an osmocenyl moiety and a rhodium center would behave in catalysis or in medical applications, even though benefits from such mixed metal systems may be substantial.

1.2. Aims of the study

With the above background, the following aims of this study were identified:

1. Synthesis and characterization of the new osmocene-containing β-diketones of the form $OcCOCH_2COR$ with Oc (osmocenyl) R = CF_3, CH_3, C_6H_5 (phenyl), Fc (ferrocenyl), Rc (ruthenocenyl) and H;

2. Determination of the rates of conversion between the enol and keto isomers of the new osmocene-containing β-diketones by means of ^{1}H-NMR spectroscopy;

3. Complexation of these osmocene-containing β-diketones with rhodium(I) to obtain complexes of the type [Rh(OcCOCHCOR)(cod)];

4. Determination of the group electronegativity of the osmocenyl group by utilization of spectroscopic (IR, $\nu_{C=O}$ values), thermodynamic ($pKa^{/}$) and electrochemical measurements;

5. Determination of the rate and substitution mechanism in reactions during which the β-diketonato ligand in [Rh(OcCOCHCOR)(cod)] is substituted with 1,10-phenanthroline by means of a stopped flow kinetic study.

Chapter 1
Introduction and aim of the study

References:

[1] W.H. Saine, Dissertation, University of Kansas, (1978).

[2] L.L. Gershbein, *Res. Comm. Chem. Path. Pharmacol*., 139, **27** (1980).

[3] E.I Edwards, R. Epton, G. Marr, G.K. Rodgers and K.I. Thompson, *Spec. Publ. Chem Soc.*, 92, **28** (1977).

[4] G. Wilkinson, Editor, *Comprehensive Organomettalic Chemistry*., M.A. Bennett, M.I. Bruce and T.W. Matheson, Pergamon Press, Oxford, pp. 774-775, **vol. 4**, (1982).

[5] S.L. Waters, *Coord. Chem. Rev*., 171, **52** (1983).

[6] N.J. Long, *Metallocene: An introduction to sandwich complexes*, Blackwell Science, London, p. 258, (1998).

[7] P. Beagley, M.A.L. Blackie, K. Chibale, J.R. Moss and P.J. Smith, *J. Chem. Soc., Dalton Trans*, 4426, (2002).

[8] P. Köpf-Maier and H. Köpf, *Metal Compounds in Cancer Therapy*, Chapman & Hall, London., p.104, (1994).

[9] B.K. Keppler, C. Friesen, H. Vangerchton and E.Vogel, *Metal Compounds in Cancer Therapy*,VCH, Weinheim, p.297. (1993).

[10] G. Wilkinson, Editor, *Comprehensive Organomettalic Chemistry*, Pergamon Press, Oxford., pp. 474-545, **vol. 3**, (1982) and the references therein.

[11] V.A.E. Barrios, A. Petit, F. Pla and R.H. Najera, *Eur. Polym. J*., 1151, **39** (2003).

[12] N.J. Long, *Metallocene: An introduction to sandwich complexes*, Blackwell Science, London, p. 23, (1998).

[13] E.W. Neuse, J.R. Woodhouse, G. Mantaudo and S. Puglisi, App*l. Organomet. Chem*., 53, **2** (1988).

[14] N.J. Long, *Metallocene: An introduction to sandwich complexes*, Blackwell Science, London, pp. 148-154, (1998).

[15] G. Wilkinson, Editor, *Comprehensive Organomettalic Chemistry*, Pergamon Press, Oxford., pp.331-426, **vol. 3**, (1982) and the references therein.

[16] D. Forster and T.W. Dekleva, *J.Chem.Educ.*, 204, **63** (1986).

[17] P.M. Matilis, A. Haynes, G.J. Sunley and M.J. Howard, *J.Chem.Soc.,Dalton Trans.*, 2187, (1996).

[18] W.R. Cullen, S.J. Rettig and E.B. Wickenheiser, *J.Mol.Catal*., 251, **66** (1991).

[19] F.A. Cotton, G. Wilkinson and P.L. Gaus, *Basic Inorganic Chemistry, 3rd edition*, John Wiley & Sons, London, 1995, pp 718-719.

[20] F. Basolo and R.G. Pearson, *Prog. Inorg. Chem*., 381, **4**(1962).

Chapter 1
Introduction and aim of study

Chapter 2
Literature survey

2.1. General Chemistry of Osmocene

2.1.1. Osmocene Synthesis

Although the chemistry of ferrocene has developed rapidly since its discovery in 1951, ruthenocene has received relatively little attention[1,2] and the chemistry of osmocene remains virtually unexplored. [2,3] This is largely attributed to the lack of convenient synthetic routes that produce ruthenocene and especially osmocene cheaply, in substantial amounts.[1-3] This study is aimed at developing synthetic routes to new osmocene complexes, exploring the use of osmocene derivatives as ligands and to explore some of the kinetic, electrochemical and thermodynamic properties of new osmocene-containing complexes.

The first reported synthesis of osmocene was in 1959 by Fischer and Grubert. They synthesized osmocene, **1**, in 23% yield by extended reflux of $OsCl_4$ in the presence of excess NaC_5H_5 in THF or dimethoxyethane (Scheme 2.1) .[4] More recently yields of 72% were obtained from the reaction of the polymer $\{[(\eta^4\text{-}C_8H_{12})OsCl_2]_x\}$ with $[(C_5H_5)Sn^nBu_3]$ in methanol at 65 ^{0}C.[5] This proved to be a reproducible route and was successful on a scale of several grams .

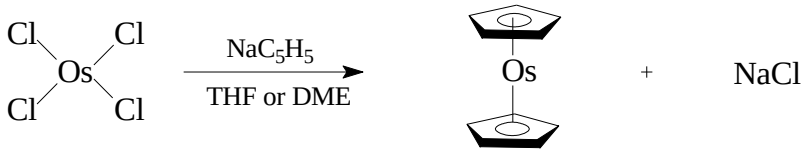

1

Scheme 2.1. Synthesis of osmocene.

Other methods include the reactions of $C_5H_6/[(Bu_4N)_2OsCl_6]/Zn/EtOH$. [6] Osmocene is obtained as a colourless, crystalline solid (m.p. 229-230 ^0C) which undergoes sublimation, is air and moisture stable and soluble in most organic solvents.[6]

2.1.2. Stability and reactivity of osmocene and substituted osmocenes

Group 8 metals consist of iron, ruthenium and osmium. These three metals form the characteristic sandwich-type metallocenes ferrocene, $Fe(C_5H_5)_2$, ruthenocene, $Ru(C_5H_5)_2$ and osmocene, $Os(C_5H_5)_2$. The known organic chemistry of osmocene closely resembles that of ferrocene and ruthenocene. All three of these metallocenes undergo reactions characteristic of an aromatic system. However, as one makes a downward migration in the periodic table's 8^{th} group the cyclopentadienyl ligands of the metallocenes become more and more unreactive towards aromatic substitution reactions. Osmocene is the least reactive metallocene in this group. In contrast, the ruthenium core of ruthenocene is most difficult to oxidise. Osmocene is thermally more stable towards degradation than ferrocene or ruthenocene.[7]

Friedel-Crafts acylation, metallation, arylation, formalation and sulphonation reactions are all possible but the degree of aromatic reactivity is markedly different in ferrocene, ruthenocene and osmocene. From an exhaustive series of competitive acylation reactions, the following order of reactivity was observed:

$$[Fe\ (C_5H_5)_2] > [Ru\ (C_5H_5)_2] > [Os\ (C_5H_5)_2]$$

This is in agreement with the relative availability of metal electrons for $C_5H_5^-$ bonding or ring basicity. The η^5-cyclopentadienyl rings in ruthenocene and osmocene are bound more tightly to the central metal atom than in ferrocene.[8] Tighter bonding would result in a lower π-electron density around the rings in the ruthenium and osmium complexes, thus accounting for the observed decreased electrophilic reactivity.

Chapter 2
Literature survey

The suppressed ability of osmocene and many other η^5-cyclopentadienyl metal compounds to form functionally substituted derivatives by ring-substitution routes has severely impeded the development of η^5-cyclopentadienyl metal chemistry.[9-11] An example of this is the exceptional stabilisation of the α-metallocenylcarbenium ions (Figure 2.1). In contrast to the electrophilic substitution reactivity, α-carbenium ions are stabilised by the metals in the following order:

osmocene> ruthenocene> ferrocene.

Stabilisation results from electron donation from metal to ligand through the overlap of a filled metal *d*-orbital of appropriate symmetry with the lowest unoccupied molecular orbital (LUMO) of the ligand. Therefore, this must be evidence of improved overlap of the Ru 4*d* and Os 5*d* orbitals with the cyclopentadienyl carbon *p*-orbitals compared with iron. This overlap in turn stabilizes the exocyclic carbon.[7]

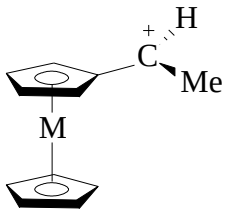

Figure 2.1. A α-metallocenylcarbenium ion. M= Fe, Os or Ru

Proton nuclear magnetic resonance spectra of several mono- and diacyl derivatives of the ferrocene-ruthenocene-osmocene triad have been obtained. It was found that there is a gradual deshielding of all the corresponding ring protons proceeding from the iron (C_5H_5 signal at 4.10 ppm) to the ruthenium (C_5H_5 signal at 4.48 ppm) to the osmium (C_5H_5 signal at 4.67 ppm) analogs.[11]

In contrast a gradual shielding of the methyl protons of acetylmetallocenes was noted. This shielding and deshielding may be attributed to a variety of factors, including both diamagnetic and paramagnetic contributors as well as the electronegativities of the

different substituents. This shielding of α- and β-protons and the deshielding of C_5H_5 protons in osmocene and ruthenocene relative to ferrocene, becomes more pronounced as reactivity towards, for example, acylation decreases.

2.1.3. General reactions of osmocene

Most aspects of the organic chemistry of osmocene (**1**) parallel the much-studied ferrocene chemistry (Scheme 2.2). It undergoes Friedel-Crafts mono-acylation to acylated species (**2**) but not alkylation.[8] Lithiation reactions are thought to involve nucleophilic attack of the hydrocarbon portion of the Li-containing reagent on a hydrogen atom of the compound undergoing the metallation. This proton must be relatively acidic. Ring hydrogen atoms in metallocenes are indeed weakly acidic. The extent of lithiation can be controlled through the selection choice of reaction conditions.

Lithiation of $[OsCp_2]$ by Bu^nLi gives a mixture of mono- and di-lithioosmocene intermediates (**3**) and (**4**) which, when condensed with carbon dioxide, yield a mixture of mono- (**5**) and di-carboxylic acids (**6**). However in the presence of $SiMe_3Cl$ trimethylsilylosmocene is yielded (**7**).[12] Separation of the mono- and di-acids is very difficult.

Acylosmocenes can be reduced to the corresponding hydroxyalkylosmocenes (**8**) or alkylosmocenes (**9**). Osmocene has an extraordinary ability to stabilize α-metallocenyl carbonium ions and can be converted to the azides (**10**).[13] Acylosmocenes react with $CH_3CN/NaNH_2$ to give β-hydroxynitriles (**11**) which can be dehydrated to the α,β-unsaturated nitriles (**12**).[14]

Chapter 2
Literature survey

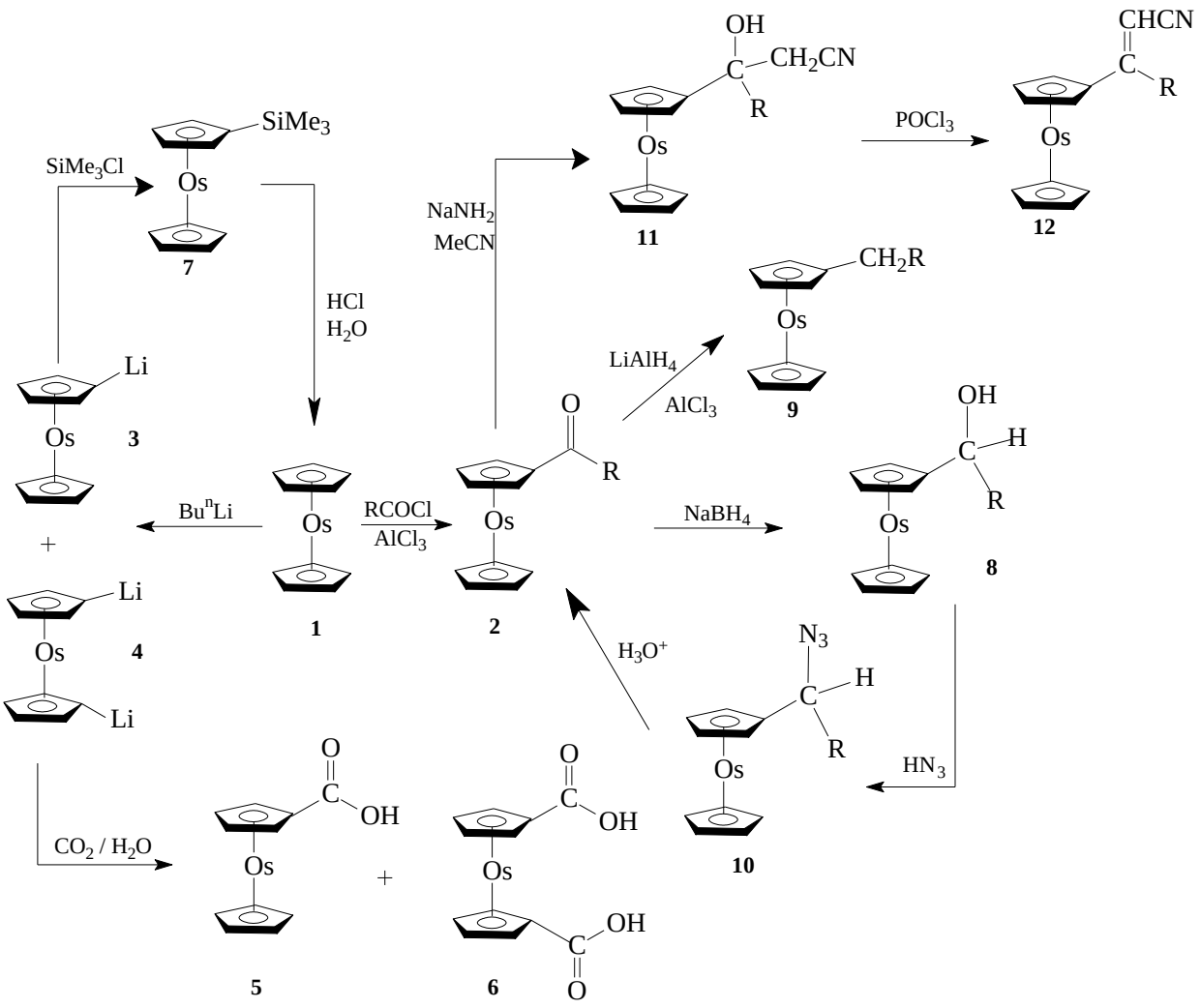

Scheme 2.2. Synthesis of a variety of osmocene precursors relevant to this study. (Bu^nLi = *n*-butyllithium, R = Me, Ph and Fe(Cp)(C_5H_4).

2.2. Synthesis

2.2.1. Synthesis of acetyl metallocenes

Friedel-Crafts acetylation reactions have mostly been performed on group 8 metallocenes as shown in Scheme 2.3.

Chapter 2
Literature survey

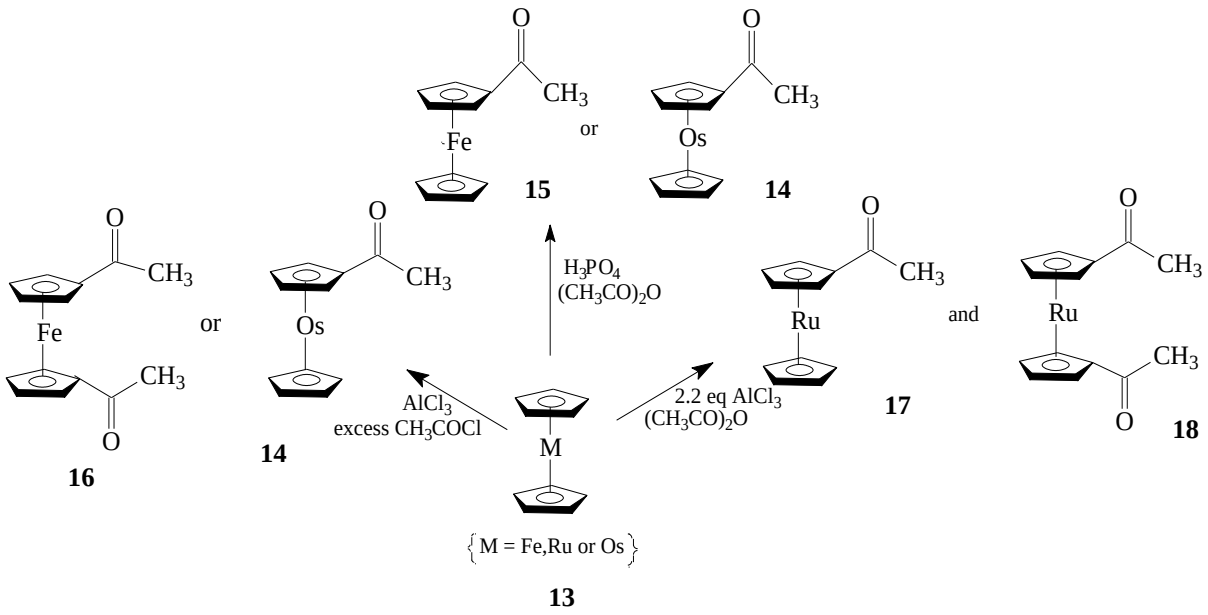

Scheme 2.3. Acetylation reactions of the group 8 metallocenes.

Graham and co-workers acetylated ferrocene using electrophilic aromatic substitution.[15] Acetic anhydride in the presence of 85% meta-phosphoric acid dissociated into acetic acid and an aldehyde cation, which in turn acts as an electrophile seeking out the electron-rich β-clouds of the ferrocene in order to displace a hydrogen atom from the ring. This acetylation agent results in a 71% yield of mono-acetylated ferrocene after chromatographic separation, due to the acetylaldehyde's electron-withdrawing properties which increase binding energy.[16] Rausch and co-workers found that due to the reactivity decrease of metallocenes down group 8, the Lewis acid aluminium trichloride had to be used to produce 89% mono-acetylated osmocene, **14**, after sublimation. Under these conditions the diacetylated products of ferrocene (21%), **16,** and ruthenocene (22%), **18,** are also obtained.

Even though the results of Rausch and Grubert show that osmocene requires more vigorous acetylation conditions than ferrocene and ruthenocene, Hill and Richards[17] found that there are a number of reasonable possibilities for the reversal in the reactivity sequences, especially due to the small differences in reactivities. It is not possible to use these observed differences as strong arguments in favour of any specific type of metal

effect, as a yield of 85% mono-acetylated osmocene was obtained with the use of 85% phosphoric acid as the Lewis acid.

2.2.2. Synthesis of metallocene carboxylic acids

The synthesis of metallocene esters needs the availability of the appropriate metallocene carboxylic acid. These esters are in turn needed to synthesize β–diketones by utilising the Claisen condensation route.

Various routes can obtain metallocene carboxylic acids. Synthesis of ferrocene carboxylic acid, **19** has mainly been documented.[17, 18, 19] Some of these reactions are shown in Scheme 2.4.

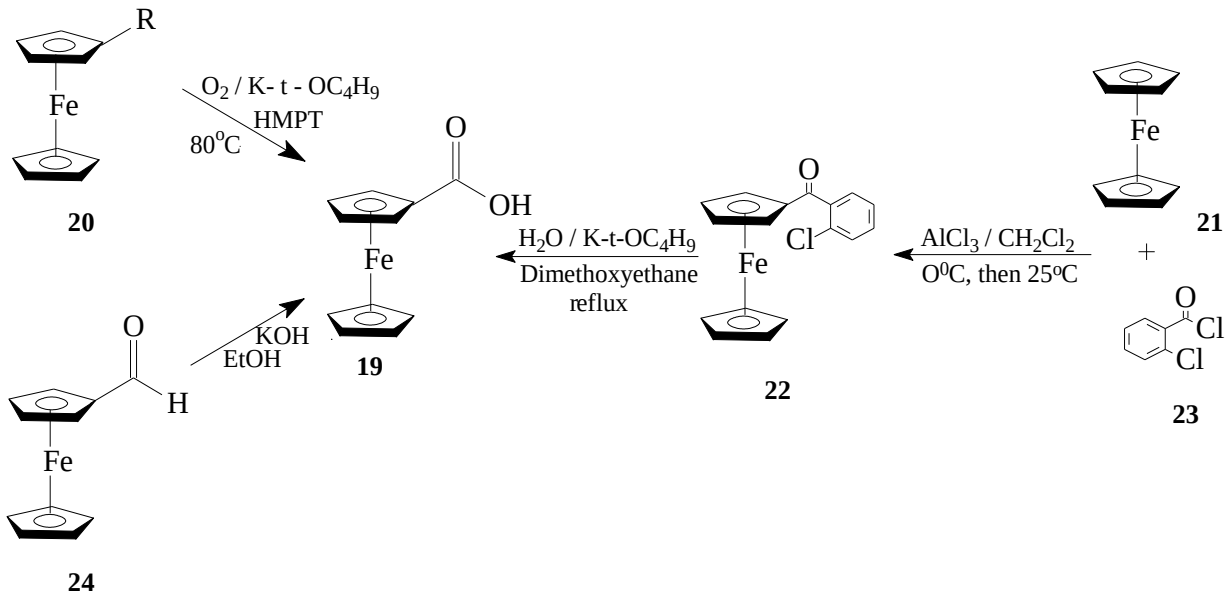

Scheme 2.4. Synthesis of ferrocene carboxylic acid *via* three pathways. (K-*t*-OC_4H_9 = Potassium *tertiary*-butoxide, HMPT = hexamethylphosphoric triamide, R = CH_2OH, CHO, $COCH_3$ to $CH_2N(CH_3)_2$).

Schmitt and Ozman synthesized ferrocene carboxylic acid, **19** from aliphatic substituted ferrocenes. The latter reacted with potassium *tert*-butoxide in the presence of hexamethylphosphoric triamide (HMPT) with yields of between 25-86%, where the R-group varied from R = CH_2OH, CHO, $COCH_3$ to $CH_2N(CH_3)_2$, **20**.[17]

The method described in the Organic Synthesis series firstly converted ferrocene, **21**, to 2-chlorobenzoylferrocene, **22**, after reacting with 2-chlorobenzoylchloride, **23**. The product was then reacted with potassium *tert*-butoxide in water to yield 74-83% of the desired carboxylic acid, **19**.[19] The ferrocene aldehyde, **24**, in the presence of potassium hydroxide in ethanol can also be converted to the ferrocene carboxylic acid, **19**.[20]

Lithiation with the use of n-butyllithium can also be employed to yield the desired carboxylic acids. The mono-lithiated and di-lithiated ruthenocene can be obtained by reacting ruthenocene with n-butyllithium.[8, 21]

Benkeser and co-workers lithiated ferrocene, **21**, with n-butyllithium to yield a mixture of the mono- and di-lithiated products, with the former predominating.[18] These mono- and di-lithiated products, **25**; **26**, of both ruthenocene and ferrocene can be converted to the carboxylic acids, **27**; **28**, by reacting them with carbon dioxide followed by hydrochloric acid. [8,21,22] These reactions are shown in Scheme 2.5.

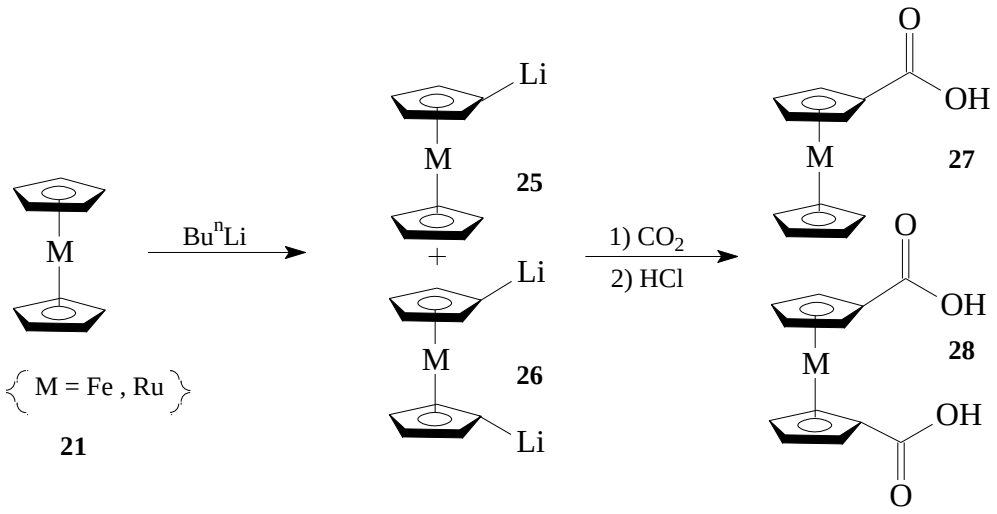

Scheme 2.5. Lithiation reactions of ferrocene and ruthenocene.

2.2.3. Synthesis of metallocene esters

Various routes exist for obtaining esters, but only a few are relevant to the synthesis of metallocene esters. Normally metallocene esters are obtained by reacting a carboxylic

acid with an alcohol in the presence of a catalytic amount of a mineral acid such as H_2SO_4 or HCl. [23]

Esterification based on the use of diazomethane to synthesize the methyl ester of 2-methylruthenocene acid, **30**, is an alternative route, which is shown in Scheme 2.6.[24]

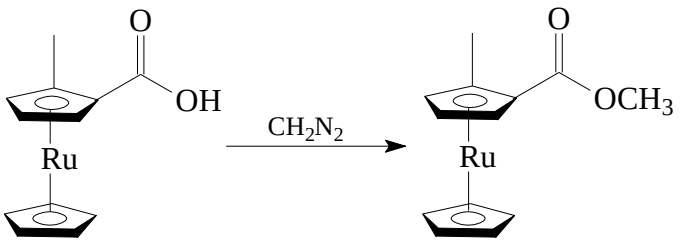

29 **30**

Scheme 2.6. Synthesis of a methyl-ruthenocene ester.

By reducing cobaltocene, **31**, to the cobaltocenium anion, **32**, containing Co(I) and then carbonating it in a dimethylformamide/methyl iodide solution the cobaltocene methyl ester, **33**, can be synthesized as indicated in Scheme 2.7.[25]

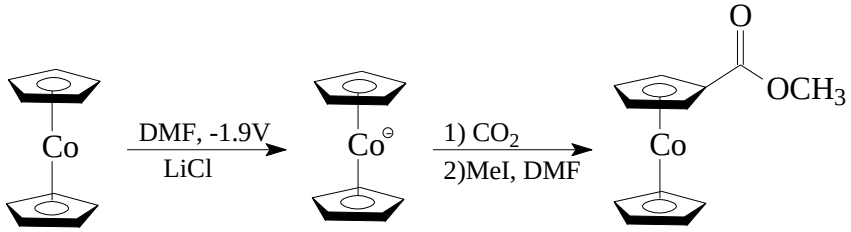

31 **32** **33**

Scheme 2.7. Synthesis of the cobaltocene methyl ester.

2.2.4. Synthesis of β-diketones

As this study is concerned with the synthesis of new osmocene β-diketone complexes, a brief discussion of various routes for β-diketone synthesis is appropriate.

Chapter 2
Literature survey

Roth and co-workers formed β-diketones by converting thioesters with tri tertiary butyl phosphine under basic conditions.[26] Butyl butanethioate, **34**, was converted to octane-3,5-dione, **35**, a yield of 72% was obtained. This reaction is indicated in Scheme 2.8.

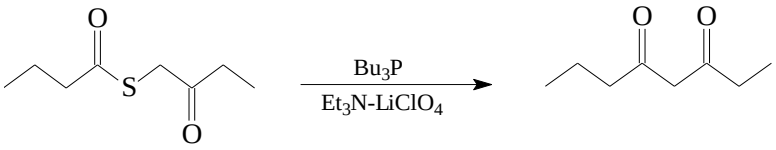

34 **35**

Scheme 2.8. Synthesis of octane-3, 5-dione by the method of Roth.

BF_3-catalysed condensation of a ketone and acetic anhydride was employed by Cravero and co-workers to synthesize para-nitrobenzoylacetone, **37**.[27] The latter was obtained by adding para-nitroacetophenone, **36** and acetic anhydride to an acetic acid-BF_3 complex at O^0C for 30 minutes and then at 25^0C for 24 hours. Scheme 2.9. illustrates this reaction.

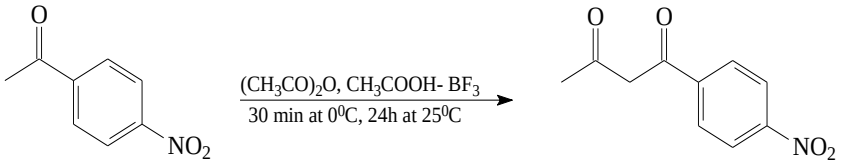

36 **37**

Scheme 2.9. Synthesis of para-nitrobenzoylacetone through the method of Cravero.

β-diketones can also be formed by pinacol rearrangement as shown by Suzuki and co-workers.[28] A yield of 80% 2-methyl-3,5-hexanedione, **39**, was obtained by heating 2-methyl-3,4-epoxy-5-hexanone, **38**, to between 80-140^0C in toluene, with the addition of a small amount of $(Ph_3P)_4Pd$ and 1,2-bis(diphenylphosphino)ethane (dppe). This reaction is shown in Scheme 2.10.

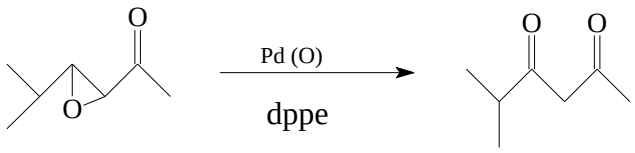

38 **39**

Scheme 2.10. Synthesis of 2-methyl-3, 5- hexanedione according to the method of Suzuki.

Umetani and co-workers adopted an alternative method.[29] The 4-pivaloyl-3-methyl-1-phenyl-5-pyrazolone complex, **41**, was synthesized by the condensation reaction of 3-methyl-1-phenyl-5-pyrazolone, **40**, with pivaloyl chloride in the presence of calcium hydroxide with a yield of 19%. This reaction is depicted in Scheme 2.11.

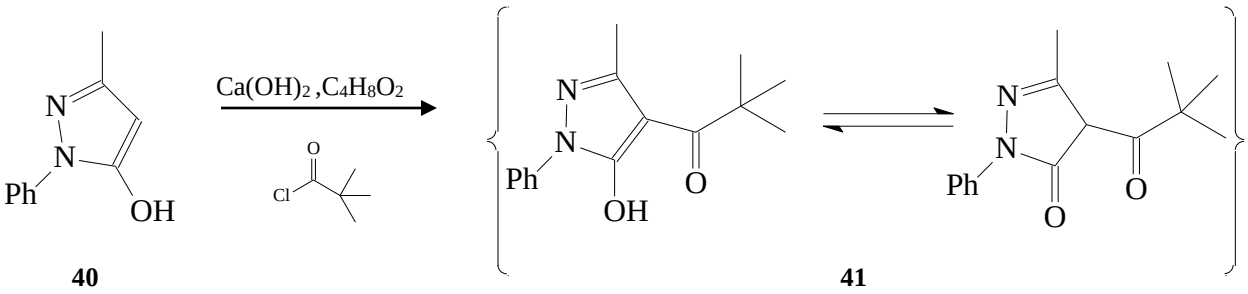

40 **41**

Scheme 2.11. Synthesis of 4-pivaloyl-3-methyl-1-phenyl-5-pyrazolone according to the method of Umetani.

2.2.5. Synthesis of metallocene β-diketones

Metallocene β-diketones are usually synthesized by the Claisen condensation route.[30] In these reactions a ketone, which possesses an α-hydrogen, reacts with a suitable acylation reagent (ester, acid anhydride, acid chloride) in the presence of an appropriate base (Scheme 2.12). The mechanism is as indicated in Scheme 2.13.

For this illustration the base lithium diisopropylamide (LDA) and the ester R^2COOEt are used.

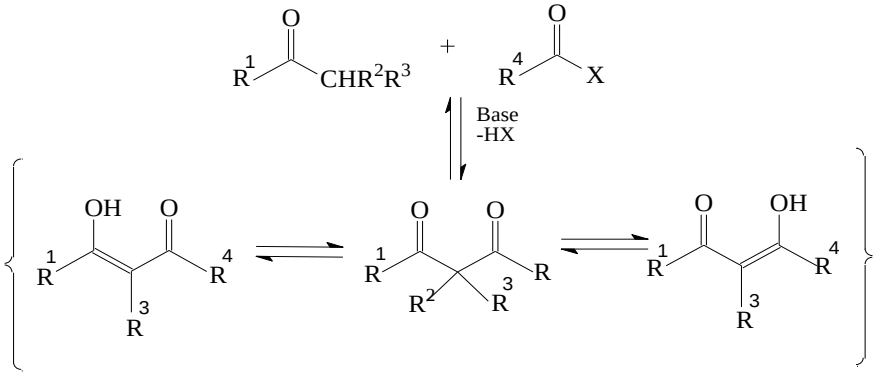

Scheme 2.12. The synthesis of β-diketones. End form R^2 =H.

Chapter 2
Literature survey

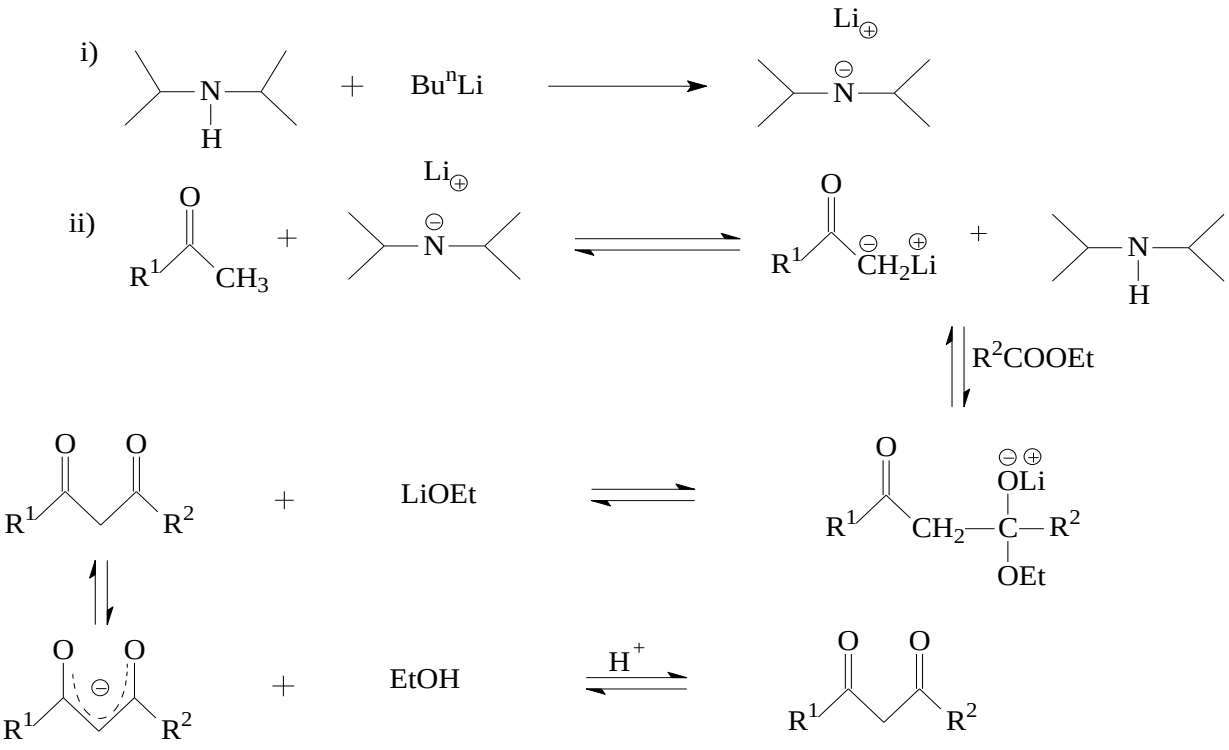

Scheme 2.13. Mechanism for the formation of a β-diketones.

Most β-diketones existing in solution are in equilibrium involving the keto- and enol-forms, provided that there is at least one methine hydrogen present. In the solid state, however, the enol form is often the sole form observed. The methine proton in the keto-form and the hydroxyl proton in the enol-form of the β-diketones are acidic. Their removal generates 1,3-diketonato anions, which are the source of an extremely broad class of coordination compounds.

Hauser and co-workers synthesized ferrocene-containing β-diketones, **42**, with potassium amide as the strong base in a mixture of liquid ammonia and diethyl ether.[31] Yields of 65% for 1-ferrocenylbutane-1,3-dione (R=CH_3), **43**, and 63% for 1-ferrocenyl-3-phenylpropane-1,3-dione (R=C_6H_5), **43**, were achieved.

Chapter 2
Literature survey

An alternative route for obtaining ferrocene-containing β-diketones is to use the base sodium methoxide as demonstrated by Weinmayr.[32] This base yielded 80% 1-ferrocenyl-4,4,4-trifluorobutan-1,3-dione (R= CF_3) while 29% of the 1-ferrocenylbuthane-1,3-dione (R=CH_3) was yielded.

The lower yield of 1-ferrocenylbutane-1,3-dione by Weinmayr can be explained by the fact that the base sodium methoxide is a weaker base than potassium amide. These reactions are shown in Scheme 2.14.

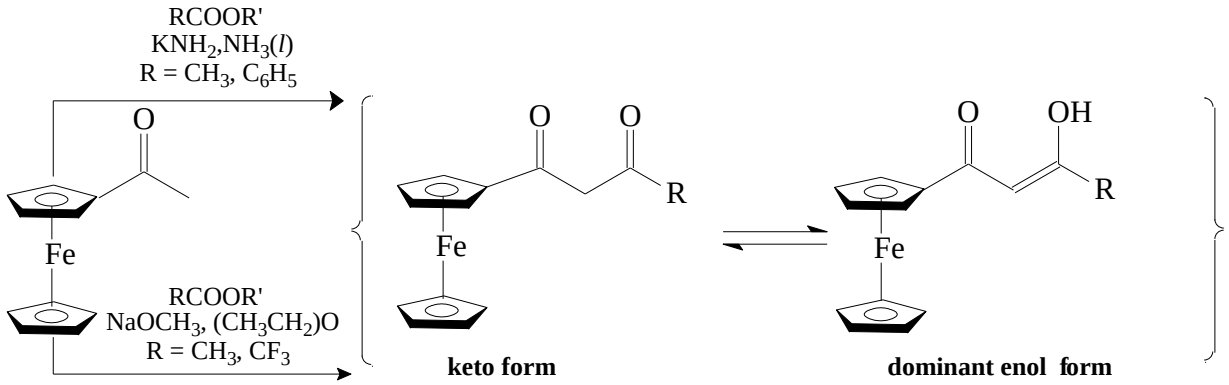

Scheme 2.14. Synthesis of ferrocene-containing β-diketones by Claisen condensation with the use of two different bases (R' = methyl or ethyl).

The Claisen condensation performed by Cain and Hauser resulted in the formation of a bis-β-diketonatoferrocene and is shown in Scheme 2.15.[33,34] This reaction between diacetylferrocene, **44,** and an appropriate ester yielded 46% 1,1-bis[1-(3-phenyl)propane-1,3-dione]ferrocene (R=C_6H_5), **45**, and 72% for 1,1-bis(1-butane-1,3-dione)ferrocene (R=CH_3), **45**.

Chapter 2
Literature survey

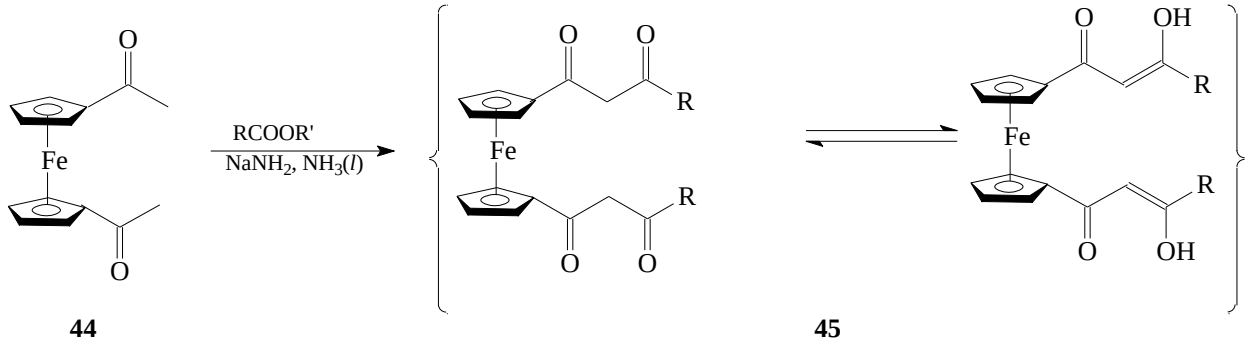

44 **45**

Scheme 2.15. Synthesis of ferrocene-containing bis-β-diketones. R = CH_3 or C_6H_5, R' = CH_3 or C_2H_6.

2.3. Medicinal properties of metal complexes

2.3.1. Transition metal complexes in chemotherapy

In 1951[35] the cytostatic activities of various transition metal complexes of Cu, Pb, Mn, Fe, Co, Ni, Ru, Rh and Os were investigated. In general these various complexes showed no activity.

Studies by Furst showed a connection between chelate formation, carcinogenicity and cancer combating properties.[36] In his book Furst postulates that the majority of non-metal carcinogens are potential complexation reagents. The carcinogenic activity is probably due to the complexation reactions with essential metals found in the body. During this complex formation process, essential metals are removed from their reaction sphere. Due to non-selective complexation reactions, these reagents complex with a wide variety of metals.

High-lipid soluble metal complexes penetrate cells by pinocytosis. In high concentration these metals disturb the normal equilibrium between essential metals, enzymes and complexing agents in the cell. This equilibrium disturbance affects cell metabolism negatively, leading to neoplastic cell transformation. Thus cancer-combating reagents, with complexing properties, have the ability to complex "foreign" metals to a higher degree than essential metals in the cell.

Chapter 2
Literature survey

During the design of new potential metal-containing chemotherapeutic substances, consideration was given to the complexation ability of metals, reaction selectivity, formation constants, and cell penetration properties of which the target molecule disposed.

The kinetic abilities of potential chemotherapeutic substances, however, did not receive a great deal of attention. This information is important for understanding the mechanism by which chemotherapeutic agents destroy cancer cells.

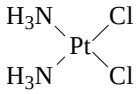

Figure 2.2. The structure of cisplatin.

Cisplatin (Figure 2.2) is an inorganic complex. It consists of a central metal, platinum, with four inorganic ligands. Until recently cisplatin has been the most frequently used chemotherapeutic agent in the U.S.A., Europe and Japan. It does, however, have a number of side effects, which include stimulating lung adenomas. Certain of these side effects have been countered by the simultaneous use of other drugs in a synergistic manner.[37]

In reality cisplatin is not the active chemotherapeutic species. In water, the labile chloro-ligands are substituted by water molecules.[38] This is shown in Scheme 2.16.

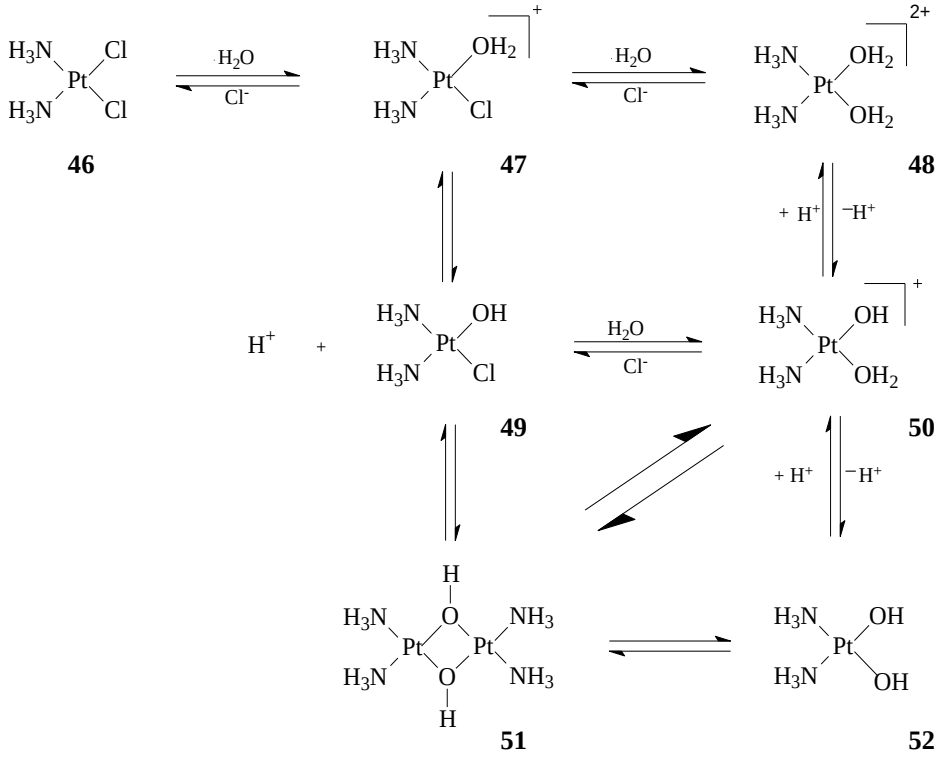

Scheme 2.16. Aqua-substitution reactions of cisplatin.

Resistance of cancer cell lines to cisplatin have been addressed through the use of other platinum coordination compounds such as carboplatin.[39] However, even this new generation of platinum drugs has severe side effects, and thus the search for new cancer drugs is a worldwide priority.

2.3.2. Rhodium and metallocenes in cancer therapy

Giralsi and co-workers compared rhodium and ruthenium complexes with cisplatin.[40] Less histological damage was shown by [(acetylacetonato)(cycloocta-1,5-diene)rhodium] than by isplatin. The complex acetylacetonate-1,5-cyclooctadiene rhodium(I), shown in Figure 2.3, is analogous to the osmocene compounds synthesised in this study.

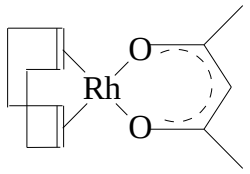

Figure 2.3. Structure of acetylacetonate-1,5-cycloctadiene rhodium (I).

Various rhodium– and ruthenium-containing complexes have been used in the fight against cancer. New antineoplastic ruthenium compounds have been developed that show cytotoxicity prevention induced by other chemotherapeutic drugs.[41,42,43]

Ruthenocene compounds have also been used in cancer therapy. The radiopharmaceutical acetyl-(^{103}Ru)-ruthenocene has been used in the investigation of the affinity of acetylruthenocene for the adrenal glands of mice. This labelled compound was prepared by heating acetyl ferrocene with ^{103}ruthenium trichloride. Results showed that the compound had an affinity for the regions of the adrenal gland, where androgen and glucocorticoid syntheses occurred.[44] A study was then carried out to show the effect of hormones on the localization of acetylruthenocene. It was found that if the hormones could be controlled, the target of the acetyl ruthenocene could also be controlled *in vivo*.[45]

Other metallocenes investigated included ferrocene derivatives. Ferrocene was linked to water-soluble polymers, so that the dose-limiting factors in chemotherapy in terms of poor solubility could be overcome. It was also found that for the water-soluble polymeric drug, fewer drug units were needed for the same effectiveness than when the drug was administered in monomeric form.[45]

This study showed[45] that both the size of the spacer between the ferrocene drug from the polymer backbone, as well as the formal reduction potential of the ferrocenyl group play an important role in drug activity. Longer spacers and lower ferrocenyl formal reduction potentials both enhance the anticancer activity.

2.4. Electrochemistry

2.4.1. Introduction

Cyclic voltammetry (CV) is possibly the simplest and most versatile electroanalytical technique for the study of electro-active species. The effectiveness of CV is its ability to

obtain the redox behaviour of electro-active species fast over a wide potential range.[46] CV is a simple and direct method for the measurement of the formal reduction potential of a reaction when both oxidized and reduced forms are stable during the time when the voltammogram is recorded.[47] Thermodynamic and kinetic information is available in one experiment. Therefore, both reduction potential and heterogeneous electron transfer rates can be measured. The rate and nature of a chemical reaction coupled to the electron transfer step can also be studied. Knowledge of the electrochemistry of a metal complex can be useful in the selection of the proper oxidizing agent to place the metal complex in an intermediate oxidation state.

More information can be gained in a single experiment by sweeping the potential very slowly ($\nu < 2$ mV/s) with time and recording the *i*-E curve directly. The potential scanning takes place in either the anodic or the cathodic direction without obtaining current reversal. This method is known as Linear Sweep Voltammetry (LSV).

2.4.2. Cyclic Voltammetry

2.4.2.1. The basic cyclic voltammetry experiment[46]

CV entails oscillating the potential of an electrode, in an unstirred solution, and measuring the resulting current. The potential of the small, static, working electrode is controlled relative to a reference electrode. The reference electrode could be, for example, a saturated calomel electrode (SCE) or a silver/silver chloride electrode (Ag/AgCl). The controlled potential, which is applied over these two electrodes, can be viewed as an excitation signal. This excitation signal for the CV is a linear potential scanning with a triangular waveform, from an initial value, E_i, to predetermined limit $E_{\lambda 1}$ (switching potential) where the direction of the scan is reversed (Figure 2.4). The scan can be stopped anywhere or a second cycle, as indicated by the broken line, can be initiated. Single or multiple cycles can be measured. The scanning rate as indicated by the slope, may be anything between $\pm$ 15 mV s^{-1} to 40000 mV/s.

Chapter 2
Literature survey

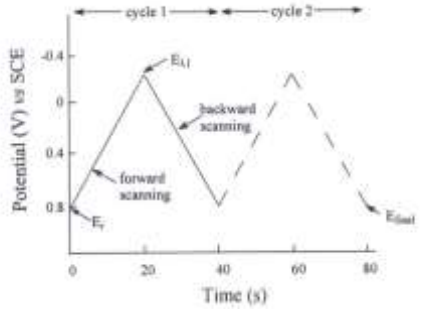

Figure 2.4. Typical excitations signal for cyclic voltammetry - a triangular potential waveform. Figure taken from: J. Chem. Educ.,702, **60** (1983).

The current response on a cyclic voltammogram (vertical axis) is plotted as a function of the applied potential (horizontal axis); see Figure 2.5 for a typical CV. Often there is very little difference between the first and successive scans. However, the changes that do appear on repetitive cycles are important in obtaining and understanding information about reaction mechanisms.

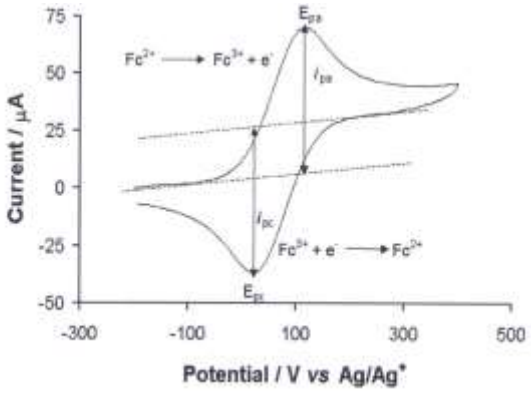

Figure 2.5. Cyclic voltammogram of a 3.0 mmol dm^{-3} Fe^{3+} solution measured in 0.1 mol dm^{-3} tetrabutylammonium hexafluorophosphate/acetonitrile on a glassy carbon electrode at 25 ^{0}C, scan rate 100 mVs^{-1}. Figure taken from: J. Chem. Educ., 702, **60** (1983).

2.4.2.2. Important parameters of cyclic voltammetry[46,48]

The most important parameters of cyclic voltammetry are the peak anodic potential, E_{pa}, peak cathodic potential, E_{pc}, peak anodic current, i_{pa}, and peak cathodic current, i_{pc}. (Figure 2.5). One method of measuring peak currents involves the extrapolation of a baseline. Establishing the correct baseline is essential for accurate measurement of the peak currents.

A redox couple may or may not be electrochemically reversible. Electrochemical reversibility implies that the rate of electron transfer between the electrode and substrate is fast enough to maintain the concentration of the oxidised and reduced species in equilibrium at the electrode surface.

The formal reduction potential for an electrochemically reversible redox couple is midway between the peak potentials (Equation 2.1).

$$E^{01} = (E_{pa} + E_{pc})/2$$

Equation 2.1.

This E^{01} is an estimate of the polarographic $E_{1/2}$ value provided that the diffusion constants of the oxidised and reduced species are equal.

The polarographic $E_{1/2}$ value can be calculated from E^{01} *via* Equation 2.2.

$$E_{1/2} = E^{01} + (RT/nF) \ln(D_R/D_O)$$

Equation 2.2.

Here D_R = diffusion coefficient of the reduced species, D_O = diffusion coefficient of the oxidised species. In cases where $D_R/D_O \approx 1$, $E_{1/2} \approx E^{01}$.

For electrochemically reversible couples the difference in peak potentials (ΔE_p) should theoretically be 59 mV at 25 ^{0}C for a one-electron transfer process. The number of electrons (*n*) transferred in the electrode reaction for a reversible couple can be determined from the separation between the peak potentials of Equation 2.3.

$$\Delta E_p = E_{pa} - E_{pc} \approx \left(\frac{59}{n} \right) \text{ mV}$$

Equation 2.3.

This 59/*n* mV separation of peak potentials is independent of the scan rate of the reversible couple, but slightly dependent on the switching potential and cycle number.[49] In practice, within the context of this research program, a redox couple with a ΔE_p value up to 90 mV will still be considered electrochemically reversible. Peak separation increases due to slow electron transfer kinetics at the electrode surface.

The peak current, i_p, is dependent on a few variables and is described by the Randle-Sevcik equation for the first sweep of the cycle at 25 ^{0}C (Equation 2.4).

$$i_p = (2.69 \times 10^5) n^{3/2} A D^{1/2} \nu^{1/2} C$$

Equation 2.4.

i_p = peak current (A), n = amount of electrons per molecule, A = working electrode surface (cm^2), C = concentration (mol cm^{-3}), ν = scan rate (V s^{-1}) and D = diffusion coefficient (cm^2 s^{-1}).

The values of i_{pa} and i_{pc} should be identical for a reversible redox couple, which is not followed by any chemical reaction (Equation 2.5).

$$i_{pa}/i_{pc} = 1$$

Equation 2.5.

Systems can also be quasi-reversible or irreversible (Figure 2.6). An electrochemically quasi-reversible couple is one in which both the oxidation and reduction processes take place, but the electrochemical kinetics are slow and $\Delta E_p > 59$ mV. With respect to this study peak separation values of 90 mV $\leq \Delta E_p \leq$ 150 mV will be considered to imply quasi-reversibility. A completely chemically irreversible system is one where only oxidation or reduction is possible.[52] In cases where the system is quasi-reversible or irreversible, Equations 2.1, 2.3 and 2.4 are not applicable.

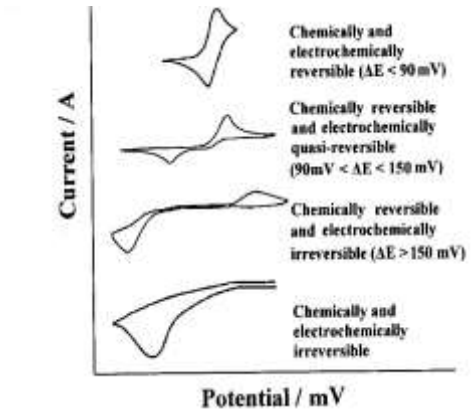

Figure 2.6. A schematic representation of the cyclic voltammogram expected from an electrochemical reversible, electrochemically irreversible, electrochemically quasi-reversible and chemical irreversible systems. Figure taken from: J. Chem. Educ., 702, **60** (1983).

2.4.3. Electrochemistry of some metallocene complexes

2.4.3.1. Ferrocene

Ferrocene, with a formal reduction potential of 400 mV *vs.* NHE ,[51] can be used in CV experiments as an internal reference system in a wide range of non-aqueous solvents,[52] or when using different reference electrodes.[53]

The Fc/Fc^+ couple is reversible and has a ΔE_p = 59 mV under ideal conditions. Different formal reduction potentials of Fc in solvents such as tetrahydrofuran (THF), DCM and CH_3CN referred to the same reference electrode have been measured (Table 2.1).

Table 2.1. Redox potentials in solutions *vs.* Ag/Ag^+ and SCE (Pt auxiliary electrode and supporting electrolyte 0.2 M *n*-Bu_4NPF_6 of ferrocene (Fc).

Substance	**Solution**	**$E_{1/2}$ *vs.* Ag/Ag^+ /V**	**$E_{1/2}$ *vs.* SCE /V**	**i_{pa}/i_{pc}**	**ΔE_p /V**
Fc	THF	0.20	0.53	1.0	100
	DCM	0.21	0.43	1.0	100
	CH_3CN	0.10	0.43	1.0	80

Irrespective of the shift in E^{01} (Fc/Fc^+) in different solvents, the formal reduction potential of another compound (e.g. $[IrCl_2(fctfa)(COD)]$) *vs.* Fc/Fc^+ as an internal standard, remains unchanged.[54] Complexes with two or three ferrocenyl ligands bound to them, showed different oxidation and reduction peaks for the different Fc moieties (Figure 2.7).[55,56,57]

The observed inequalities is due to the improbability of all ferrocenyl groups of the same molecule, coming simultaneously in reaction contact with the electrode to invoke three simultaneous one-electron transfer processes.[58,59]

Chapter 2
Literature survey

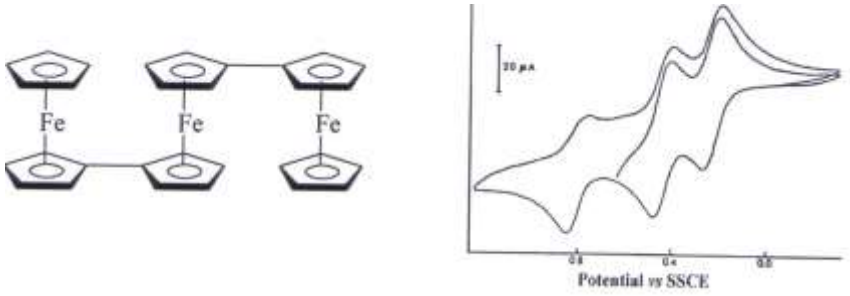

Figure 2.7. Left: Structure of 1,1'-terferrocene(1+). Right: Cyclic voltammogram of 1,1'-terferrocene(1+) in 1:1 CH_2Cl_2:CH_3CN containing 0.1M TBAH at scan rate 200 mV s^{-1}. Figure taken from: *Can. J. Chem*.**,** 378**, 77** (1999).

In the complexes in which two ferrocenyl ligands are bound to each other, the binding mode could be either by one or two covalent bonds (Figure 2.8).[60] This leads to quite a dramatic difference in their electrochemical polarographic behaviour (Table 2.2), which can be related to cyclic voltametric behaviour *via* Equation 2.2. In a bridged ferrocene with two linkages, the Fe atoms are kept very close to one another. Its CV data shows that the second oxidation step is more difficult than the first. Electron interaction can take place *via* two ways: 1) through the conjugated carbon skeleton of the ligands, 2) through direct metal-metal interaction (a through-space field effect). The CV results of a bridged ferrocene with one linkage show that its second oxidation step is easier than that found for the bridged ferrocenes with two linkages, thus the potentials of the two redox couples are closer to one another. This was attributed to the direct electrostatic field interaction between the Fe atoms, as, for steric reasons, the mono-bridged ferrocene derivative can adopt a conformation in which the two Fe atoms are pseudo-*trans* to one another.

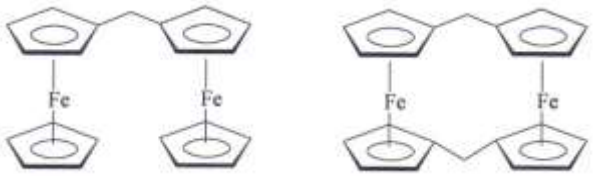

Figure 2.8. Ferrocene derivatives, which are linked *via* either one or two connecting CH_2 groups.

Table 2.2. Polarographic half potentials of ferrocene derivatives, bridged ferrocenes that are linked *via* either one or two linkages.

Bridged ferrocenes	**$E_{1/2}$ /V**	**$\Delta E_{1/2}$ / V *vs.* Fc (0.34 V)**
One CH_2 linkage	0.30, 0.40	-0.04, 0.06
Two CH_2 linkages	0.25, 0.44	-0.09, 0.10

When ferrocene is bound in a complex such as a β-diketone ($FcCOCH_2COR$), the E^{O1} value of the Fc/Fc^+ couple is influenced by the group electronegativity of the R group (Figure 2.9, Table 2.3),[58] due to the good communication between the ferrocenyl ligand and the R group *via* the backbone of the pseudo-aromatic β-diketone core. With increasing electronegativity of the R group on the β-diketone, the E^{O1} value of the Fc/Fc^+ couple also increases as R withdraws electron density from it.

There is also a linear relationship between the pK_a of the β-diketone and the E^{O1} value of the Fc/Fc^+ couple, and with increasing pK_a there is a decrease in the E^{O1} value of the Fc/Fc^+ couple.

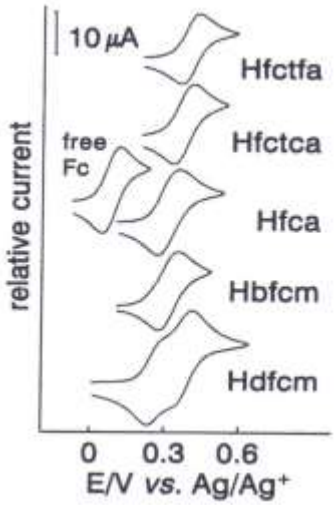

Figure 2.9. Cyclic voltammograms of 2 mmol dm^{-3} solutions of ferrocene (Fc) and ferrocene-containing β-diketones measured in 0.1 mol dm^{-3} $TBAPF_6/CH_3CN$ at a scan rate of 50 mV s^{-1} on a Pt working electrode at 25.0(1) ^0C versus Ag/Ag^+. Acronyms are defined in Table 2.3. Figure taken from: *Can. J. Chem*., 378, **77** (1999).

Table 2.3. E^{01} *vs.* Ag/Ag^+ of the β-diketones of the type $FcCOCH_2COR$, R = CF_3, CCl_3, CH_3, Ph and Fc group electronegativities of the R groups on the β-diketones and pKa values of the β-diketones.

β-diketone	R group on the β-diketone	E^{01} *vs.* Ag/Ag^+ /mV	Group electronegativity of the R group	pK_a of the β-diketone
Hfctfa	CF_3	0.394	3.01	6.53
Hfctca	CCl_3	0.370	2.76	7.15
Hfca	CH_3	0.313	2.34	10.01
Hbfcm	Ph	0.306	2.21	10.41
Hdfcm	Fc	0.265; 0.374	1.87	13.1

2.4.3.2. Ruthenocene

Traditionally the view has been that the oxidation of ruthenocene proceeds by a $2e^-$ irreversible process.[61] This result was observed by using tetrabutylammonium perchlorate as supporting electrolyte. However, this electrolyte has weak coordinating properties. A non-coordinating solvent however results in a $1e^-$ reversible electrochemical process.[62]

A reduction potential of 1.03 V was obtained for ruthenocene versus an aqueous AgCl/Ag (1.0 M KCl) reference electrode when the electrolyte was tetrabutylammonium tetrakis[3,5-bis(trifluoromethyl)phenyl]borate (TBA^+TFPB^-). Figure 2.10 depicts the CV.

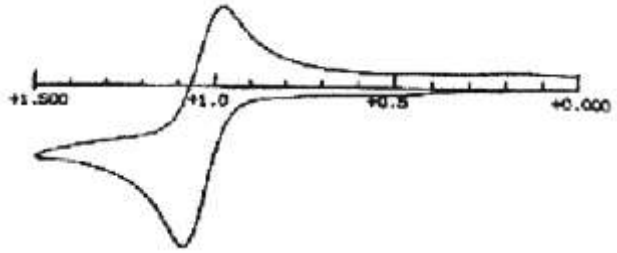

Figure 2.10. Cyclic voltammetry of a 0.5 mmol dm^{-3} solution of ruthenocene in 0.1 mol dm^{-3} $TBA^{+}TFPB^{-}$ /dichloromethane at a scan rate of 100 mV s^{-1}, indicating a 1e^{-} reversible electrochemistry. Figure taken from: *Inorg. Chem*., 4687, **30** (1991).

Jacob and co-workers dissolved ruthenocene in a mixture of 0.8:1 $AlCl_3$:1-butylpyridinium chloride, resulting in a quasi-reversible 1e^{-} oxidation reaction shown in Figure 2.11.[63]

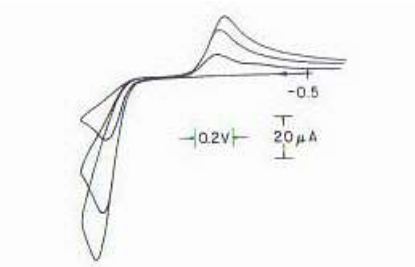

Figure 2.11. Cyclic voltammetry of 22.2 mmol dm^{-3} solution of ruthenocene in Lewis acid-base molten salts, indicating a quasi-reversible 1e^{-} oxidation. Figure taken from: *J. Electroanal. Chem*., 161, **427** (1997).

It was recently shown by Jacob and co-workers that the electrochemistry of the newly synthesised novel ruthenocene–substituted derivatives is irreversible. In this study there were two oxidation peaks at 740 mV and 910 mV for the compound dodecyl-dimethyl(methylruthenocenyl)-ammonium bromide in a 1.0 M aqueous NaCl solution.[63]

Sati and co-workers found irreversible electrochemistry for binuclear ruthenocene compounds.[64] Their study showed two oxidation potentials for the compound 1,4-bis(ruthenocenyl)benzene, 0.42 V and 0.56 V respectively, versus the

ferrocene/ferrocenium couple with the reduction peak at 0.28 V. This binuclear compound's CV is shown in figure 2.12.

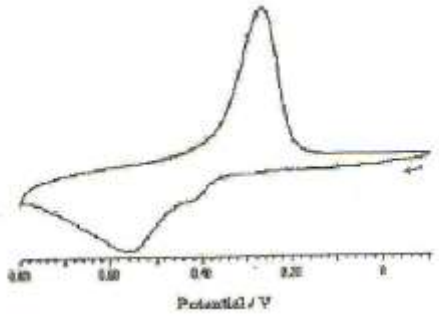

Figure 2.12. Irreversible electrochemistry of 1,4-bis(ruthenocenyl)benzene in dichloromethane utilising a glassy carbon electrode. Scan rate 0.1 V s^{-1} and supporting electrolyte $TBAClO_4$. Figure taken from: *J. Organomet. Chem*., 23, **655** (2002).

2.4.3.3. Osmocene

Gubin and co-workers found that at a dropping mercury electrode (DME), the oxidation of the osmocene proceeds reversibly as a one-electron process. At the Pt electrode the oxidation of the osmocene is irreversible and occurs in two consecutive one-electron steps, while the potentiometric oxidation is a reversible two-electron process.[65]

During a study of the reactivity of 17- and 19-electron organometallic complexes by Kukharenko and co-workers, the redox behaviour of various indenyl sandwich complexes was studied by means of cyclic voltammetry at a Pt-electrode at –85-20 ^{0}C in THF, CH_3CN and DCM.[66]

The complex $(C_9H_7)_2$ Os at 20 ^{0}C in CH_2Cl_2 exhibited two anodic one-electron diffusion-controlled peaks on the CV, while in THF there was a reversible two-electron oxidation and in CH_3CN an irreversible two-electron oxidation.

Oxidation-reduction potentials obtained by chronopotentiometric methods at a platinum electrode in a CH_3CN solution indicate a two step, one electron each oxidation by osmocene.[67] Kuwana and co-workers also found that electron-withdrawing substituents decrease the ease of oxidation, while electron-donating substituents increase the ease of oxidation with respect to the parent metallocenes.

2.5. Acid dissociation constants

The acid dissociation constant is the equilibrium constant for the ionisation of a weak acid, as shown in Scheme 2.17.[68]

$$HA_{(aq)} + H_2O_{(l)} \overset{K_a}{\rightleftharpoons} H_3O^+_{(aq)} + A^-_{(aq)}$$

Scheme 2.17. Ionization of a weak acid.

From this reaction the equilibrium constant in Equation 2.6 can be derived.

$$K_c = \frac{[H_3O^+][A:^-]}{[HA][H_2O]}$$

Equation 2.6.

When rewritten, this gives Equation 2.7.

$$K_a = K_c\,[H_2O] = \frac{[H_3O^+][A:^-]}{[HA]}$$

Equation 2.7.

Note $pK_a = -\log K_a$.

The pK_a' for the β-diketones synthesized by Du Plessis[59] refers to the process shown in Scheme 2.18.

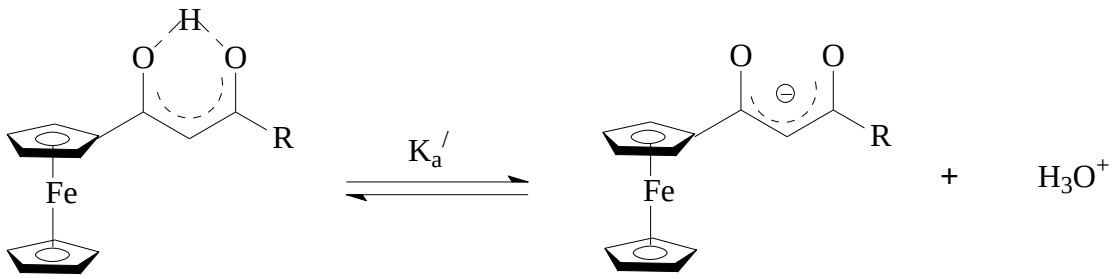

Scheme 2.18. A schematic definition of the acid dissociation constant equilibrium for metallocene-containing β-diketones.

The authors preferred the symbol pK_a' over pK_a, since there was no attempt to partition between the separate pK_a values for the enol and keto tautomers.

Values for pK_a can be determined through two methods. The conductomeric method involves conductometric measurements of dilute solutions to obtain a value for the equivalent conductance as well as the limiting conductance. From these data it is possible to determine the pK_a for very weak acids.

This method was adapted by Fuoss and Kraus to determine the acid dissociation constants due to low pH values.[69,70]

In their study, they applied Equation 2.8:

$$Ka = \frac{\Lambda_c}{\Lambda_o} = \frac{\alpha^2 c}{1-\alpha}$$

Equation 2.8. Λ_c = equivalent conductance, α = degree of ionization, Λ_o = limiting conductance.

From this equation, pK_a was obtained after refinement by applying the activity coefficient corrections.

Ballinger and Long used the conductometric method to determine the pK_a values for substituted methanols.[71] Values obtained varied from pK_a = 15.5 for propan-1-ol and an extrapolated value of pK_a = 15.9 for ethanol.

The second method involves the spectroscopic monitoring of an acid-base titration, also known as the absorbance method. Du Plessis and co-workers adapted this method in their study of ferrocene β-diketones.[59]

The $pK_a^{/}$ values were obtained by means of Equation 2.9,

$$A_T = \frac{A_{HA}10^{-pH} + A_A10^{-pKa^{/}}}{10^{-pH} + 10^{-pK_a^{/}}}$$

Equation 2.9.

which, together with the pH data, was inserted in the fitting program MINSQ.[58]

During the course of this study the author made exclusive use of the spectroscopic method for determining the pK_a's of a series of new osmocene-containing β-diketones.

2.6. Electronegativities[72,73]

Electronegativities (χ) are an empirical measure of the tendency of an atom in a molecule to attract electrons. Observed atomic electronegativities vary with the oxidation state of the atom, the number of outer lying energy levels, the atom bonded to the atom of which the electronegativity is to be determined, bond distance between the atoms and various other factors. The numerical values that have been assigned are only useful as a semi-quantitative notion. There are a number of different scales for expressing χ, including the Pauling, Allred and Rochow , Allen, as well as the Gordy scale for electronegativity.[73]

Pauling makes use of "excess" covalent bond energies to determine differences in electronegativity between atoms. Fluorine has the largest electronegativity, χ_F =3.98. Allred and Rochow utilised the fact that atoms will attract electron density in a chemical bond according to Coulomb's law in their determination of χ. Allen related the one - electron ionisation enthalpies of all p and s electrons in the valence shell of an atom to the atomic electronegativity.

Central to this study, however, are electronegativity values measured on the Gordy scale. The method of calculating χ according to the Gordy scale suggests that χ values for atoms on the Gordy scale may be related to the number of valence electrons *n* and the covalent radius *r* (in Å). Equation 2.10 is used in this determination:

$$\chi_G = 0.31\frac{(n+1)}{r} + 0.50$$

Equation 2.10.

This arises from the interpretation of χ as the potential due to the *effective* nuclear charge Z^*, at the covalent boundary by employing Equation 2.11.

$$Z^* = n - 0.50(n-1) = 0.5(n+1)$$

Equation 2.11.

This equation can only be applied if all electrons in closed shells below the valence shell exert a full screening effect, while the screening constant for one valence electron on another is 0.5. Values obtained for χ *via* the Gordy method are shown in comparison with the other methods in Table 2.4.

Table 2.4. Comparison of the atomic electronegativity values, χ, determined by the Pauling (χ_p), Allred and Rochow (χ_{A+R}), Allen (χ_{spec}) and Gordy (χ_G) methods.

Atom	χ_p	χ_{A+R}	χ_{spec}	χ_G
H	2.20	2.20	2.30	2.17
Li	0.98	0.97	0.91	0.96
Na	0.93	1.01	0.87	0.90
F	3.98	4.10	4.19	3.94
Cl	3.16	2.83	2.87	3.00
Br	2.96	2.74	2.69	2.68

The concept of atomic electronegativities can also be extended to include group electronegativities, χ_R. The rationale is that the group also has an influence on the shared electron pair in any covalent bond between two atoms. It is clear that the trifluoromethyl group in $-H_2C^1-C^2F_3$ will result in the covalent bonding electrons between C^1 and C^2 being closer to C^2. In the case of $-H_2C^1-C^2-(CH_3)_3$, the *tert*-butyl group will lead to the bonding electrons being closer to C^1 than to C^2.

A linear or near-linear dependence was found between χ_R and a variety of physical quantities such as pK_a, formal reduction potential, E^{o1}, and IR carbonyl stretching frequencies. Thus by utilizing data for a group of methyl esters the group electronegativity of the ferrocenyl group χ_{Fc} could be determined.[59]

This was achieved by plotting known IR ester carbonyl stretching frequencies versus known χ_R. χ_{Fc} was obtained by extrapolating this plot.

Chapter 2
Literature survey

2.7. Kinetics

In this study the kinetics of the isomerization of osmocene-containing β-diketones was studied as well as the substitution kinetics relating to β-diketonato substitution in [Rh(β-diketonato)(cod)] complexes with 1,10-phenanthroline.

2.7.1. Isomerization kinetics

All β-diketones exist in principle as a mixture of keto and enol forms as shown in Scheme 2.19.

Du Plessis and co-workers found that although two enol isomers for $FcCOCH_2COR$ are possible, the dominant enol-isomer in solution had the OH-group on the carbon furthest from the ferrocenyl moiety.[59] This equilibrium is shown in Scheme 2.19.

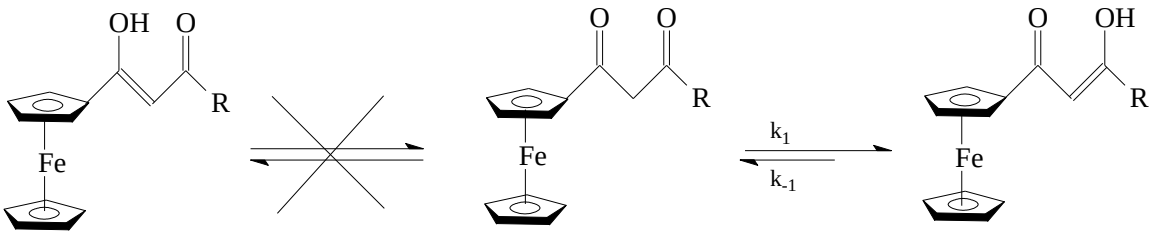

enol isomer A keto isomer enol isomer B

Scheme 2.19. The keto-enol tautomerizations studied by Du Plessis (R= CF_3, CCl_3, CH_3, C_6H_5 and ferrocenyl).

The rate of conversion between the keto isomer and enol isomer B was studied using ^1H NMR spectroscopy. The rate law applicable for the formation of keto isomer is

$$-\frac{d}{dt}[\text{enol isomer}] = (k_1 + k_{-1})[\text{enol isomer}] = k_{obs}[\text{enol isomer}]$$

Equation 2.12.

with k_{obs} the kinetic measurable quantity. To determine K_c, the equilibrium percentage of keto isomer present in solution was first determined by comparing the relative intensities of the appropriate enol/keto ^{1}H NMR signal pairs. Once the % keto isomer was known, the equilibrium constant (Equation 2.13) for equilibrium could be evaluated.

$$K_c = \frac{[\text{enol isomer}]}{[\text{keto isomer}]} = \frac{k_1}{k_{-1}} = \frac{\%\ \text{enol isomer at equilibrium}}{\%\ \text{keto isomer at equilibrium}}$$

Equation 2.13

This is indicated in Scheme 2.20.

$$\text{Fc-CO-CH}_2\text{-CO-R} \underset{k_{-1}}{\overset{k_1}{\rightleftharpoons}} \text{Fc- CO-CH=C(OH)-R}$$

Scheme 2.20. Representation of the forward and backward rate constants.

The equilibrium constant was independent of the β-diketone concentration, but by increasing the temperature from 20 ^{0}C to 60 ^{0}C the percentage keto isomer increased for R = ferrocene, CH_3, C_6H_5 and CCl_3 while decreasing for R = CF_3. It is important to note that after leaving the β-diketone in the solid state for two months, the enol form B (scheme 2.19) is the only observed isomer.

Solvents can also affect the keto-enol equilibrium.[74] Blokzijl and co-workers found that by increasing the alcohol in the alcohol:water ratio the enol isomer of pentane-2,4-dione was favoured.

In the work of Cravero[27] the tautomeric equilibrium between the two enol isomers of para-substituted benzoylacetones was studied with the use of ^{13}C NMR. It was found that with electron-withdrawing para-groups the equilibrium shifts towards the keto form. This equilibrium is shown in Scheme 2.21.

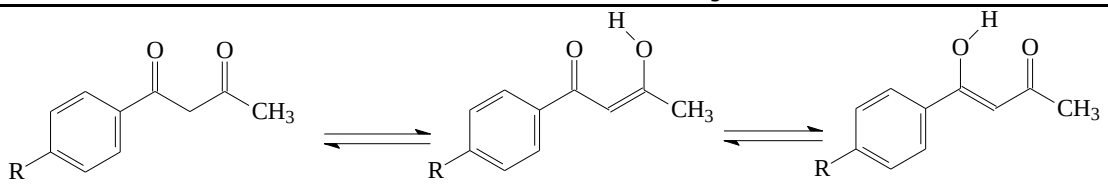

Scheme 2.21. Types of keto-enol equilibria studied by Cravero.

2.7.2. Substitution kinetics

2.7.2.1. Introduction

Kinetics is the study of reaction rates and how these rates change under a variety of conditions. Substitution reactions or ligand exchange are usually divided into three main groups: nucleophilic substitution, electrophilic substitution and oxidative addition followed by reductive elimination.[75] These substitution reactions involve the interaction between 18-electron and 16-electron species.

2.7.2.2. Mechanism of substitution reactions

The two main mechanisms of ligand substitution that can be identified are (A) the dissociative mechanism and (B) the associative mechanism.

(A) The dissociative mechanism

The dissociative mechanism resembles S_N1 substitution in organic chemistry. Firstly the leaving monodentate ligand X in $[L_nM\text{-}X]$ dissociates from the coordination sphere of the metal, thus reducing the number of monodentate ligands bonded to the central metal atom. Secondly, the incoming ligand, Y reacts with the transition state $[L_nM]$, to form the final product $[L_nM\text{-}Y]$. The intermediate transition state, $[L_nM]$, is coordinatively unsaturated and very reactive. Scheme 2.22 illustrates this mechanism.

Slow step: $[L_nM\text{-}X] \xrightarrow{k,\ slow} [L_nM] + X$

Fast step: $[L_nM] + Y \xrightarrow{fast} [L_nM\text{-}Y]$

Scheme 2.22.

The kinetic rate law for the dissociative mechanism of substitution takes the form of equation 2.14:

$$Rate = k[L_nM\text{-}X]$$

Equation 2.14.

A feature of this rate law is that the rate of the reaction is independent of the concentration of the incoming ligand, Y. This means that the reaction is zero order in Y.

The entropy of activation, ΔS^*, is positive because the transition state is less ordered than the starting materials. In a dissociative substitution mechanism, the stereochemistry may be retained or racemization may take place. Racemization depends on the rate at which the incoming ligand traps the intermediate.[76]

(B) The associative mechanism

The associative mechanism for ligand substitution in metals resembles S_N2 substitution in organic chemistry. The incoming ligand Y, initially binds to the metal centre in $[L_nM\text{-}X]$, leading to an intermediate with an increased coordination number, $[L_nMX\text{-}Y]$. The intermediate subsequently undergoes a further reaction, where the leaving group, X, detaches to give the substituted product $[L_nMY]$. This mechanism is illustrated in Scheme 2.23.

Slow step: $[L_nMX] + Y \xrightarrow{k,\ slow} [L_nMX\text{-}Y]$

Fast step: $[L_nMX\text{-}Y] \xrightarrow{fast} [L_nM\text{-}Y] + X$

Scheme 2.23.

A different kinetic rate law applies for this mechanism, Equation 2.15, compared with the rate law for the dissociative mechanism:

$$Rate = k[L_nMX][Y]$$

Equation 2.15.

From this rate law it can be seen that ligand substitution occurring through an associative mechanism in first order with respect to the incoming ligand, Y [77].

The entropy of activation, ΔS^*, is negative, which implies that the transition state is more ordered than the starting materials. Electron-deficient complexes (e.g. 16 or 17 valence electron compounds) favour the associative mechanism, but some 18 electron compounds also follow the associative mechanism.[76] The associative mechanism often involves solvolysis (Scheme 2.24), especially if the solvent is polar or has a tendency to solvate. If solvolysis takes place the kinetic rate law describing an associative mechanism changes to (Equation 2.16):

$$Rate = (k_s + k_2[Y])[L_nM\text{-}X] = k_{obs}[L_nM\text{-}X]$$

Equation 2.16.

In

$$k_{obs} = k_s + k_2[Y]$$

Equation 2.17.

k_s = rate constant of solvent pathway and k_2 = rate constant of the direct pathway.

Chapter 2
Literature survey

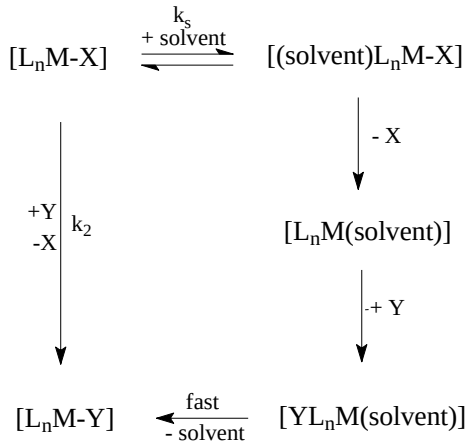

Scheme 2.24. Schematic representation of the direct and solvent pathway for the associative mechanism.

An example of the above can be found in a study by Vosloo and co-workers[77].

These authors conducted studies on ferrocene-containing β-diketonato complexes of the type [Rh(FcCOCHCOR)(cod)] with R = CF_3, CCl_3, CH_3, C_6H_5 and Fc = ferrocenyl, where the β-diketonato ligand is replaced by 1,10-phenanthroline. They found that an associative substitution mechanism, in addition a solvent pathway mechanism was followed that was most pronounced for the $FcCOCH_2COC_6H_5$ complex.[77] The plots of rate constants versus 1,10-phenanthroline concentrations can be seen in Figure 2.13. An associative mechanism was assigned, due to the large negative activation energies.

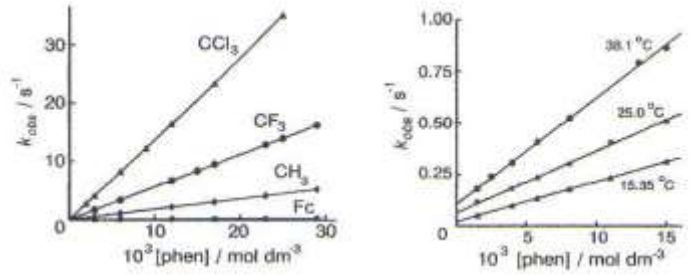

Figure 2.13. Plots of the pseudo first-order rate constants versus [phenanthroline] for the non-solvent pathway (left) and solvent pathway (right for R = C_6H_5) for the β-diketonato substitution from [Rh(FcCOCHCOR)(cod)] with 1,10-phenanthroline, R = CCl_3, CF_3, CH_3, Fc or C_6H_5. Figure taken from *Inorg. Chim. Acta*., 188, **331** (2002).

From Equation 2.17 it follows that the y-intercept give k_s and the slope of the above graphs give the second order rate constant k_2.

2.7.2.3. Factors influencing substitution reaction rates[78]

Factors that may influence the rate of substitution involve the type and nature of all the relevant ligands (entering, leaving and remaining), the central metal atom and the solvent.

(A) Effect of the entering ligand

As expected for an associative mechanism, the entering ligand has a first order influence on the rate of the reaction. The nucleophilicity of the incoming ligand is one of the most important factors influencing the reaction rate. Nucleophilicity is a measure of the ability of an incoming ligand to attack the positive metal centre or the ability to supply the electrons needed for the reaction to proceed. The ability of an incoming ligand to induce bond making and breaking processes thus determines the rate of a substitution reaction. A strong nucleophile will attack the metal centre of a complex more readily than a weaker one, thus forming a more stable bond with the central metal atom. Consequently, the reaction rate will increase with increasing strength of the incoming ligand nucleophilicity.

This has been confirmed by the rate constants obtained for the substitution of Cl^- with a large variety of ligands from *trans*-$[Pt(py)_2(Cl)_2]$ (Scheme 2.25 and Table 2.5).[79,80] These rate constants have been fitted to the Swain-Scott equation (Equation 2.18) and are used to set up a scale of nucleophilic power for ligand substitution.

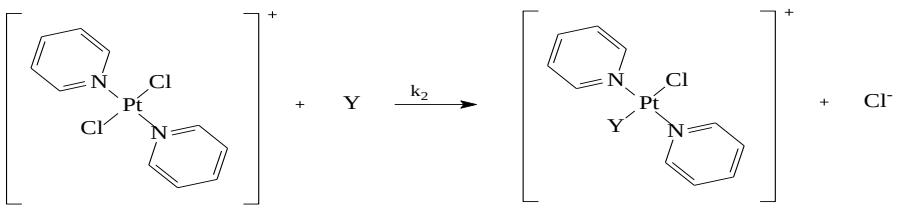

Scheme 2.25. Substitution of Cl^- by a large variety of ligands (Y) from *trans*-$[Pt(py)_2(Cl)_2]$.

Table 2.5. Second order rate constants (k_2) of the substitution reaction of *trans*-$[Pt(py)_2(Cl)_2]$ with a number of nucleophiles in CH_3OH.

Nucleophile	10^3 k_2 / dm^3 mol^{-1} s^{-1}	n_{Pt}	pK_a^*
CH_3OH	1×10^{-5}	0.0	-1.7
NH_3	0.47	3.07	9.25
I^-	107	5.46	-10.7
PPh_3	249000	8.93	2.73

pK_a^* values in water [79,80]

$$\log k_2 = s n_{Pt} + \log k_s$$

Equation 2.18.

In Equation 2.18 k_2 = second order rate constant of the substitution reaction of the nucleophile, k_s = rate constant for solvation reaction, *s* = nucleophilic discrimination factor (measure of the sensitivity of the substrate) and n_{Pt} = nucleophilic reactivity constant. The terms *s* and k_s depend only on the Pt complex and not the incoming ligand. The n_{Pt} value can be used to correlate kinetic data for Pt(II) complexes. Values of n_M and *s* can be used to predict reaction rates.

Basicity is a thermodynamic term defined by the pK_a of the conjugated acid of the Lewis base (a nucleophile), and differs significantly from nucleophilicity, which is a kinetic term. There is also no correlation between the pK_a and nucleophilicity of an incoming ligand. The basicity of the incoming ligand (in contrast to the nucleophilicity) has a rather limited effect on the rate of associative substitution reactions. This can be seen from the substitution reaction rates of [Rh(acac)(cod)] with derivatives of 1,10-phenanthroline and 2,2'-dipyridyl (Scheme 2.26 and Table 2.6).[81]

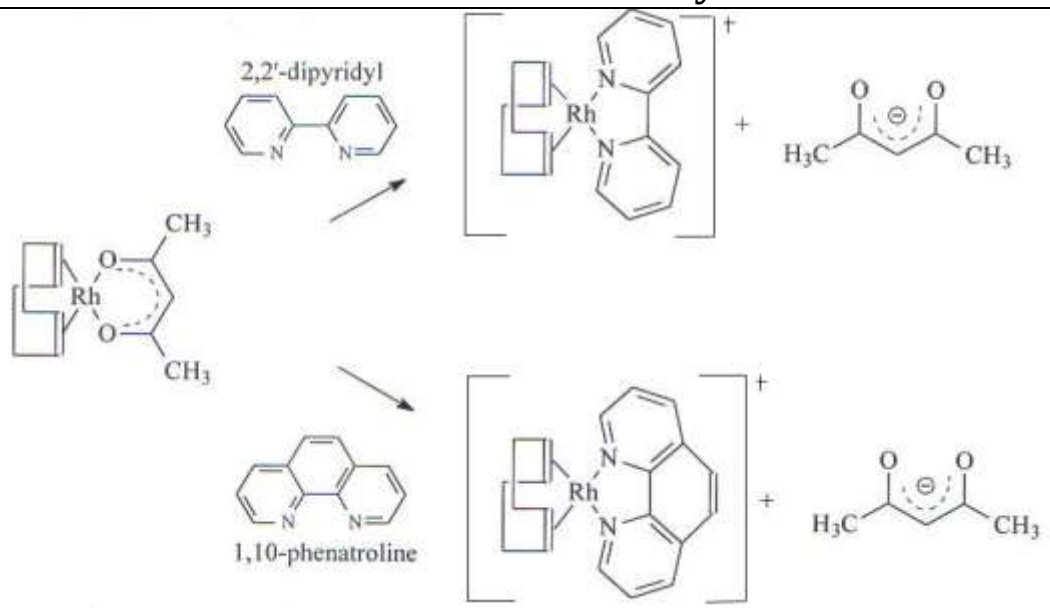

Scheme 2.26. Substitution reactions of β-diketonato ligand by various derivatives of 1,10-phenanthroline and 2,2'-dipyridyl from [Rh(acac)(cod)].

Table 2.6. Second order rate constants (k_2) and activation parameters for the substitution of β-diketonato ligand by various derivatives of 1,10-phenanthroline and 2,2'-dipyridyl from [Rh(acac)(cod)] in CH_3OH.

Incoming ligand	$pK_a^{\#}$	$k_2/dm^3\ mol^{-1}s^{-1}$	$\Delta H^*/\ JK^{-1}\ mol^{-1}$	$\Delta S^*/JK^{-1}mol^{-1}$
5-nitro-phenanthroline	3.57	12.40	30.80	-121
1,10-phenanthroline	4.96	29.00	32.60	-108
5,6-dimethyl-phenanthroline	5.20	19.90	38.70	-90
4,7-dimethyl-phenanthroline	5.97	18.80	36.70	-97
3,4,7,8-tetramethyl-phenanthroline	6.31	19.60	40.70	-84
2,2'-dipyridyl	4.30	12.4	36.80	-112

$^{\#}pK_a$ values in water.[83]

(B) Effect of the leaving group

In contrast to the incoming ligand, the second order rate constant (k_2) of the substitution reaction, shown in Scheme 2.26, is influenced by the basicity (pK_a) of the leaving group,

provided that pK_a < 10. When the pK_a > 11, the substitution reaction was almost independent of β-diketonato pK_a. This is shown in Figure 2.14.[82]

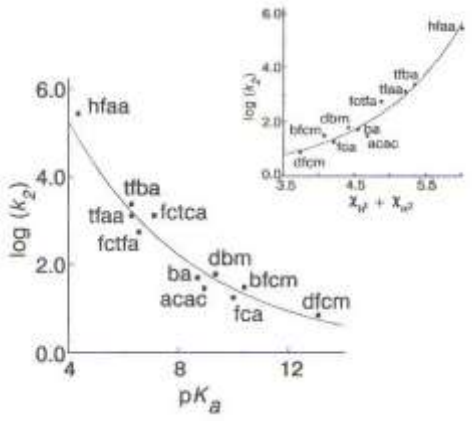

Figure 2.14. Plot of log k_2 versus acid dissociation constant values for the free β-diketones for the substitution of RCOCHCOR′ in complexes of the type [Rh(RCOCHCOR′] with 1,10-phenanthroline. Insert: plot of log k_2 versus accumulative electronegativities of R groups on β-diketone.

As the basicity of the leaving group decreases the second order rate constant of substitution increases.

This is illustrated by the substitution of the β-diketonato ligands from [Rh(β-diketonato)(cod) with 1,10-phenanthroline (Scheme 2.24 and Table 2.7).

Table 2.7. Second order rate constants (k_2) and activation parameters for the reaction between [Rh(β-diketonato)(cod)] and 1,10-phenanthroline in CH_3OH.

β-diketonato	pK_a[#]	k_2/dm^3 mol^{-1} s^{-1}	ΔH^*/ JK^{-1} mol^{-1}	ΔS^*/ JK^{-1} mol^{-1}
$CH_3COCHCOCH_3$	8.95	29.0	32.6	-108
$CH_3COCHCOPh$	8.70	51.2	31.6	-106
PhCOCHCOPh	9.35	61.4	27.3	-119
$CH_3COCHCOCF_3$	6.30	1330	30.5	-83
$PhOCHCOCF_3$	6.30	2420	26.2	-93
$CF_3COCHCOCF_3$	4.35	276000	23.2	-63

[#]pK_a values in water.[81,84]

The effect of the leaving group is often related to the strength of the M-X bond (metal-ligand bond, where X = the atom in the leaving ligand bound to the metal). A stronger M-X bond makes it more difficult for X to be substituted by another ligand, resulting in a decrease in the substitution rate. The opposite applies to a weaker M-X bond.

However, to explain this, the insert of Figure 2.14 is very instructive. Group electronegativities constitute the key property that is involved. It turns out that as χ_R for each R group in the β-diketonato ligands $(RCOCHCOR)^-$ decreases (meaning the R groups become more electron-donating), the ligand becomes more electron-rich. Due to this phenomenon a stronger interaction with the positively charged Rh cation is allowed. Hence the Rh-O bond must get shorter and stronger, thus the decrease in the rate of substitution.

From a study by Vosloo and co-workers,[77] it was shown that the rate-determining step is the breaking of Rh-O bonds rather than the formation of Rh-N bonds when β-diketonato ligands are substituted by 1,10-phenanthroline from complexes of the type [Rh(β-diketonato)(cod)].

(C) Effect of the remaining ligand

The remaining ligands in the coordination sphere of the metal, *cis* and *trans* to the leaving group also play an important part in the rate of substitution. The *trans*-influence is a thermodynamic property, which can be defined as the influence a fixed ligand has on the metal-ligand bond *trans* to it. In particular it influences the crystallographic bond length *trans* to it. The *trans*-effect is a kinetic property, which is defined as the effect a fixed ligand has on the rate of substitution of a ligand *trans* to it.[85]

The kinetic *cis*-effect of a coordinated ligand is defined very similarly to the *trans*-effect, except that it is the effect a fixed ligand has on the rate of substitution for another ligand *cis* to it. The influence of the two groups *cis* to the leaving group is far less pronounced than that found for the group *trans* to the leaving group.

Chapter 2
Literature survey

The similarity between the *cis*- and *trans*-effects stems from the direct communication between *cis*-ligands *via* the metal p_y and d_{x2-y2} orbitals. In cases where a relatively poor nucleophile acts as the entering group, the relative ability of ligands to act as *trans* labilizers is the same as their ability to act as *cis* labilizers. (Shown in Scheme 2.27)

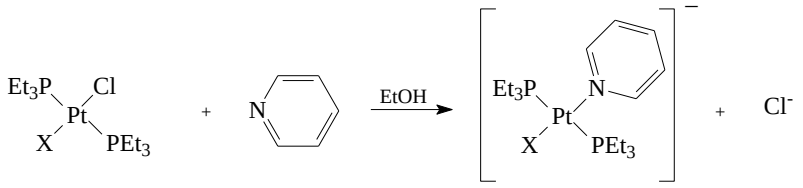

(A) [largest *trans*-effect] X = H^- (>10000) > CH_3^- (>170) > $C_6H_5^-$ (40) > Cl^-(1) [smallest *trans*-effect]

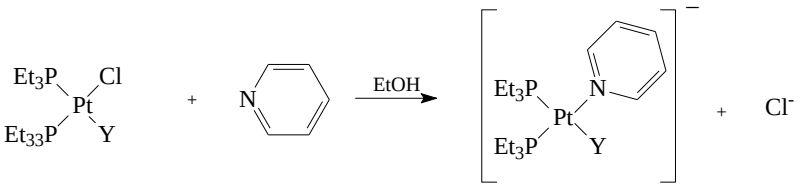

(B) [largest *cis*- effect] Y = CH_3^- (3.6) > $C_6H_5^-$ (2.3) > Cl^- (1) [smallest *cis*-effect]

Scheme 2.27. (A) Illustration of the *trans*-effect by measuring the kinetic substitution rate of Cl^- with pyridine. X = ligand exerting the *trans*-effect. Rate constants, expressed as the ratio k(X)/k(Cl), are given in brackets after each X. (B) Illustration of the *cis*-effect by measuring the kinetic substitution rate of Cl^- with pyridine. Y = ligand exerting the *cis*-effect. Rate constants, expressed as the ratio k(Y)/k(Cl), are given in brackets after each Y.

From molecular orbital calculations it has been shown that ligands that weaken bonds *trans* to themselves also weaken bonds *cis* to them, but not too much.[86] In the transition state, bond breaking becomes somewhat easier for good *cis*-directors and the reaction rate increases, but not quite as much as it would have if the *cis* ligand was in the *trans* position.

The steric hindrance of bulky ligands coordinated to the metal centre also influences the rate of substitution. In sterically crowded complexes, bulky ligands shield the metal centre, thereby blocking the attack of the incoming ligand. An example of this is the hydrolysis of *cis*-[Pt(Cl)L(PEt_3)$_2$] where Cl^- is replaced,[87] and there is a decrease in reaction rate the more bulky the ligand becomes. Shriver and co-workers indicated that

increasing the steric hindrance of ligands coordinated to a metal complex progressively retards the substitution rate of the incoming ligand.

Also, *cis* hindrance is more effective than *trans* hindrance. In [PtCl(2,6-dimethylpyridine)(PEt_3)$_2$] the *ortho*-CH_3 of 2,6-dimethylpyridine block the positions above and below the plane of the complex, causing steric hindrance for the position *cis* to it. Figure 2.15 shows the structures of *cis*-and *trans*-[PtCl(2,6-dimethylpyridine)(PEt_3)$_2$].

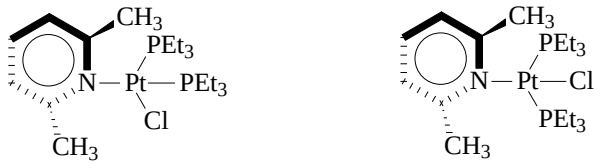

Figure 2.15. Structure of *cis*-and *trans*-[PtCl(2,6-dimethylpyridine)(PEt_3)$_2$].

(D) Effect of the central metal atom

The dependence of the rate of substitution on the central metal is based on the ability of the metal (with coordination sphere of four) to form a five-coordinated transition state in an associative mechanism and the metal's ability to form a three-coordinated transition state in a dissociative mechanism.

The relative rate of substitution decreases from top to bottom in a given group of transition metals in the periodic table as well as going from right to left in a given row of the transition metals of the periodic table.[88]

(E) Effect of the solvent

The influence of the solvent lies in its ability to solvate the metal. This influences the energetics of the activation process from the ground and in activated states. It can also act

as a nucleophile in the reaction (Scheme 2.24), to change the kinetic rate law to (Equation 2.19):

$$Rate = (k_s + k_2[Y])[complex]$$

Equation 2.19.

Here k_s is the rate constant of the solvent pathway. A large k_s is observed for solvents that have a good ability to donate electrons to the metal and coordinates strongly to the metal. The general order of stronger solvation power by solvents is:

$$(CH_3)_2SO > CH_3NO_2, H_2O > ROH$$

Solvents like benzene and chloroform, which coordination very poorly to metals, have little or no influence on the reaction rate, as $0 \approx k_s << k_2$.

2.7.2.4. Activation parameters

The rates of chemical reactions increase with temperature. The Arrhenius equation describes the dependence of the rate constant on temperature (Equation 2.20):[89]

$$k = Ae^{(-E_a/RT)}$$

Equation 2.20.

The higher the activation energy, E_a, the slower the reaction at any given temperature.

More important activation parameters include ΔH^*, ΔS^*, ΔG^* and ΔV^*. The signs and magnitudes of these thermodynamic parameters also often indicate the mechanism of a reaction. The transition state theory postulates that an activated transition state complex is in equilibrium with reagents before the reaction takes place and that the reaction rate is given by the rate of decomposition of the activated complex to form the products (Scheme 2.28).

The rate constant for the overall reaction is given by Equation 2.21.

$$A + B \underset{}{\overset{K_c^*}{\rightleftharpoons}} [A\cdot B]^* \xrightarrow{k} \text{products}$$

Scheme 2.28.

$$k = (RT/Nh)K_c^*$$

Equation 2.21.

Here K_c^* = equilibrium constant, R = universal gas constant, h = Planck's constant, N = Avogadro's constant and T = absolute temperature.

The information of this activated complex is governed by thermodynamic considerations similar to those of ordinary chemical equilibria. The Gibbs energy of activation is thus defined thermodynamically as shown in Equation 2.22.

$$\Delta G^* = -RT \ln K_c^*$$
$$= \Delta H^* - T\Delta S^*$$

Equation 2.22.

A combination of Equations 2.21 and 2.22 gives Equation 2.23.

$$\ln k = \ln\left[\frac{(RT)}{(Nh)}\right] + \frac{\Delta S^*}{R} - \frac{\Delta H^*}{RT}$$

or

$$\ln \frac{k_2}{T} = -\frac{\Delta H^*}{RT} + \frac{\Delta S^*}{R} + \ln \frac{R}{Nh}$$

Equation 2.23.

The magnitude of ΔS^* can be used to determine whether the mechanism of substitution is associative or dissociative in nature. A distinctly positive ΔS^* value indicates a

dissociative mechanism and a large negative ΔS* value indicates an associative mechanism of substitution.

The volume of activation, ΔV*, relating to Scheme 2.28 consists of two parts, an intrinsic part, $\Delta V^*_{intr,}$ and a solvation part ΔV^*_{solv}, and is defined in Equation 2.24.

$$\Delta V^* = \Delta V^*_{intr} + \Delta V^*_{solv}$$

Equation 2.24.

The volume changes that arise during the formation of the transition state due to the variations in bond lengths and angles are represented by ΔV^*_{intr}, while the change in solvation is reflected by ΔV^*_{solv}. For a dissociative mechanism ΔV^*_{intr} is positive due to bond cleavage and ΔV^*_{solv} is negative due to electrostriction, thus ΔV* is approximately zero for a dissociative mechanism.[90] For an associative mechanism ΔV* is much more negative, due to the contribution from a negative ΔV^*_{intr} value, which arises from the bond formation and only a minor contribution from ΔV^*_{solv}. Hence, a dissociative mechanism is indicated by ΔS* (measured in JK^{-1} mol^{-1}) and ΔV* values, whereas large negative ΔS* and ΔV* values indicate an associative mechanism.

Leipoldt and co-workers studied the substitution of carbonyl ligands in β-diketonatocarbonylrhodium(I) complexes by cyclooctadiene.[82,84,91] (Scheme 2.29)

$$[Rh(\beta\text{-diketonato})(CO)_2] + cod \xrightarrow{k_2} [Rh(\beta\text{-diketonato})(cod)] + 2CO$$

Scheme 2.29.

The Beer-Lambert law applied to UV/Vis spectroscopy (Equation 2.25) was found to be valid for all complexes in the concentration range utilised for this kinetic study.

$$A = \varepsilon C l$$

Equation 2.25. A = UV/Vis absorbance, ε = molar absorptivity, C = concentration and *l* = path length, normally 1 cm.

The experimentally determined rate law from this study is depicted in Equation 2.26:

$$\frac{d[Rh(\beta\text{-diketonato})(cod)]}{dt} = (k_s + k_2[cod])[Rh(\beta\text{-diketonato})(CO)_2] = k_{obs}[Rh(\beta\text{-diketonato})(CO_2)]$$

Equation 2.26.

In equation 2.25, k_s is a rate constant describing solvent participation and

$$k_{obs} = k_s + k_2[cod]$$

Equation 2.27.

Activation parameters ΔH* and ΔS* for the study were obtained from a fit of k_2/T against 1/T (in Kelvin) according to the Equation 2.28.

$$\ln \frac{k_2}{T} = -\frac{\Delta H^*}{RT} + \frac{\Delta S^*}{R} + \ln \frac{R}{Nh}$$

Equation 2.28. k_2 = the experimentally determined second order rate constant, ΔH* = the activation enthalpy, ΔS* = activation entropy, R = universal gas constant, h = Planck's constant, N = Avogadro's constant and T = absolute temperature.

The slope of the graph of $\ln (^{k2}/_{T})$ *vs*.$(^{1}/_{T})$ gives a slope of $-(^{\Delta H^*}/_{R})$ and ΔS* can be determined from the intercept with the y-axis = $(^{\Delta S^*}/_{R}) + \ln (^{R}/_{Nh})$. From the large negative ΔS* values obtained it was concluded that the reaction shown in Scheme 2.29 occurs *via* an associative mechanism. A high-pressure study on the same reaction yielded large negative ΔV* values, which also included an associative mechanism.

Activation parameters may therefore be used to provide more insight on reaction mechanism, especially where substitution reactions are concerned.

References:

[1] M.A. Bennett, M.I. Bruce and T.W. Matheson, G. Wilkinson, Editor, *Comprehensive Organometalic Chemistry*, Pergamon Press, Oxford, pp. 759-776, vol. **4**, (1982).

[2] M.O. Albers, D.J. Robinson and E. Singleton, *Coord. Chem. Rev*., 1, **79** (1987).

[3] R.D. Adams and J.P. Selegue, G. Wilkinson, Editor, *Comprehensive Organometalic Chemistry*, Pergamon Press, Oxford, pp. 1019-1020, vol. **4** (1982).

[4] E.O. Fischer, H. Grubert, *Chem. Ber*., 2302, **92** (1959).

[5] M.O. Albers, D.C. Liles, D.J. Robinson, A. Shaver, E. Singleton and M.B. Wiege, *J. Organomet. Chem.*, 2321, **5** (1986).

[6] N.J. Long, *Metallocene: An introduction to sandwich complexes*, Blackwell Science, London, pp. 60-61, (1998).

[7] N.J. Long, *Metallocene: An introduction to sandwich complexes*, Blackwell Science, London, pp. 129-132, (1998).

[8] M.D. Rausch, E.O. Fischer and H. Grubert, *J. Am. Chem. Soc*., 76, **82** (1960).

[9] M.D. Rausch, D.W. Macomber and W.P. Hart, *J. Am. Chem. Soc*., 1198, **102** (1980).

[10] R.B. Woodward, M. Rosenblum and M.C. Whiting, *J. Am. Chem. Soc*., 3458, **74** (1952).

[11] M.D. Rausch and V. Mark, *J. Org. Chem. Soc*., 3225, **28** (1965).

[12] F.G.A. Stone and E. Abel, G. Wilkinson, Editor *Comprehensive Organometalic Chemistr.,* Pergamon Press, pp.1018-1019,vol. **4** (1982).

[13] J.M. Birmingham, *Adv. Organomet. Chem*., 365, **2** (1964).

[14] A.A. Koridze and A.A. Lubovich, *Bull. Acad. Sci. USSR, Div. Chem. Sci.(Engl. Transl.)*., 1586, **21** (1972).

[15] P.J. Lindsay, R.V. Parshall, G.W. Peterson and M.L. Whitman, *J.Am. Chem. Soc*., 3416, **79** (1957).

[16] E.A. Hill and H. Richards, *J. Am. Chem. Soc*., 3840, **83** (1961).

[17] G. Schmitt and S. Ozman, *J. Org. Chem*., 3331, **41** (1976).

[18] R.A. Benkeser, D. Goggin and G. Schroll, *J. Am. Chem. Soc*., 4025, **76** (1954).

[19] J. McMurry, *Organic Chemistry*, John Wiley & Sons, New York, pp. 28-31, **5th** ed(1999).

[20] A.J, Pearson, *Metallo-Organic Chemistry*, John Wiley & Sons, New York, pp. 310-322, (1985).

[21] F.G. Stone and E. Abel, G. Wilkinson, Editor *Comprehensive Organometalic Chemistr.,* Pergamon Press, pp.771-773 ,vol. **4** (1982).

[22] O. Hofer and K. Schloegel, *J. Organomet. Chem*., 443, **13** (1968).

[23] J. McMurry, *Organic Chemistry*, John Wiley & Sons, New York, pp. 855-857, **5th** ed (1999).

[24] F.G.A. Stone and E. Abel, G. Wilkinson, Editor, *Comprehensive Organometalic Chemistry,*

Pergamon Press, pp.771-773, vol. **4** (1982).

[25] A.J. Pearson, *Metallo-Organic Chemistry*, John Wiley & Sons, New York, pp. 335-341, (1985).

[26] M. Roth, P. Dubs, E. Gotschi and A. Eschenmoser, *Helv. Chim. Acta*, 710, **54** (1971).

[27] R.M.Cravero, M. Gonzalez-Sierra and A.C. Oliveri, *J. Chem. Soc., Perkin Trans*., 1067, **2** (1993).

[28] M. Suzuki, A. Watanabe and R. Noyori, *J. Am. Chem. Soc*., 2095, **102** (1980).

[29] S. Umetani, Y. Kawase, O.T.H. Le and M. Matusi, *J. Chem. Soc., Dalton Trans*., 2787, (2000).

[30] A.I. Vogel, *Practical Organic Chemistry and Qualitative Organic analysis*, Longman, London, pp. 864-865, **3rd** ed(1977).

[31] C.R. Hauser and J.K. Lindsay, *J. Org. Chem*., 482, **22** (1957).

[32] V. Weinmayr, *Naturwissenchaften*., 311, **45** (1958).

[33] C. E. Cain, T.A. Mashburn, Jr. and C.R. Hauser, *J. Org. Chem*., 1030, **26** (1961).

[34] C.R. Hauser and C.E. Cain, *J. Org. Chem*., 1142, **23** (1958).

[35] B. Rosenberg, *Naturwissenchaften*, 399, **60** (1954).

[36] A. Furst, *The Chemistry of Chelation in Cancer*, JC Press, Springfield, pp768-772, **3rd** ed (1963).

[37] S. Adachi, T. Ogasawara, E. Wakimoto, Y. Tsuji, T. Takemura, K. Kayama, Y. Takayasu, J. Inoue and N. Nakao, *Cancer (N.Y.)*., 74, **91** (2001).

[38] J.W. Reishus and D.S. Martin jr., *J. Am. Chem. Soc*., 245, **83** (1961).

[39] J.H. Burchenal, K. Kalaher, T. O'Toole and J. Chrisholm, *Cancer Res*., 1238, **37** (1977).

[40] J.C. Swarts and C.J. van Rensburg, *Ferrocene compounds for cancer treatment*, patent no.: PCT/IBOI/02258, Dated 29 Jan. 2003.

[41] T. Tsurui, H. Iida, S. Tsukagoshi and Y. Sakuari, *Biochem. Pharm*., 213, **30** (1981).

[42] V. Conter and W.T. Beck, *Biochem. Pharm*., 723, **32** (1983).

[43] R. Herken and M. Wenzel, *Eur. J. Nucl. Med*., 56, **10** (1985).

[44] J. Shani, T. Livshitz and M.Wenzel, *Int. J. Nucl. Med. Bio*., 13, **12** (1985).

[45] J.C. Swarts, D.M. Swarts, M.D. Maree, E.W. Neuse, C. La Madeleine and J.E. van Lier, *Anticancer Res*., 1, **20** (2000).

[46] P.T. Kissinger and W.R. Heineman, *J. Chem. Educ*., 702, **60** (1983).

[47] D.H. Evans, K.M.O'Connell, R.A. Peterson and M.J. Kelly, *J. Chem Educ*., 290, **60** (1983).

[48] G.A. Mabbot, *J. Chem. Educ*., 697, **60** (1983).

[49] A.J. Bard and L.R. Faulkner, *Electrochemical Methods: Fundamentals and Applications*, Wiley and Sons, New York, pp. 215, (1980).

[50] P.A. Christen and A. Hammett, *Techniques and Mechanisms in Electrochemistry*, Blackie Academic & Professional, London, pp. 55-67, pp.170-175, (1994).

[51] H.M. Koepp, H. Wendt and H. Stehlow, *Z. Electrochem*., 483, **64** (1960).

[52] G. Gritzner and J. Kuta, *Pure Appl. Chem*., 461, **56** (1984).

[53] R.R. Gagne, C.A. Koval and G.C. Lisensky, *Inorg. Chem*., 2855, **19** (1980).

[54] J. Conradie, Ph.D. Study, University of the Orange Free State, R.S.A., (1999).

[55] C. La Vanda, P.O. Cowan, C. Leitch and K. Bechgaard, *J. Am. Chem. Soc*., 6788, **96** (1974).

[56] W.H. Morrison, Jr., S. Krogsrud and D.N. Hendrickson, *Inorg. Chem*., 1998, **12** (1973).

[57] G.M. Brown, T.J. Meyer, D.O. Cowan, C. LeVanda, F. Kaufman, P.V. Roling and M.D. Rausch, *Inorg. Chem*., 506, **14** (1975).

[58] W.C. du Plessis, J.J.C. Erasmus, G.J. Lamprecht, J. Conradie, T.S. Cameron, M.A.S. Aquino and J.C. Swarts, *Can. J. Chem*., 378, **77** (1999).

[59] W.C. du Plessis, T.G. Vosloo and J.C. Swarts, *J. Chem. Soc., Dalton Trans*., 2507, (1998).

[60] J.E. Gorton, H.L. Lentzner and W.E. Watts, *Tetrahedron*, 4353, **27** (1971).

[61] M.G. Hill, W.M. Lamanna and K.R. Mann, *Inorg. Chem*., 4687, **30** (1991).

[62] R.J. Gale and R. Job, *Inorg. Chem*., 42, **20** (1981).

[63] C. Jacob, A.Y. Sfronov, S. Wilson, H.A.O. Hill and T.F. Booth, *J. Electroanal. Chem*., 161, **427** (1997).

[64] M. Sati, G. Maruyama and A. Tanemura, *J. Organomet. Chem*., 23, **655** (2002).

[65] S.P. Gubin, S.A. Smirnova, L.L. Denisovich, A.A. Lubovich, *J. Organomet. Chem*., 243, **30** (1971).

[66] S.V. Kukharenko, V.V. Strelets, A.R. Kudinov, A.Z. Kreidin, M.G. Peterleitner, L.I. Denisovich and M.I. Rybinskaya, *J. Organomet. Chem*., 1, **519** (1996).

[67] T.Kuwana, D.E. Bublitz and G. Hoh, *Chem Ind.*, 635, (1959).

[68] A. Albert and E.P. Serjeant, *The Determination on Ionization Constants*, Chapman and Hall, London, pp. 70-101, **3rd** ed(1984).

[69] R.G. Mortimer, *Physical Chemistry*, The Benjamin Cummings Publishing company inc., pp. 910-913, (1993).

[70] B. Stevens, *Chemical Kinetics*, Chapman & Hall, London, pp.37-43, (1965).

[71] P. Ballinger and F.A. Long, *J. Am. Chem. Soc*., 795, **82** (1960).

[72] F.A. Cotton, G. Wilkinson and P.L. Gaus, *Basic Inorganic Chemistry*, Wiley and Sons Inc., pp. 63-67, **3rd** ed(1995).

[73] P.R. Wells, *Progress in Physical Organic Chemistry*, pp. 111-145, **6th** ed(1968).

[74] W. Blokzijil, J.B.F.N. Engberts and M.J. Blandamer, *J. Chem. Soc., Perkin Trans*., 455, **2** (1994).

[75] R.J. Cross, *Chem. Soc. Rev*., 197, **14** (1985).

[76] F. Mathey and A. Servin, *Molecular Chemistry of the Transition Elements*, Wiley and Sons, Chichester, pp. 28– 50, (1996).

[77] T.G. Vosloo, W.C. du Plessis and J.C. Swarts. *Inorg. Chim. Acta*., 188, **331** (2002).

[78] R.G. Wilkens, *Kinetics and Mechanisms of Reactions of Transition Metal Complexes*, VCH, Weinheim, pp. 103, 232-242, **2nd** ed(1991).

[79] U. Belluco, L. Cattalini, F. Basolo, R.G. Pearson and A. Turco, *J. Am. Chem. Soc*., 241, **87** (1995).

[80] R.G. Pearson, H.Sabel and J. Songstad, *J. Am. Chem. Soc*., 319, **90** (1968).

[82] J.G. Leipoldt, E.C. Steynberg and R. van Eldik, *Inorg. Chem*., 3068, **26** (1987).

[81] J.G. Leipoldt, S.S. Basson, G.J. van Zyl and G.J.J. Steyn, *J. Organomet. Chem*., 241, **418** (1991).

[83] W. Robb and C.G. Nicolson , *S. Afr. J. Chem*., 1, **31** (1978).

[84] J.G. Leipoldt and E.C. Grobler, *Trans. Met. Chem*., 110, **11** (1986).

[85] A. Wernar, *Z. Anorg. Chem*., 267, **3** (1993).

[86] S.S. Zumdahl and R.S. Drago, *J. Am. Chem. Soc*., 6669, **90** (1968).

[87] D.F. Shriver, P. Atkins and C.H. Langford, *Inorganic Chemistry*, Freeman, New York., p.467, **2nd** ed(1994).

[88] F. Basolo, J. Chatt, H.B. Gray, R.G. Pearson and B.L. Shaw, *J. Chem. Soc*., 2207, (1961).

[89] S. Arrhenius, *Z. Phys. Chem*., 226, **4** (1889).

[90] E. Whalley, *J. Chem. Phys.*, 1400, **38** (1963).

[91] J.G. Leipoldt, G.J. Lambrecht and E.C. Steynberg, *J. Organomet. Chem*., 259, **402** (1991).

Chapter 3
Results and discussion

3.1. Introduction

The compound number system of each chapter starts at 1.

This chapter describes the results obtained by the author during the present study.

New derivatives of osmocene were synthesized. The compounds 1-osmocenyl-4,4,4-trifluorobutan-1,3-dione (osmocenoyltrifluoroacetone, Hoctfa), 1-osmocenylbutane-1,3-dione (osmocenoylacetone, Hoca), 1-osmocenyl-3-phenylpropane-1,3-dione (benzoylosmocenoylmethane, Hbocm), 3-ferrocenyl-1-osmocenylpropane-1,3-dione (ferrocenoylosmocenoylmethane, Hocfcm), 1-osmocenyl-3-ruthenocenylpropane-1,3-dione (osmocenoylruthenocenoylmethane, Hocrcm) and 1-osmocenyl-1,3-propanedione (osmocenoylacetaldehyde, Hoch) were prepared by Claisen condensation of acetyl osmocene and the appropriate ester under the influence of lithium diisopropylamide.

[Rh(β-diketonato)(cod)] complexes were obtained by treating the appropriate β-diketone with $[Rh_2(cod)_2Cl_2]$.

The pK_a' values for the new β-diketones were obtained by measuring the absorbance at different pH during an acid-base titration in a solvent system of water containing 9% acetonitrile and 1% tetrahydrofuran.

Formal reduction potentials, or if this was not possible, peak anodic potentials (E_{pa} values *vs*. Ag/AgCl) of the redox active metal centers in the osmocene-containing β-diketones and the [Rh(β-diketonato)(cod)] complexes in dichloromethane (DCM) were determined during a cyclic voltammetry study.

Kinetic results for the conversion of the β-diketones from the enol to the keto-isomer and vice versa are described. Substitution kinetic results for the $(OcCOCHCOR)^{-1}$-moiety from the [Rh(OcCOCHCOR)(cod)] with 1,10-phenanthroline are also presented.

Chapter 3
Results and discussion

Where possible, results are related to the group electronegativity of each R group in the present series of compounds.

3.2. Syntheses

3.2.1. Acetyl osmocene

Acetyl osmocene, **2**, was prepared in 78 % yield by Friedel-Crafts acetylation of osmocene, **1**, with acetic anhydride in the presence of 85 % phosphoric acid according to a known method.[1] The yield obtained is influenced by the temperature of the reaction vessel. Temperatures below 70 ^{o}C resulted in low yields, while tar was formed at temperature exceeding 80 ^{o}C. The synthetic route is shown in Scheme 3.1. Ferrocenoic and ruthenocenoic acid were synthesized *via* the 2-chlorobenzoyl ferro or ruthenocene intermediate and esterfied by refluxing in MeOH according to a known method.

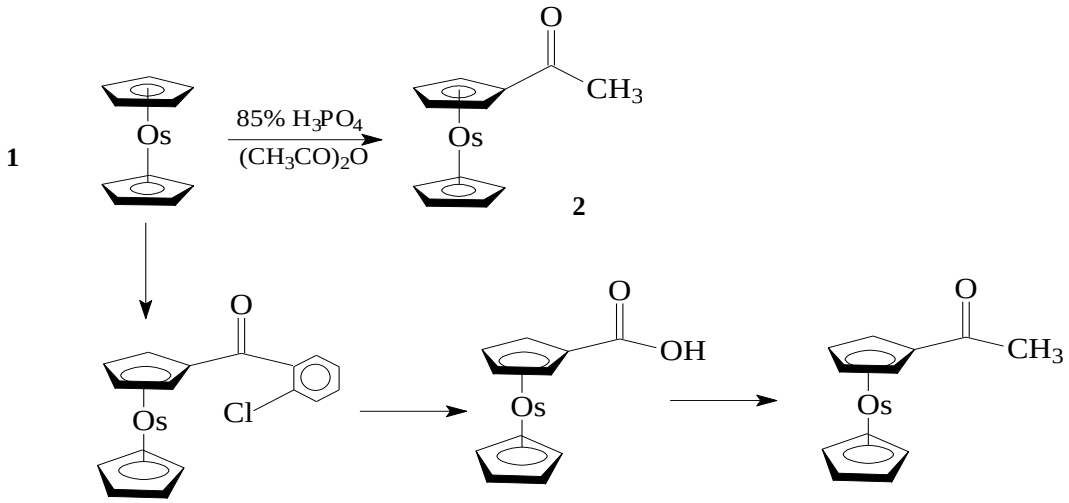

Scheme 3.1. Synthetic route for the preparation of acetyl osmocene and methyl osmocenoate

Chapter 3
Results and discussion

3.2.2. β-diketones

The new light yellow osmocene-containing β-diketones, Hoctfa, **3**, Hoca, **4**, Hbocm, **5**, Hocfcm, **6** (red in color), Hocrcm, **7**, and the β-keto aldehyde Hoch, **8**, (Scheme 3.2) were prepared by Claisen condensation of acetyl osmocene, **2**, with the esters RCOOMe (R = C_6H_5, Fc, Rc, H) or RCOOEt (R = CF_3, CH_3), under the influence of the hindered base lithium diisopropylamide (LiDPA).

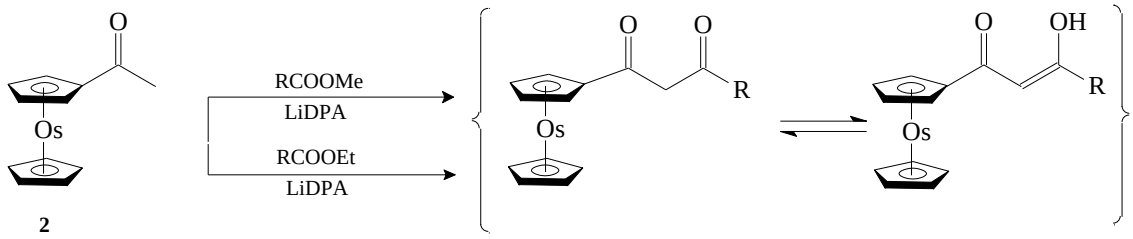

2

R = CF_3 (**3**), CH_3 (**4**), C_6H_5 (**5**), Fc (**6**), Rc (**7**) or H (**8**).

Scheme 3.2. Reaction scheme for the preparation of the new osmocene-containing β-diketones, $OcCOCH_2COR$, Hoctfa (**3**, R = CF_3), Hoca (**4**, R = CH_3), Hbocm (**5**, R = C_6H_5), Hocfcm (**6**, R = Fc), Hocrcm (**7**, R = Rc) and the β-keto aldehyde Hoch (**8**, R = H). LiDPA = lithium diisopropylamide.

Apart from Hoctfa, **3**, which was obtained in 68 % yield, the reactions were inefficient with yields being: 17 % of Hoca, **4**, 18 % of Hbocm, **5**, 26 % of Hocfcm, **6**, 9 % of Hocrcm, **7**, and 24 % of Hoch, **8**, respectively. Hocfta, **3**, and Hoch, **8**, could not be purified by column chromatography as decomposition caused them to become fixed on the silica gel. Hoctfa, **3**, and Hoch, **8**, could only be purified by recrystallisation.

The high yield for Hoctfa, **3**, syntheses is probably in part related to the high acidity of **3** (see section 3.3) and the high reactivity of the ester precursor CF_3COOEt. The triflate ester, CF_3COOEt, is probably more susceptible to attack from the in *situ* generated $OcCOCH_2^-$ group as the trifluoromethyl electron-withdrawing group generates a more positive charge on the carbonyl carbon of the ester than on the other esters. The reactions were done under argon to protect the oxygen and moisture-sensitive LiDPA, and the labile intermediate $OcCOCH_2^-$, which is generated when **2** reacts with LiDPA.

Hoca, **4**, synthesis failed if the ethyl acetate used was not freshly purified and dried. This is necessary because CH_3COOEt mixes partially with water and is much more hygroscopic then any of the other esters. Moisture and ethyl acetate hydrolysis products such as acetic acid would destroy the $OcCOCH_2^-$ reactive species as well as any unreacted LiDPA base, thereby terminating Hoca, **4**, formation.

3.2.3. Complexation reaction of β-diketones with rhodium

The rhodium dimer, **11**, was obtained by published methods [2] in yields up to 78 %. The method (Scheme 3.3) involved refluxing of $RhCl_3.H_2O$, **9**, and cyclooctadiene, **10**, in the presence of ethanol for 2½ hours at 78 °C to yield $[Rh_2Cl_2(cod)_2]$, **11**, as a yellow powder.

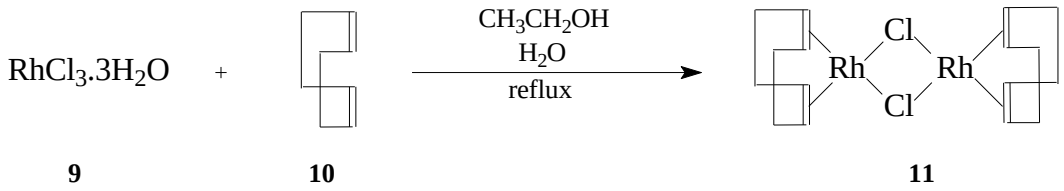

9 **10** **11**

Scheme 3.3. Synthesis of the rhodium dimer, **11**.

Complexation of the osmocene-containing β-diketones, **3**-**8**, with $[Rh_2Cl_2(cod)_2]$, **11**, in dimethylformamide yields the complexes, [Rh(octfa)(cod)], **12** (51%), [Rh(oca)(cod)], **13** (49%), [Rh(bocm)(cod)], **14** (46%), [Rh(ocfcm)(cod)], **15** (36%), and [Rh(och)(cod)], **16** (46%).

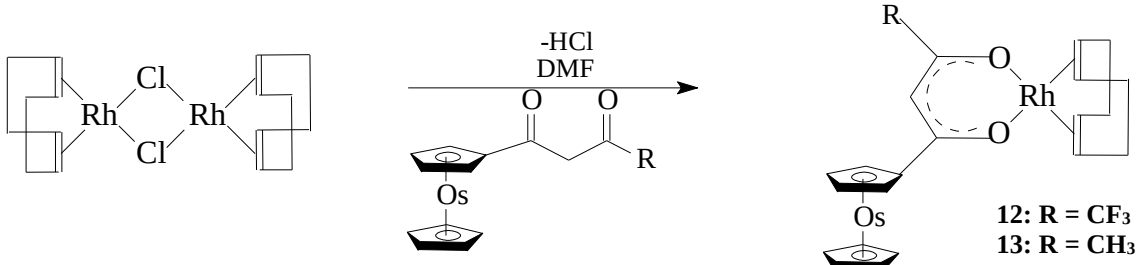

11 **3 - 8**

12: R = CF_3
13: R = CH_3
14: R = C_6H_5
15: R = Fc
16: R = H

Scheme 3.4. The complexation reaction of osmocene-containing β-diketones with the rhodium dimer $[Rh_2Cl_2(cod)_2]$, **11**, to give complexes of the type [Rh(OcCOCHCOR)(cod)] with R= CF_3, CH_3, C_6H_5, Fc and H.

Chapter 3
Results and discussion

Except for the synthesis of **15**, mixtures were stirred for up to 5 hours to allow complex formation to proceed to completion, due to slow formation kinetics. However [Rh(ocfcm)(cod)], **15**, was isolated after 30 minutes of reaction time. Complex **15** and the precursor, **6**, are extremely susceptible to acid. HCl is liberated in the complexation reaction due to the breaking of the Cl-bridges of the rhodium dimer. It was found that the yield of **15** decreased substantially during longer reaction times.

3.3. $pK_a^{/}$ determinations

There is referred to the observed $pK_a^{/}$ rather than pure thermodynamic pK_a values, in this study, because no attempt was made to partition the experimentally observed $pK_a^{/}$ value into the separate pK_a values for the keto and enol tautomers of the β-diketones, **3**-**8**. The $pK_a^{/}$ values were obtained by measuring the absorbance at different pH during an acid-base titration in water-acetonitrile-tetrahydrofuran 90:9:1 by volume, μ = 0.100 mol dm^{-3} (sodium perchlorate monohydrate, $NaClO_4$) at 25(1) ^oC with β-diketone concentrations $\pm$ 0.04 mmol dm^{-3}.

Acetonitrile was chosen as co-solvent because it is known to have very little influence on $pK_a^{/}$ values, and it assists in keeping the β-diketones in solution. A 1 % THF co-solvent system was used since the β-diketones, **3**-**8,** precipitate from the water/acetonitrile system, as they form upon titration with acid.

The UV/visible spectra of the protonated (enolic) and deprotonated (basic) forms of β-diketones Hoctfa, **3**, Hoca, **4**, Hbocm, **5**, Hocfcm, **6**, Hocrcm, **7**, and Hoch, **8**, are shown in Figure 3.1.

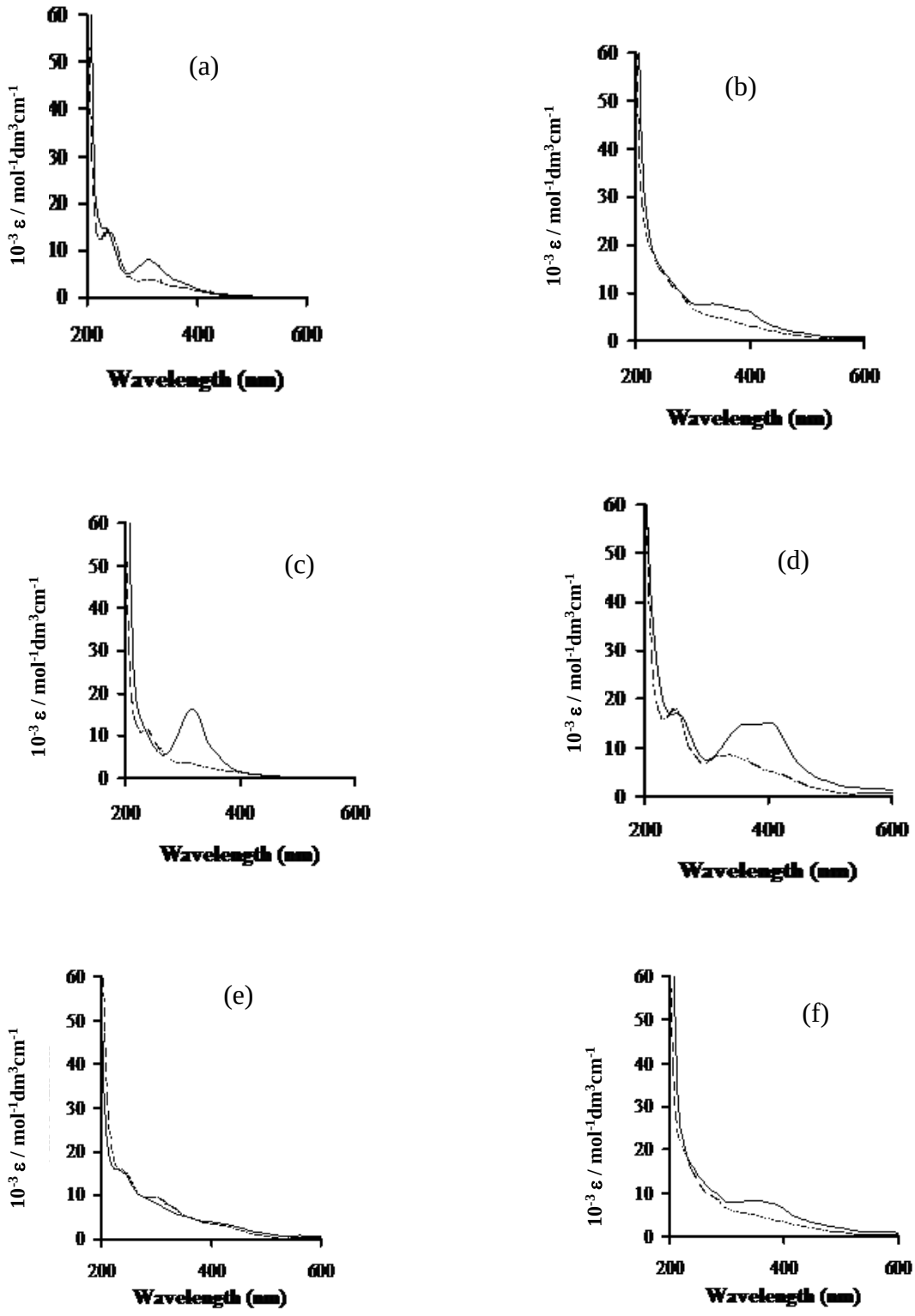

Figure 3.1. Electronic spectra of free β-diketones (----------) and deprotonated β-diketonato anions (_____) in water containing 9 % CH_3CN and 1 % THF for (a) Hoctfa, **3**, (b) Hoca, **4**, (c) Hbocm, **5**, (d) Hocfcm, **6**, (e) Hocrcm, **7**, and (f) Hoch, **8**.

Chapter 3
Results and discussion

From Figure 3.1 suitable wavelengths were identified to follow the titration in Figure 3.2. The basicity of β-diketones increased (i.e. higher $pK_a^{/}$ values) as the electronegativity of R groups decreased. The keto-aldehyde (R = H) was found to be the most acidic (i.e. least basic, $pK_a^{/} \approx 7$) and Hocfcm, **6**, the most basic β-diketone studied in the project. Base titrations are defined as the addition of base to an $OcCOCH_2COR$ solution during $pK_a^{/}$ determination, while acid titration is the addition of an acid to a $[OcCOCHCOR]^-$ solution. The new $pK_a^{/}$ values obtained from the obtained S-curves are summarized in Table 3.1. These $pK_a^{/}$ values are obtained by applying a least squares fit of UV absorbance versus pH data obtained from the acid (or base) titration of the β-diketone to Equation 3.1.

Table 3.1. $pK_a^{/}$ values (determined at λ_{exp}) and molar absorptivity ε (at λ_{max}) of the new osmocene-containing β-diketones Hoctfa, **3**, Hoca, **4**, Hbocm, **5**, Hocfcm, **6**, Hocrcm, **7**, and Hoch, **8**, in 9 % acetonitrile/ 1 % tetrahydrofuran mixture at 25 °C in 90 % water.

Compound	**$pK_a^{/}$** **(for base titration)**	**$pK_a^{/}$** **(for acid titration)**	**λ_{exp}/nm**	**10^{-3} ε/ $dm^3mol^{-1}cm^{-1}$**	**β-diketone λ_{max}**	**β-diketonato λ_{max}**	**χ_R**
Hoctfa (**3**), R=CF_3	7.90(2)	8.01(3)	310	8.09	309	309	3.01
Hoca (**4**), R=CH_3	10.39(3)	10.44(2)	320	8.43	319	294	2.34
Hbocm (**5**), R=C_6H_5	10.59(2)	10.55(1)	380	14.82	340	390	2.21
Hocfcm (**6**), R=Fc	13.04(1)	13.08(1)	305	16.32	349	340	1.87
Hocrcm (**7**), R=Rc	11.42(1)	11.37(2)	395	6.25	399	340	1.99
Hoch (**8**), R=H	7.54(3)	7.16(2)	390	9.79	284	299	2.20

Chapter 3
Results and discussion

$$A_T = \frac{A_{HA}10^{-pH} + A_A10^{-pKa'}}{10^{-pH} + 10^{-pK_a'}}$$

Equation 3.1.

In this Equation A_T = total absorption, A_{HA} = absorption of the β-diketone, $OcCOCH_2COR$, and A_A = absorption of the β-diketonate species, $(OcOCHCOR)^-$. The general instability of β-diketones towards strong aqueous alkali media, which led to cleavage at the methane position, made it difficult to determine the pK_a' of the β-diketones Hocfcm, **6**, and Hocrcm, **7**, by the spectroscopic method.

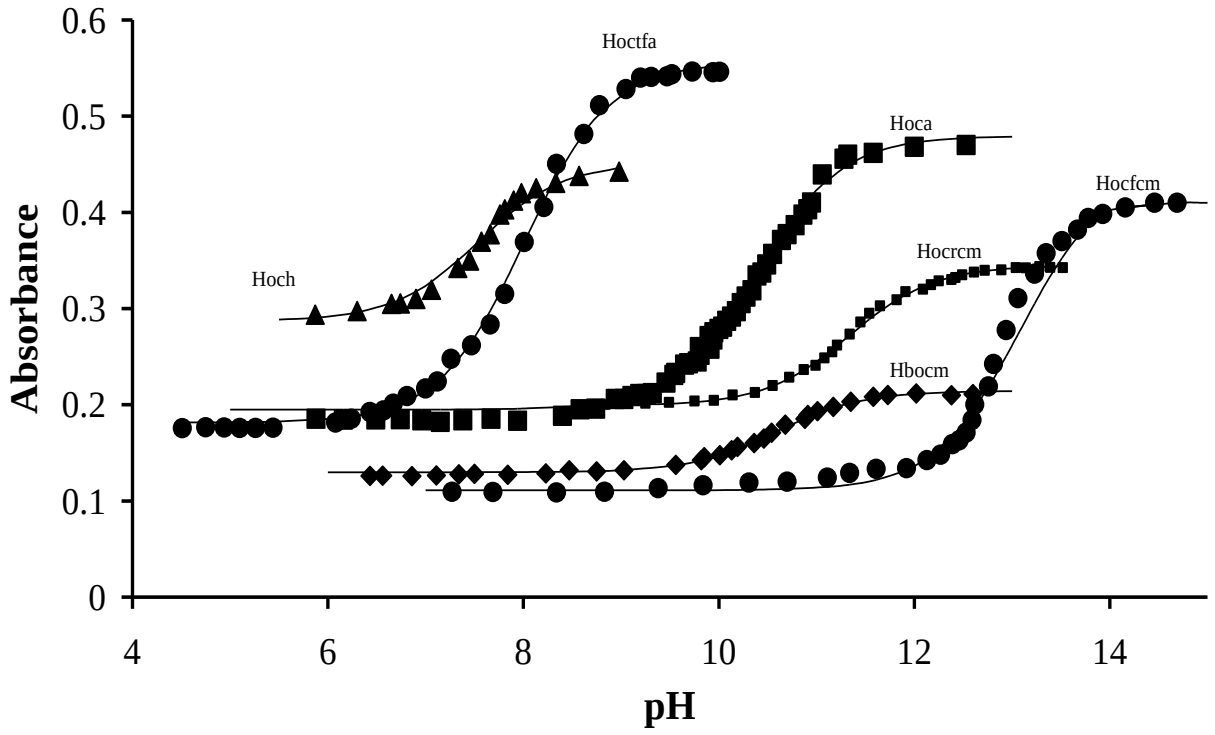

Figure 3.2. Relative absorbance dependence on pH for Hoctfa, **3**, Hoca, **4**, Hbocm, **5**, Hocfcm, **6**, Hocrcm, **7**, and Hoch, **8**, in water-acetonitrile-tetrahydrofuran 90:9:1 by volume with μ = 0.100 mol dm^{-3} (sodium perchlorate monohydrate, $NaClO_4$) at 25(1) ^oC, for the acid titration.

Chapter 3
Results and discussion

3.4. Isomerization kinetics between the keto-and enol-tautomers of the β-diketones

3.4.1. The observed solution phase equilibrium constant, K_c

In principle, β-diketones exist as a mixture of keto and enol forms as shown in Scheme 3.5. Although two enol isomers are possible, in analogy to the ferrocene-containing β-diketones[3], the dominant osmocene-containing β-diketone enol isomer, based on ^{1}H NMR evidence, is considered as enol isomer B. This assumption is also substantiated by a recent crystal structure determination of Hbocm, **5**, which confirm B as the only isomer in the solid state. (Unpublished results, J.C. Swarts)

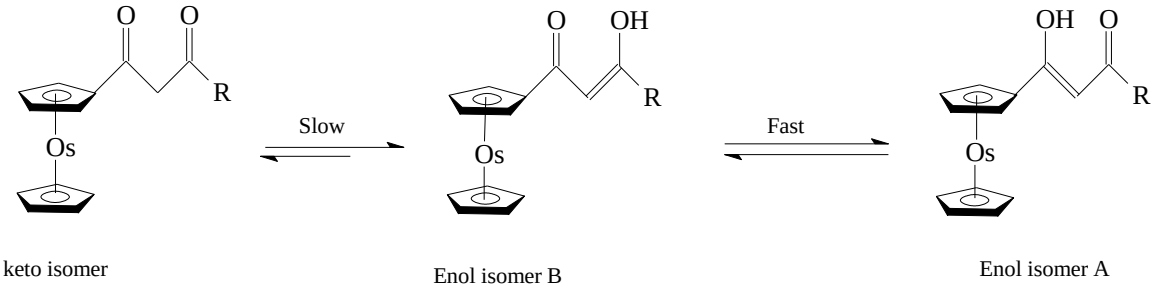

Scheme 3.5. Keto-enol equilibrium for osmocene-containing β-diketones.

The apparent absence of enol isomer A allows writing of the simplified equilibrium shown in Scheme 3.6.

$$\text{Oc-CO-CH}_2\text{-CO-R} \underset{k_{-1}}{\overset{K_c,\ k_1}{\rightleftharpoons}} \text{Oc-CO-CH=(COH)-R}$$

Scheme 3.6.

K_c can also be depicted as k_1 / k_{-1}.

$$K_c = \frac{\text{[enol isomer] at equilibrium}}{\text{[keto isomer] at equilibrium}} = \frac{\text{\% enol isomer at equilibrium}}{\text{\% keto isomer at equilibrium}}$$

$$= \frac{\text{integral value of } ^1\text{H NMR signal of a suitable enol molecular fragment}}{\text{integral value of } ^1\text{H NMR signal of a suitable keto molecular fragment}}$$

$$= \frac{k_1}{k_{-1}}$$

Equation 3.2.

For convenient K_c determination, integral values for suitable ^{1}H NMR signals from the ^{1}H NMR spectra of β-diketones at equilibrium were used (Equation 3.2). However, for kinetic data it was more convenient to use isomer percentages. To demonstrate how K_c was determined, $OcCOCH_2COCH_3$ (Hoca, **4**) will be used as an example. Figure 3.3 shows the ^{1}H NMR spectrum of Hoca, **4**, in $CDCl_3$ at equilibrium. From this spectrum, utilizing the integral values of the methyl group of the keto and enol isomers, the equilibrium constant, K_c, could be calculated as K_c = 3.032 / 2.033=1.49. From the C_5H_5 signals, K_c = 4.645 / 2.962=1.56. The two CH_2 signals result in K_c = 2.153 / 1.210=1.78 and K_c = 2.015 / 1.462=1.38. The methine signals results in K_c = 1 / ½(1.308) =1.53.

The K_c value of 1.78 is obviously too large, mainly because the enol CH_2 signal integral should be 2.00 and not 2.153 as was measured. Upon ignoring K_c=1.78, the average K_c for Hoca, **4**, is therefore 1.49. Integration of the spectrum was done in such a way that the methine proton of the enol isomer was assigned an integral value of 1.

K_c values for the other complexes in the solvent $CDCl_3$ as well as CD_3CN, were determined in a similar way, results are summarized in Table 3.2.

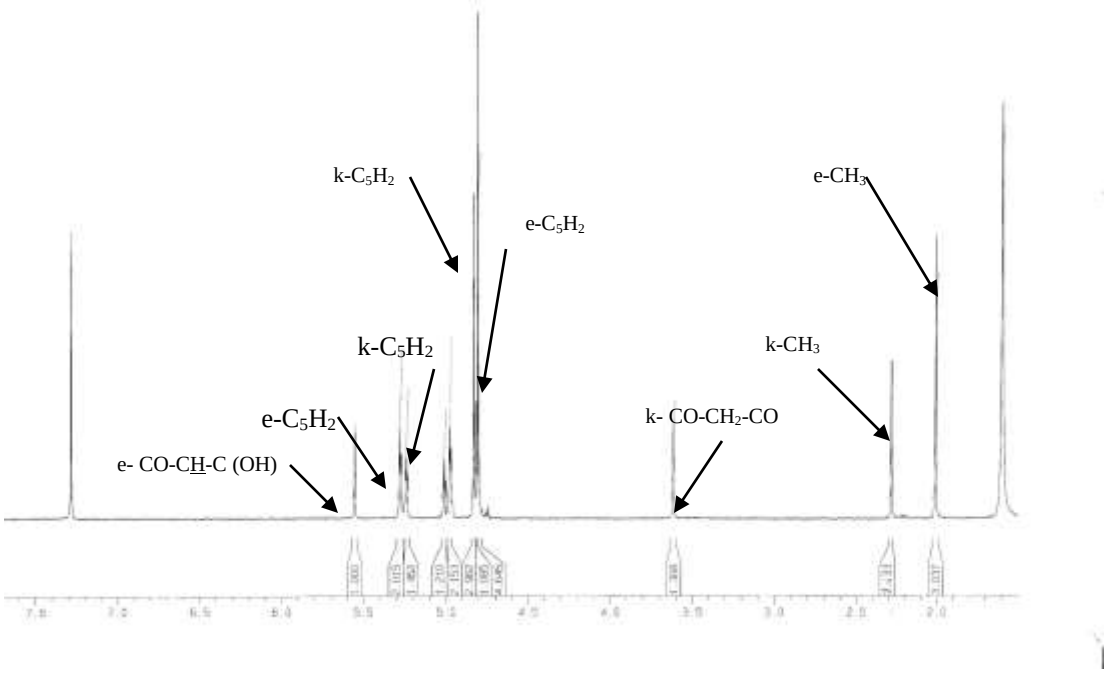

Figure 3.3. The ^{1}H NMR spectrum of Hoca, **4**, in $CDCl_3$ at equilibrium (19 ^oC): Oc-CO-CH_2-CO-CH_3 ⇆ Oc-CO-CH=C(OH)-CH_3. The spectrum was obtained after enough time elapsed to ensure that the sample was at equilibrium. The prefix 'e' implies a signal of the enol isomer, while the prefix 'k' implies a signal of the keto isomer. Oc = $C_5H_5OcC_5H_4$

To determine the percentage keto isomer at equilibrium, for a suitable set of ^{1}H NMR peaks, Equation 3.3 below was used (I= integral value). Once again, utilizing for example the methine ^{1}H NMR integral values for Hoca, **4**, in Figure 3.3, (enol at 5.53 ppm, keto at 3.36 ppm) the percentage keto isomer is

$$\% \text{ keto isomer} = \frac{(\text{I of keto signal})/2}{\{(\text{I of keto signal})/2 + (\text{I of enol signal})\}} \times 100$$

$$= [(1.308/2) / \{(1.308/2 + 1.000)\}] \times 100$$

$$= 39.5\%$$

Equation 3.3.

Utilizing the CH_3 signal, the percentage keto isomer is 40.1 %. From the C_5H_5 signal, the percentage keto signal is 38.9 %, while from the C_5H_2 signals at 5.2-5.3 ppm, it is 42.0%. The average percentage keto isomer is therefore 40.1 %. Substitution of the average keto percentage and signal values in Equation 3.4 gives

$$Kc = \frac{\%enol}{\%keto}$$

$$= \frac{100\% - \%keto}{\%keto}$$

$$= \frac{100\% - 40.1\ \%}{40.1\ \%}$$

$$= 1.49$$

Equation 3.4.

for the equilibrium

$$Oc\text{-}CO\text{-}CH_2\text{-}CO\text{-}CH_3 \rightleftharpoons Oc\text{-}CO\text{-}CH{=}C(OH)\text{-}CH_3$$

Scheme 3.7.

In a similar fashion, by using appropriately unambiguously definable ^1H NMR signals, the average K_c value and percentage keto isomer for Hbocm, **5**, Hocfcm, **6**, Hocrcm, **7**, and determined. The compound Hoctfa, **3**, is so rich in enol content that no accurate K_c value could be determined with ^1H NMR measurements.

The same enol equilibrium was investigated by determining K_c and percentage keto isomer also in acetonitrile, CD_3CN. Results are summarized in Table 3.2.

Table 3.2. Equilibrium constant, K_c, at 19 °C, applicable to Scheme 3.7, the percentage keto isomer at equilibrium for the keto-enol equilibrium, with Gibbs's energy for the mentioned β-diketones.

	CD_3CN						$CDCl_3$					
Compounds Compounds	**10^5k_{obs} / s^{-1}**	**10^5k_1 / s^{-1}**	**10^5k_{-1} / s^{-1}**	**%keto at eq**	**K_c**	**ΔG / kJmol^{-1}**	**10^5k_{obs} / s^{-1}**	**10^5k_1 / s^{-1}**	**10^5k_{-1} / s^{-1}**	**%keto at eq**	**K_c**	**ΔG / kJmol^{-1}**
Hoctfa(**3**) R = CF_3 χ_R = 3.01	-	-	-	<5	>19	<-7148	-	-	-	<5	>19	<-7148
Hoca(**4**) R = CH_3 χ_R = 2.34	3.10	1.70	1.40	44.80	1.22	-502.56	5.10	3.05	2.03	39.5	1.49	-1032.4
Hbocm(**5**) R = C_6H_5 χ_R = 2.21	168	120	47.7	28.40	2.52	-2243.8	4.02	3.37	0.65	16.17	5.18	-3075.8
Hocfcm(**6**) R = Fc χ_R = 1.87	139	60.0	79.0	56.70	0.76	666.2	1.03	0.458	0.572	55.5	0.80	541.7
Hocrcm(**7**) R = Rc χ_R = 1.99	201	48.7	152	75.49	0.32	2691.5	2.00	0.529	1.471	73.7	0.36	2480.3

K_c values were generally slightly larger in chloroform than in acetonitrile. The reason for this observation is not quite clear at this stage. However, the larger tendency of CD_3CN to solvation may have an influence on these results.

Inspection of K_c values in Table 3.2 shows Hoctfa, **3**, has the largest K_c value implying that the enol isomer becomes less dominant in moving from Hoctfa, **3**, to Hbocm, **5**, to Hoca, **4**, to Hocrcm, **7**, to Hocfcm, **6**.

The Gibbs energies for the isomerisation reactions were obtained by the application of Equation 3.5. [4]

$$\Delta G = -RT \ln K_c$$

Equation 3.5.

The Gibbs energy, ΔG, for Scheme 3.7 was calculated and results tabulated in Table 3.2. A decrease in the equilibrium keto content (increase in the equilibrium enol content) gives rise to an increase in equilibrium constant, K_c.

Inspection of ΔG values in Table 3.2 is instructive. A negative ΔG implies a spontaneous process, in this case conversion from keto to enol isomers as per Scheme 3.7. However, for **6** and **7**, ΔG became positive, implying that conversion from enol to keto isomer dominates. In these two cases, the keto isomer, in $CDCl_3$ and CD_3CN solution, is therefore thermodynamically more favored than the enol isomer. From inspection of the χ_R values it is also observed that this happens for cases in which the R-side group was the most electron-donating.

In general, from these results it is concluded that polar solvents (such as CD_3CN) and highly electron-donating β-diketone side chains stabilize the keto form.

3.4.2. Kinetics of enol-keto conversion

It was found that when β-diketone samples were allowed to age, eventually all keto isomers converted to the enol isomers. This implied that when an aged sample was dissolved and a ^1H NMR spectrum recorded, the spectrum was that of a sample which is much enriched in enol content.

By recording spectra of this solution with time, the conversion of enol to keto isomers could be followed until the equilibrium position was reached. Figure 3.4. shows the ^1H NMR spectra of an enol-enriched sample of Hocfcm.

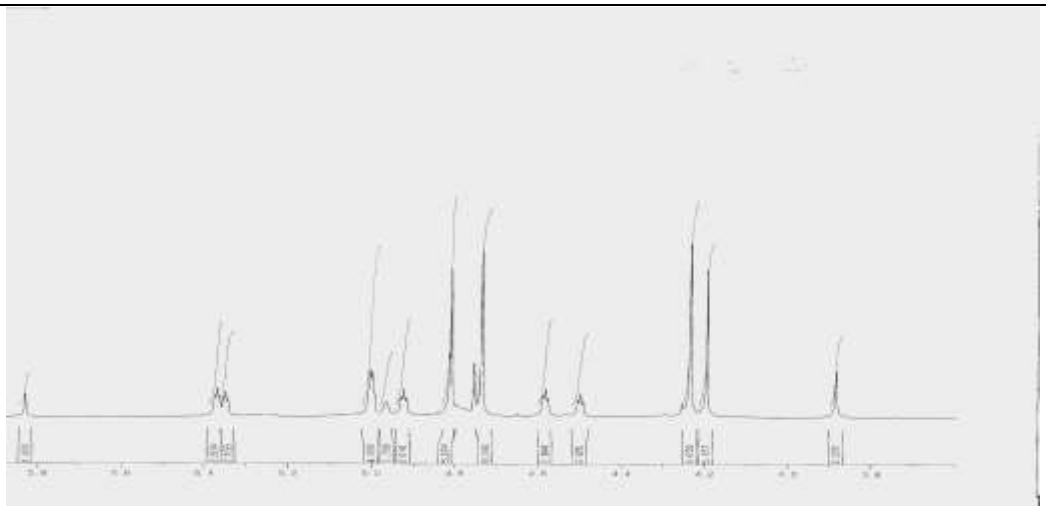

Figure 3.4. ^{1}H NMR spectrum of Hocfcm, **6**, at equilibrium.

By recording spectra of the enol-enriched sample at known time intervals, the kinetic rate of conversion from enol to keto isomer could be measured. Since this conversion is an equilibrium reaction involving a forward rate constant k_1 and a reverse rate constant k_{-1} according to scheme 3.6 (page 66), the general rate equation for the reaction is,

$$\ln \frac{C_o - C_\infty}{C_t - C_\infty} = k_{obs}\, t = (k_1 + k_{-1})t$$

Equation 3.6.

Figure 3.5 shows the time trace of keto isomer formation for Hoca, **4**, in $CDCl_3$ and CD_3CN. In both cases, the equilibrium keto/enol position is reached within 100 000 s. From the plot depicted in Figure 3.5 one is able to determine the observed first order constant k_{obs} for the reaction by application of equation 3.6.

This kinetic treatment does not allow separation of the forward, k_1, and reverse, k_{-1}, rate constant, since only $k_{obs} = k_1 + k_{-1}$ can be determined from kinetic data (See Figure 3.5, insert). However, by recognizing $K_c = k_1/k_{-1}$ as per equation 3.2, page 67, and with both K_c and k_{obs} known, these two equations may be solved simultaneously to separate k_1 and k_{-1}, from each other. Results for these mathematical treatments are shown in Table 3.2.

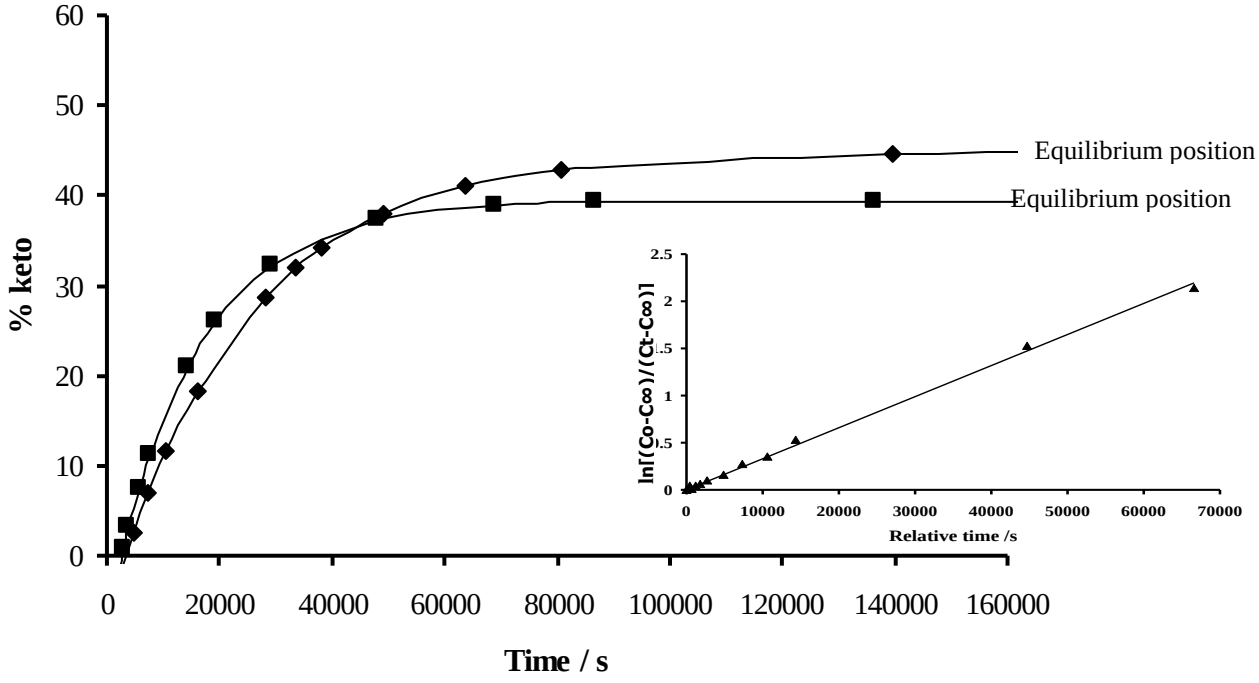

Figure 3.5. Conversion from enol to keto isomer for Hoca, **4**, in acetonitrile {CD_3CN} indicated by ◆ and $CDCl_3$. indicated by ■. **Insert:** A kinetic plot of data from this process that leads to the first order rate constant k_{obs}.

The plots of the percentage keto isomer versus time for the β-diketones Hbocm, **5** and Hocrcm, **7**, in $CDCl_3$ are shown in Figure 3.6.

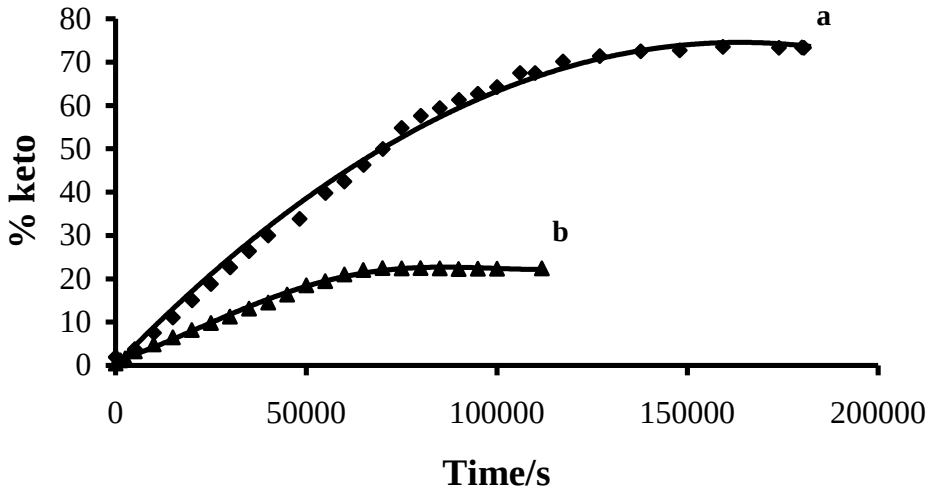

Figure 3.6. Time trace showing the conversion from the enol-isomer to the keto-isomer for (a) Hocrcm, **7**, and (b) Hbocm, **5**, at 292 K in $CDCl_3$.

3.4.3. Kinetics of keto-enol conversion

Section 3.4.2. described a kinetic treatment by studying the conversion of the enol isomer to the keto isomer. In principle the same results should be obtained if a kinetic study was performed on a solution that is enriched in keto isomer by following the rate of enol formation.

In this study the β-diketone, Hoca, **4**, was used to illustrate this phenomenon. To obtain a solution with keto-enriched content, a solution of Hoca, **4**, in diethyl ether was extracted by aqueous NaOH. The original organic layer was discarded and $CDCl_3$ was added to the aqueous layer. Acidification with HCl allowed extraction of the β-diketone in the $CDCl_3$ layer in sufficient concentrations to obtain a ^1H NMR spectrum. The aqueous layer was discarded and the $CDCl_3$ layer was quickly washed with water and a portion of the organic layer was taken to record a ^1H NMR spectra at known time intervals. For each time interval, the % keto isomer was determined and the observed first-order rate constant, k_{obs}, was obtained from Equation 3.7[5].

$$[A]_t = \{[A]_\infty + ([A]_o - [A]_\infty)\}^{[-(k_{obs})t]}$$

Equation 3.7. $[A]_t$ = % keto isomer at time t, $[A]_\infty$ = % keto isomer at infinite time, $[A]_o$ = initial % keto isomer, $k_{obs} = k_1 + k_{-1}$.

Thereafter rate constants k_1 and k_{-1} were separated by simultaneously solving the Equations $k_{obs} = k_1 + k_{-1}$ and $K_c = k_1/k_{-1}$. Data are indicated in Table 3.3.

Table 3.3. Keto to enol conversion data.

Compound **OcCOCH$_2$COR**	**χ_R**	**k_{obs}= $10^5(k_1 + k_{-1})$ / s^{-1}**	**$K_c = k_1/k_{-1}$**	**$\times 10^5 k_1$ / s^{-1}**	**$\times 10^5 k_{-1}$ / s^{-1}**	**%keto**	**ΔG kJ mol^{-1}**
Hoca (**4**), R = CH_3	2.34	5.21	1.49	3.12	2.09	40.1	-968.16

The rate constants that could be extracted for the conversion of keto to enol isomers were observed to be almost equal to the rate constants obtained for the conversion of enol to keto isomers for the β-diketone Hoca, **4**.

Time traces show the conversion from keto to enol Hoca, **4**, isomers and enol to keto Hoca, **4**, isomers are indicated in Figure 3.7.

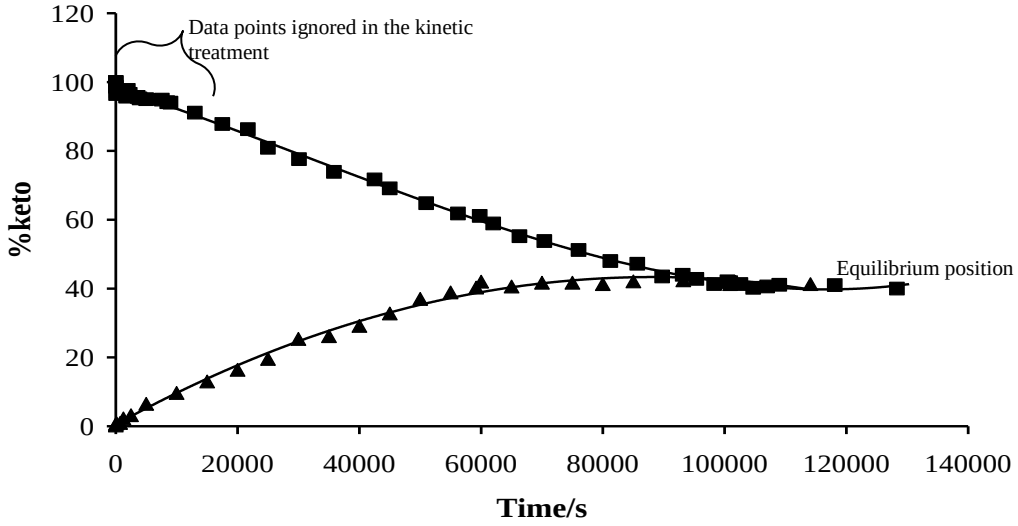

Figure 3.7. The keto to enol conversion for Hoca, **4,** indicated by ■ and the enol to keto conversion for Hoca, **4,** indicated by▲.

Figure 3.7 shows an apparent delay in conversion rate from keto to enol isomers. The reason for this "induction" period is not clear at this stage.

3.5. Kinetics of β-diketonato substitution in [Rh(β-diketonato)(cod)]

This section concerns the kinetics of substitution of the bidentate β-diketonato ligands from [Rh(β-diketonato)(cod)] complexes by 1,10-phenanthroline (phen), to give $[Rh(phen)(cod)]^+$. The reaction that takes place is indicated in Scheme 3.8.

$$[Rh(\beta\text{-diketonato})(cod)] + phen \rightarrow [Rh(phen)(cod)]^+ + (\beta\text{-diketonato})^-$$

Scheme 3.8.

3.5.1. The Beer- Lambert Law

The UV/Vis spectra of [Rh(octfa)(cod)], **12**, [Rh(oca)(cod)], **13**, [Rh(bocm)(cod)], **14**, [Rh(ocfcm)(cod)], **15**, and [Rh(och)(cod)], **16**, 1,10-phenanthroline (phen) and $[Rh(phen)(cod)]^+$, in methanol at 25 ^oC were recorded. Suitable wavelengths to follow the reaction kinetically were identified by choosing a wavelength where the spectrum of [Rh(β-diketonato)(cod)] and $[Rh(phen)(cod)]^+$ differed substantially. Figure 3.8 illustrates the UV spectrum of [Rh(octfa)(cod)], **12**, superimposed onto that of the substitution product $[Rh(phen)(cod)]^+$.

Although the biggest difference in these spectra is at $\lambda < 340$nm, in order not to move into a wavelength where quartz cells had to be used, a wavelength of 365nm was chosen to monitor the substitution reaction. Table 3.4 summarizes all the wavelengths and relative peak maxima for **12-16**.

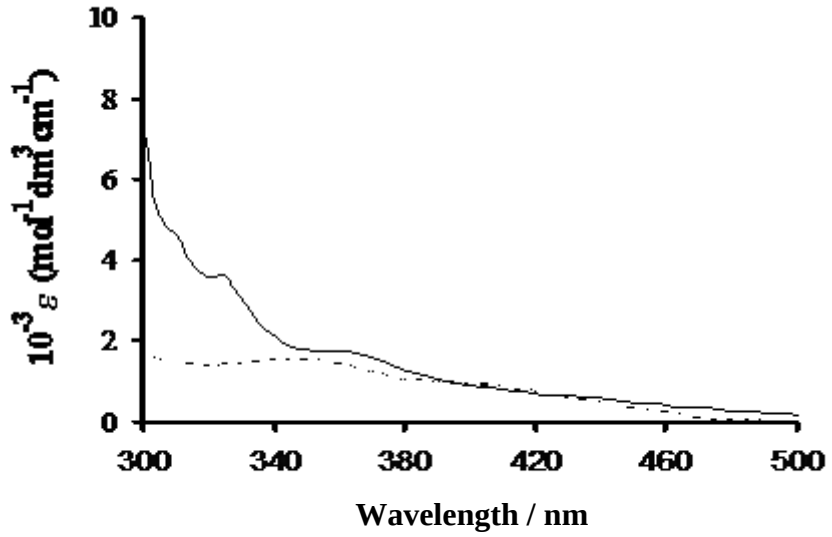

Figure 3.8. UV spectra of [Rh(octfa)(cod)], **12**, (……) and the resulting substitution product $[Rh(phen)(cod)]^+$ (_____) in methanol at 25 ^oC.

The Beer-Lambert law held for all complexes at the wavelengths at which the kinetics were performed. Figure 3.9 confirms the validity of the Beer-Lambert law ($A = \varepsilon cl$, with ε = molar absorptivity and l = path length = 1 cm) for each of the complexes under investigation.

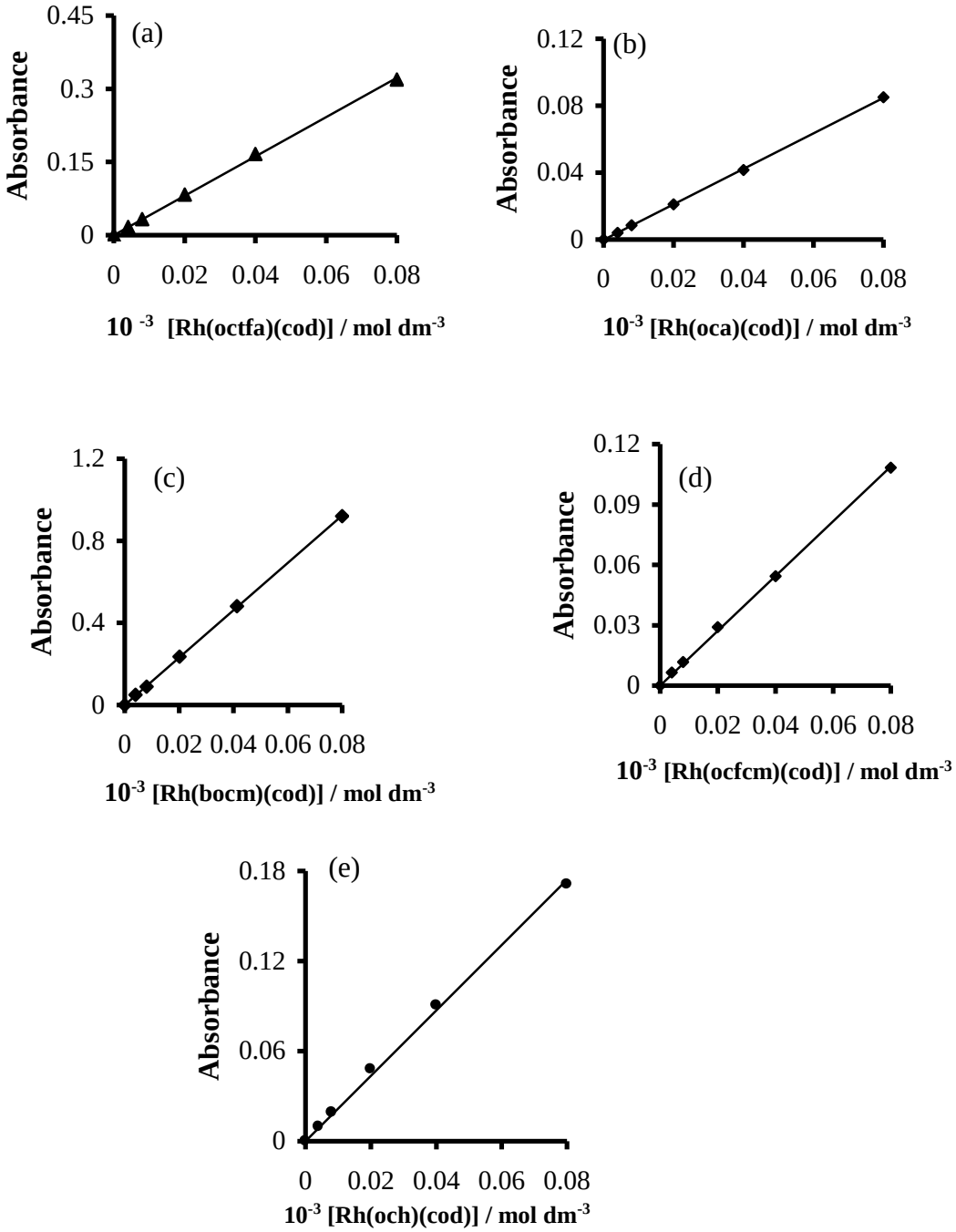

Figure 3.9. The linear relationship between absorbance and concentration of [Rh(β-diketonato)(cod)] complexes (a) [Rh(octfa)(cod)], **12**, (λ = 365 nm), (b) [Rh (oca)(cod)], **13**, (λ = 335 nm), (c) [Rh (bocm)(cod)], **14**, (λ = 350 nm), (d) [Rh(ocfcm)(cod)], **15,** (λ = 355 nm), and (e) [Rh(och)(cod)], **16**, (λ = 320 nm), at the indicated wavelength, confirming the validity of the Beer-Lambert law.

Table 3.4. Molar absorptivity, ε, at the indicated wavelength, λ, for [Rh(β-diketonato)(cod)] complexes.

Complex	λ_{exp}/ nm	ε at λ_{exp}/ $dm^3mol^{-1}cm^{-1}$
[Rh(octfa)(cod)],**12**, R= CF_3	365	4175
[Rh(oca)(cod)],**13**, R=CH_3	335	1064
[Rh(bocm)(cod)],**14**, R=C_6H_5	350	11542
[Rh(ocfcm)(cod)],**15**, R=Fc	355	1342
[Rh(och)(cod)],**16**, R=H	320	2108

3.5.2. Substitution kinetics of [Rh(β-diketonato)(cod)] with 1,10-phenanthroline

The substitution reaction between rhodium complexes of the type [Rh(OcCOCHCOR)(cod)] and 1,10-phenanthroline, **17**, to form $[Rh(phen)(cod)]^+$, **18**, is illustrated in Scheme 3.9.

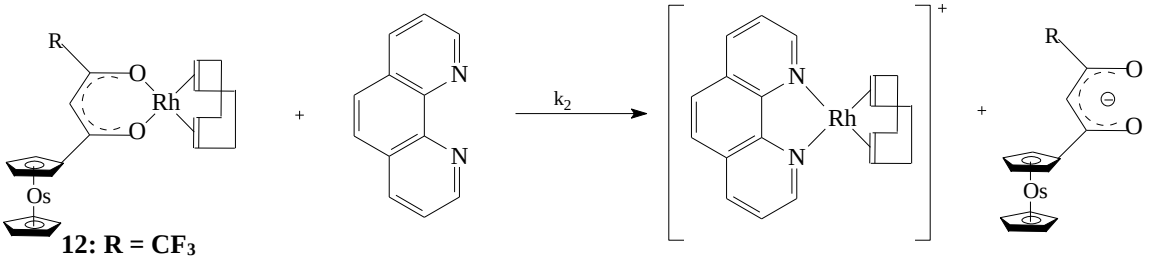

12: R = CF_3
13: R = CH_3
14: R = C_6H_5
15: R = Fc
16: R = H

17 **18** **19**

Scheme 3.9. Schematic representation for the substitution of $(OcCOCHCOR)^-$ from [Rh(OcCOCHCOR)(cod)], **12-16**, complex with 1,10-phenanthroline, **17**, to liberate $[Rh(phen)(cod)]^+$, **18**, and $(OcCOCHCOR)^-$, **19**. R = CF_3, CH_3, C_6H_5, Fc and H.

All substitution reactions were studied under pseudo first-order conditions with the concentration of 1,10-phenanthroline equal to 9 to 120 times the concentration of [Rh(β-diketonato)(cod)]. That the substitution is first order under these conditions was confirmed by a linear relationship in the plot of lnC versus time. Here, C = concentration

of [Rh(β-diketonato)(cod)] at different times t. The stopped flow apparatus used in this study uses "volt" as measured quantity and it is directly proportional to C. The pseudo first order rate constant, $k_{obs,}$ was obtained using the data analysis program 8X.18MV developed for the stopped flow system that was used.

A graph of k_{obs} against [phen] was linear in all cases as shown in Figure 3.10. All complexes, except for [Rh(OcCOCHCOPh)(cod)], showed within experimental error, a zero intercept (i.e. $k_s = 0$), thereby confirming that the solvent path did not make an observable contribution to the reaction. This was in fact expected since the displacement of bidentate ligands such as $(OcCOCHCOR)^-$ with monodentate solvent molecules (MeOH in this study) would be difficult, and hence slower than the displacement of a bidentate β-diketonato ligand with the bidentate phenanthroline ligand.

For the zero-intercept linear graph of k_{obs} *vs*. [Phen], it follows that the rate law of this substitution reaction simplifies as shown in Equation 3.8.

$$\text{Rate} = (k_s + k_2[\text{phen}])[\text{Rh(OcCOCHCOR)(cod)}]$$

$$= k_{obs}[\text{Rh(OcCOCHCOR)(cod)}]$$

Equation 3.8.

In Equation 3.8, the pseudo first-order rate constant, $k_{obs} = k_s + k_2[\text{phen}]$, with $k_s \approx 0$.

k_2 is the second-order rate constant for the substitution process and k_s is the rate constant associated with solvent taking part in the reaction. To determine k_2, plots of k_{obs} *vs*. [Phen] were constructed (Figure 3.10). The slope gave k_2 and the intercept showed $k_s \approx 0$.

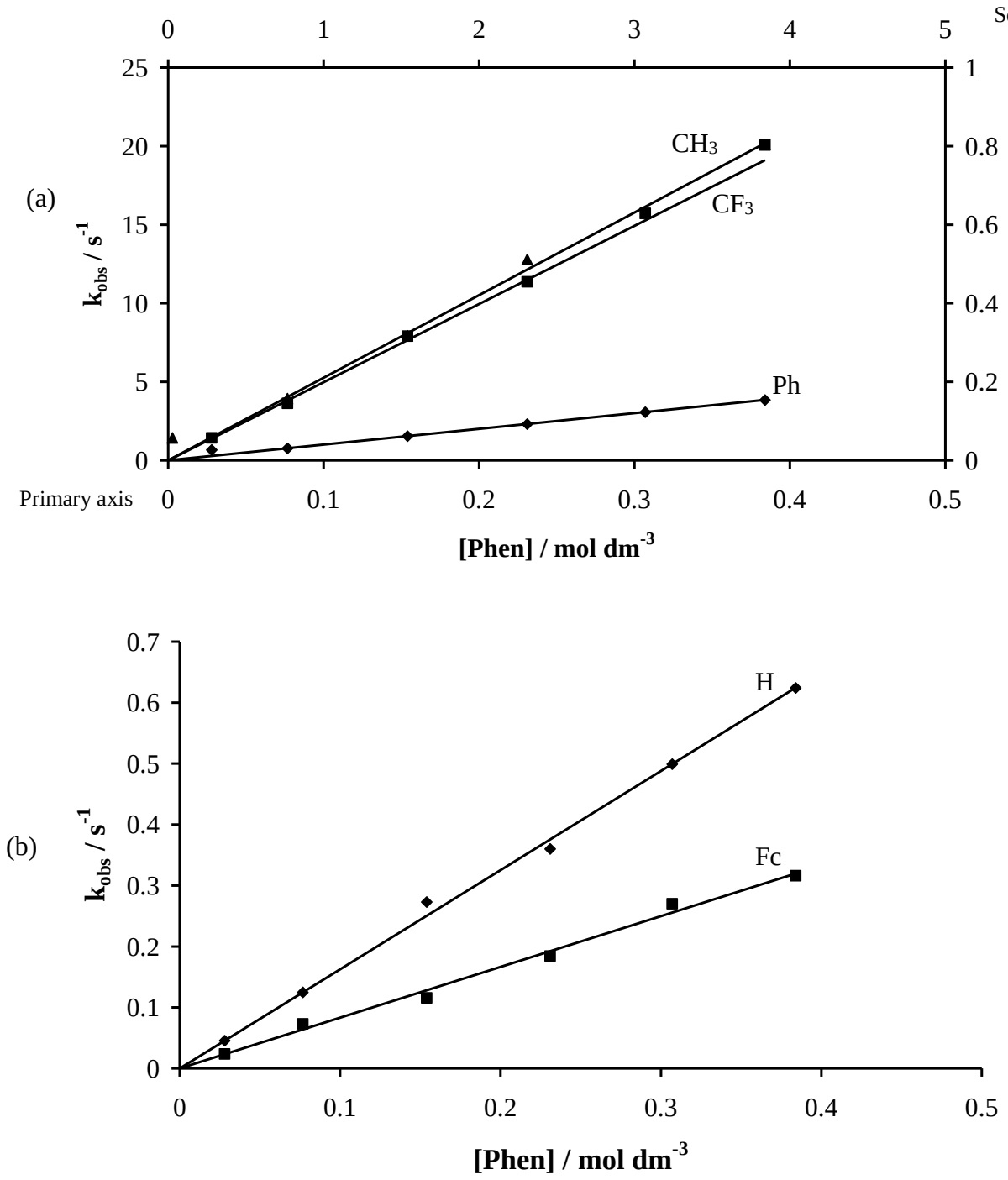

Figure 3.10(a). Graphs of pseudo first-order rate constant, k_{obs} vs. [Phen] at 25 °C for [Rh(octfa)(cod)], **12**, (primary axis), [Rh(oca)(cod)], **13**, (secondary axis) and [Rh(bocm)(cod)], **14,** (primary axis), graph **(b):** [Rh(och)(cod)] **16**, and [Rh(ocfcm)(cod)] **15.**

Chapter 3
Results and discussion

A case deserving special mention is the [Rh(bocm)(cod)], **14**, complex. Several previous studies showed that Rh complexes having a phenyl group in a β-diketonato ligand show a small non-zero intercept in the plot k_{obs} *vs*. [1,10-phenanthroline]. Vosloo and co-workers found that [Rh(FcCOCHCOPh)(cod)] had a y-intercept of k_s = 0.06(1) s^{-1} (Fc = ferrocenyl).[6] For the complex [Rh(bocm)(cod)], **14**, a y-intercept of k_s = 0.13 s^{-1} was found, the rate constant associated with a solvent participating step, k_s, is, however, very small compared with the rate constant associated with the non solvent route where k_2 = 24.4(1) $dm^3\ mol^{-1}\ s^{-1}$.

Therefore, even for **14**, the solvent pathway does not contribute significantly to substitution reactions for the complexes of this study.

Eyring plots of the experimental data over a temperature range of 15 °C to 40 °C are shown in Figure 3.11.

Activation parameters ΔH* and Δ S* for the studied substitution can be obtained from a fit of k_2 and temperature data (measured in Kelvin) to the Eyring Equation 3.9.

$$\ln \frac{k_2}{T} = -\frac{\Delta H^*}{RT} + \frac{\Delta S^*}{R} + \ln \frac{R}{Nh}$$

Equation 3.9.

k_2 = the experimentally determined second order rate constant, ΔH^* = the activation enthalpy, ΔS^* = the activation entropy, N = Avogrado's constant, *h* = Planck's constant, R = universal gas constant.

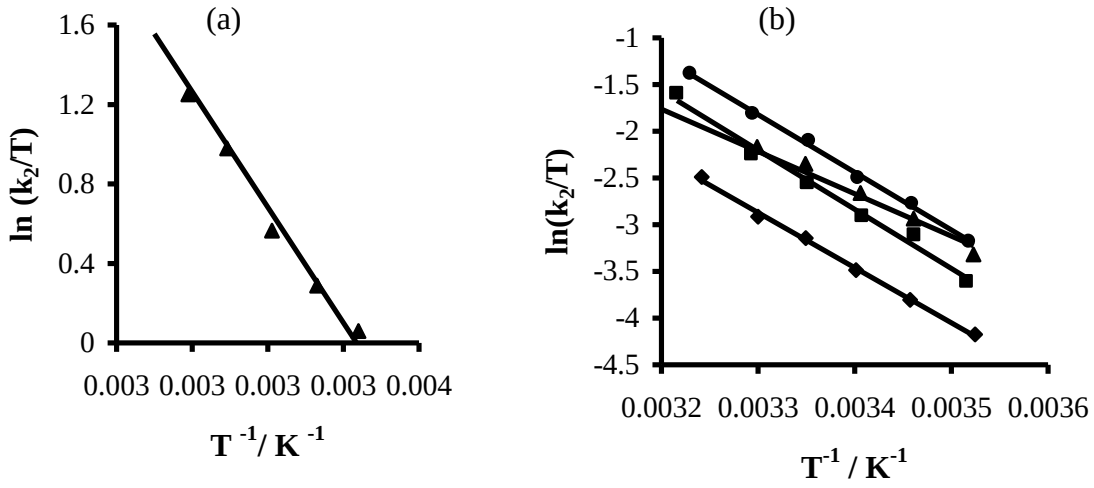

Figure 3.11. Eyring plots of $\ln(k_2/T)$ *vs*. T^{-1} at various temperatures (15 °C – 40 °C) for (a) [Rh(octfa)(cod)], **12**, (b) [Rh(bocm)(cod)], (**14**, ●); [Rh(oca)(cod)], (**13**, ▲) **;** [Rh(och)(cod)], (**16**, ■) and [Rh(ocfcm)(cod)], (**15**.◆).

The slopes of the above graphs give $(-\Delta H^*/R)$ and ΔS^* can be determined from the y-intercepts as discussed in chapter 2.

The Gibbs energy of activation can be calculated from Equation 3.10.

$$\Delta G^* = \Delta H^* - T\Delta S^*$$

Equation 3.10.

The activation parameters as well as the second order rate constants for the substitution reactions between the [Rh(β-diketonato)(cod)] complexes and 1,10-phenanthroline are tabulated in Table 3.5.

Table 3.5. Activation parameters as well as second order rate constants (k_2) for the substitution reactions between the [Rh(β-diketonato)(cod)] complexes and 1,10-phenanthroline. The wavelengths given in the table are the wavelengths at which the analyses were conducted.

Complex [Rh(OcCOCHCOR)(cod)]	ΔH^* /kJ mol^{-1}	ΔS^* /J K^{-1} mol^{-1}	ΔG^* /kJ mol^{-1}	k_2 /dm^{3}mol^{-1} s^{-1}	χ_R	λ_{exp} /nm
[Rh(octfa)(cod)], **12**, R=CF_3	48.09(2)	-31.46(3)	57.47(2)	524.1(2)	3.01	365
[Rh(oca)(cod)], **13**, R=CH_3	58.20(3)	-24.32(2)	65.45(2)	20.94(1)	2.34	335
[Rh(bocm)(cod)], **14**, R=C_6H_5	48.54(2)	-55.56(3)	65.07(2)	24.35(1)	2.21	350
[Rh(ocfcm)(cod)], **15**, R=FC	54.79(2)	-42.67(3)	67.51(2)	9.12(3)	1.87	355
[Rh(och)(cod)], **16**,R=H	51.48(3)	-48.98(2)	66.08(3)	16.23(2)	2.13	320

Although the ΔS^* values for the present series of compounds are not as negative as for example, complexes depicted in Table 2.7, they are significantly negative in size. (Values closer to 0 than –10 J K^{-1} mol^{-1} would not be regarded significantly negative in size) The negative activation entropies clearly indicate that the substitution process proceeds *via* an associative mechanism and not a dissociative mechanism. Two proposed mechanisms are depicted in Scheme 3.10.

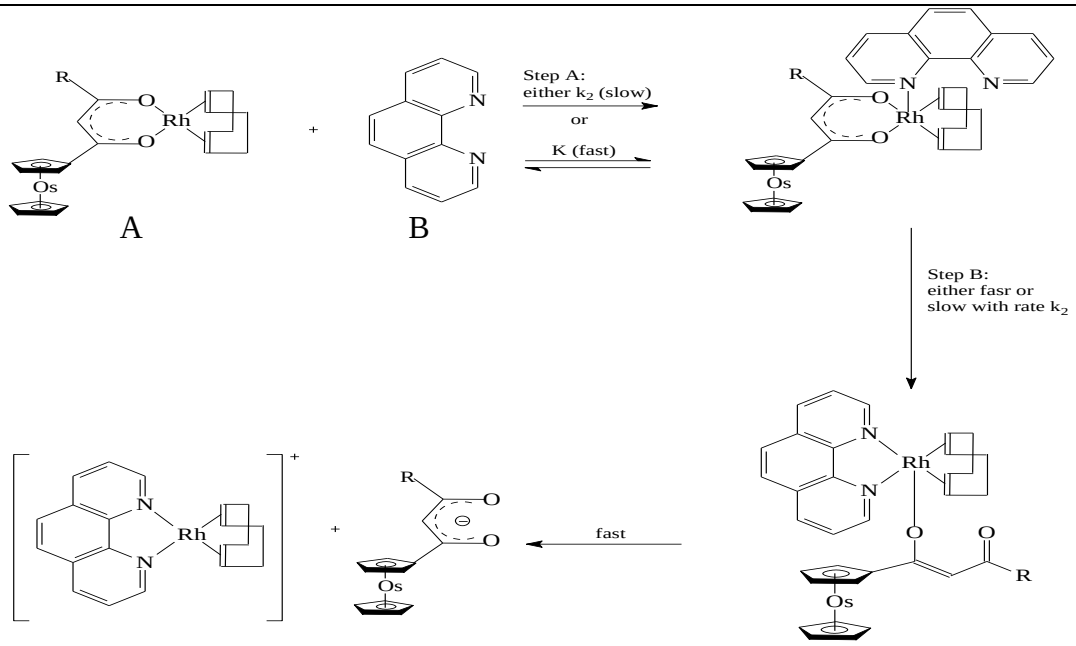

Scheme 3.10. Schematic representation of two kinetically indistinguishable associative mechanisms for the substitution reaction between the [Rh(β-diketonato)(cod)] complexes and 1,10-phenanthroline. R = CF_3, CH_3, C_6H_5, H and Fc.

In the first possible mechanism, step A is slow, with rate constant k_2, and this mechanism gives a theoretical rate law of Rate = k_2[A][B]. By comparison with Equation 3.8 the two k_2 values of each equation are identical.

However, in the second possible mechanism, the theoretical rate law is Rate = k_2K[A][B]. Comparison with Equation 3.8 implies that the measured rate constant k_2 summarized in Table 3.4 is actually the product k_2K.

The first step involves the formation of the five coordinated species in Scheme 3.10. This step is followed by breakage of one of the two Rh-O bonds of the β-diketone coordinated to the rhodium nucleus. To decide which Rh-O bond will most probably break first, a consideration of group electronegativities is instructive. From the data provided in table 3.5, it is clear that k_2 becomes smaller as χ_R, the group electronegativity of the R-group, becomes smaller. To explain this, the β-diketonato ligands with R-groups having large χ_R values intensify the positive charge on the Rhodium(I) core of these complexes. Thus complex **12**, with R = CF_3 and χ_R = 3.01 will have the most positive Rh-center and

complex **15**, with R = ferrocenyl (χ_R= 1.87) will have the least positive Rh center. The nucleophile, 1,10-phenanthroline, will therefore bind faster with complex **12** in step A, of Scheme 3.10 with the rhodium complex B, and the slowest with **15**. In step B, the oxygen atom that lowers the positive charge on the Rh center the most will stay intact, while the other oxygen atom will break its bond with the Rh nucleus. It follows that the O-atom adjacent to the R-group with the largest χ_R value will always break its bond with the Rh center first. The complex containing CF_3, having the largest χ_R value, will thus break Rh-O-bonds next to the CF_3 group the fastest, while **15**, with R = ferrocenyl, will break Rh-O bonds the slowest. Once the first Rh-O bond is broken and the second Rh-N bond has formed the second Rh-O bond will break very fast.

Figure 3.12 depicts the relationship between the group electronegativities applicable to this study.

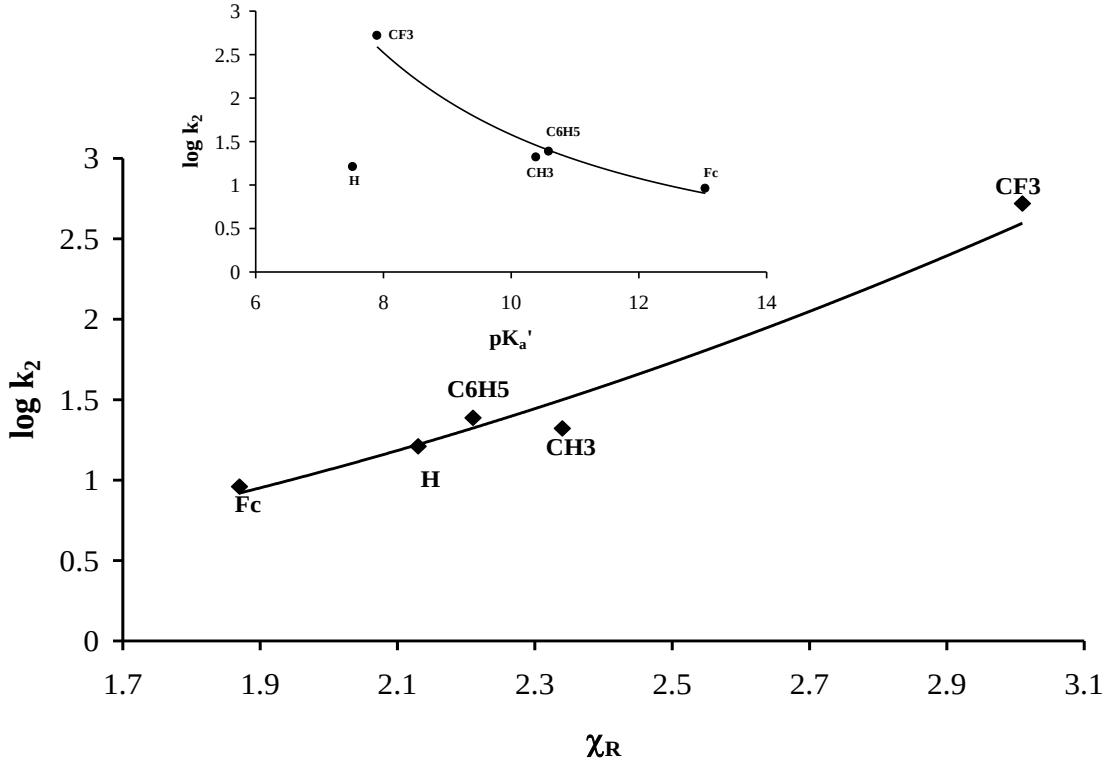

Figure 3.12. The relationship observed between the second order rate constant and group electronegativity, χR, for the substitution reaction of the β-diketonato moiety between [Rh(β-diketonato)(cod)] complexes and 1,10-phenanthroline. Inset: the relationship observed between the second order rate constant and the acid dissociation constant, $pK_a^{/}$.

The general log k_2 vs. $pK_a^{/}$ trend observed indicates that the rate of substitution becomes slower as the $pK_a^{/}$ of the free ligand becomes larger. The only exception to this observation is the β-keto-aldehyde complex [Rh(och)(cod)]. Figure 3.12 inset, shows this relationship graphically. Further research is required to understand why the aldehyde complex, **16**, does not fit the log k_2 / $pK_a^{/}$ graph as well as it fits in the log k_2 / χ_R graph.

A research program is at present underway to determine if the ferrocene and ruthenocene aldehyde complexes behaves similarly in this regard.

3.6. Cyclic Voltammetry

3.6.1. Introduction

Cyclic voltammetry (CV), Oster Young square wave voltammetry (SW) and linear sweep voltammetry (LSV) were conducted on all new osmocene-containing β-diketones, $OcCOCH_2COR$, as well as their associated [Rh(OcCOCHCOR)(cod)] complexes in the solvent electrolyte system $CH_2Cl_2/[NBu_4][B(C_6F_5)_4]$. The effects of the group electronegativity (χ_R) of substituents on the formal reduction potential (E^{01}) and peak anodic potentials (E_{pa}) of the redox-active metallic nuclei of the complex were determined.

Formal reduction potentials (E^{01}), peak cathodic potentials (E_{pc}) and peak anodic potentials (E_{pa}) are reported *vs.* Fc/Fc^+ as an internal standard, but were measured experimentally *vs* an in-house constructed Ag/AgCl reference electrode to minimise overpotentials and liquid junction potentials.

The important metallic redox-active centres studied in the synthesised complex are Oc/Oc^+, $2Rh^I/[2Rh^{II} \rightleftharpoons (Rh^{II})_2] \rightarrow Rh^{III}$ and $2Rc/[2Rc^+ \rightleftharpoons (Rc)_2^{2+}]$ with Oc = osmocenyl and Rc = ruthenocenyl fragments. These redox-active couples vary from being quasi-reversible (defined for the purpose of this study as 90 mV < ΔE < 150 mV) to electrochemically irreversible (defined as ΔE > 150 mV).

Chapter 3
Results and discussion

3.6.2. Osmocene-containing β-diketones

Analyses of the cyclic voltammetry data of the new osmocene-containing β-diketones revealed quasi-reversible to irreversible electrochemistry for the osmium metal core in the osmocene moiety.

Figure 3.13 shows the cyclic voltammograms of Hoctfa (**3**), Hoch (**8**) and Hocfcm (**6**). The CV of **3** (Figure 3.13, Left) is very simple and easily interpretable, the peak labeled 1 represents the chemically reversible and electrochemically irreversible oxidation wave of Oc/Oc^{+}, with $\Delta E > 150mV$ and $i_{pa} / i_{pc} \approx 1.0$. The source of the peak X can not at this stage be assigned with confidence. To research it in detail was also considered outside the borders of this MSc study. It will be the topic of a follow-up study.

The CV of **8** (Figure 3.13, Middle) is still easily interpretable; however an additional feature has been observed. The oxidation of osmocene shows two poorly resolved peaks labeled 1 and 2. Peaks 1 and 2 are so close to each other that even Oster Young square wave voltammetry does not resolve these two peaks to the point that two separate peak potentials can be identified. The source of the two oxidation peaks can be traced to the presence of the keto and enol isomers of (**8**) in solution. On the CV time scale the conversion from keto to enol is slow (see paragraph 3.4), thus it is possible to observe both the keto and enol forms of the β-ketoaldehyde. The equilibrium composition of Hoch, **8**, has 77 % enol and 23 % keto isomers in $CDCl_3$ solutions. The CF_3 substituted species Hoctfa, **3**, exists almost exclusively in the enol form; hence Figure 3.13 left shows only one osmocene CV wave, that of the enol form. Only peak 2 revealed a reduction peak, this is, however, still an electrochemically irreversible oxidation process because $\Delta E > 150$ mV. The absence of a cathodic reduction peak for peak 1 and the lower than expected intensity of the reduction wave of peak 2 is at this stage of our knowledge attributed to be instability of this keto aldehyde, especially when the osmocenyl group is in the oxidized (Os^{III}) state. Once, again the source of the peak labeled X could not be identified.

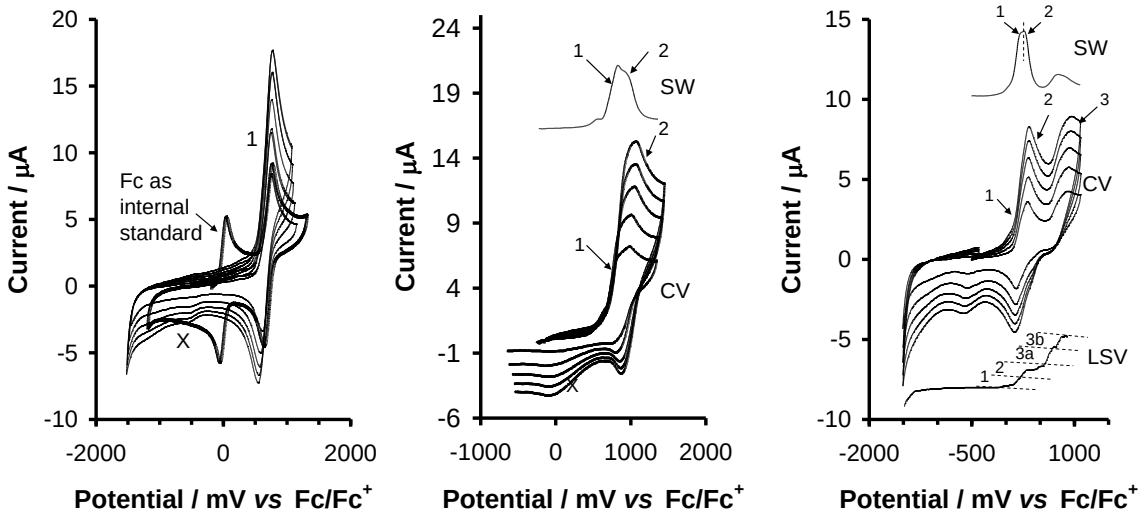

Figure 3.13. The cyclic voltammograms of 2.0 mmol dm^{-3} Hoctfa (**3**) (left), Hoch (**8**) and Hocfcm (**6**) (right), solutions at scan rates 100, 200, 300, 400 and 500 mV s^{-1}. The supporting electrolyte is 0.1 mol dm^{-3} $[NBu_4][B(C_6H_3(CF_3)_2)_4]$ in dichloromethane utilizing a glassy carbon electrode at 25 ºC. The CV of (**3**) (left) also shows a 100 mV s^{-1} scan with free ferrocene as internal marker.

The CV of **6** (Figure 3.13, Right), has two oxidation waves, belonging to the Fc/Fc^+ and Oc/Oc^+ couples respectively. The peaks labeled 1 and 2 are assigned to the electrochemically quasi-reversible and chemically reversible oxidation of the ferrocenyl moiety. Again the existence of two peaks is due to the keto (55% at equilibrium in CD_2Cl_2) and enol (45 % at equilibrium in CD_2Cl_2) forms present in solution. By analogy with the ruthenocene-containing β-diketones of a different study,[8] we assign the lower potential peak, peak 1, to the enol isomer and the higher potential peak, peak 2, to the keto isomer. Peak 3 is assigned to the chemically irreversible oxidation of the osmocenyl moiety.

This peak is very broadened and it is assumed that there are also two oxidation peaks that overlap to the extent that they cannot be separated. Consistent with Hoch, **8**, the instability of the oxidized osmocenyl center disallows observation of the cathodic reduction wave of the oxidized osmocenium center.

Oster Young square wave voltammetry (Figure 3.13, Right top) also does not resolve the enol and keto peaks. However, it can be seen from the linear sweep voltammogram (Figure 3.13, Right bottom) that the oxidation waves of the ferrocenyl moiety and the osmocenyl moiety transfer the same number of electrons. It also shows, consistent with a mixture of keto and enol isomers, two active species associated with the ferrocenyl and osmocenyl redox waves. That peak 1 and peak 3a, and also peak 2 and peak 3b, are not equal in size clearly demonstrates that the keto-enol equilibrium position of the fully reduced species does not have the same content of keto and enol isomers as the partially oxidized (or the fully oxidized) species.

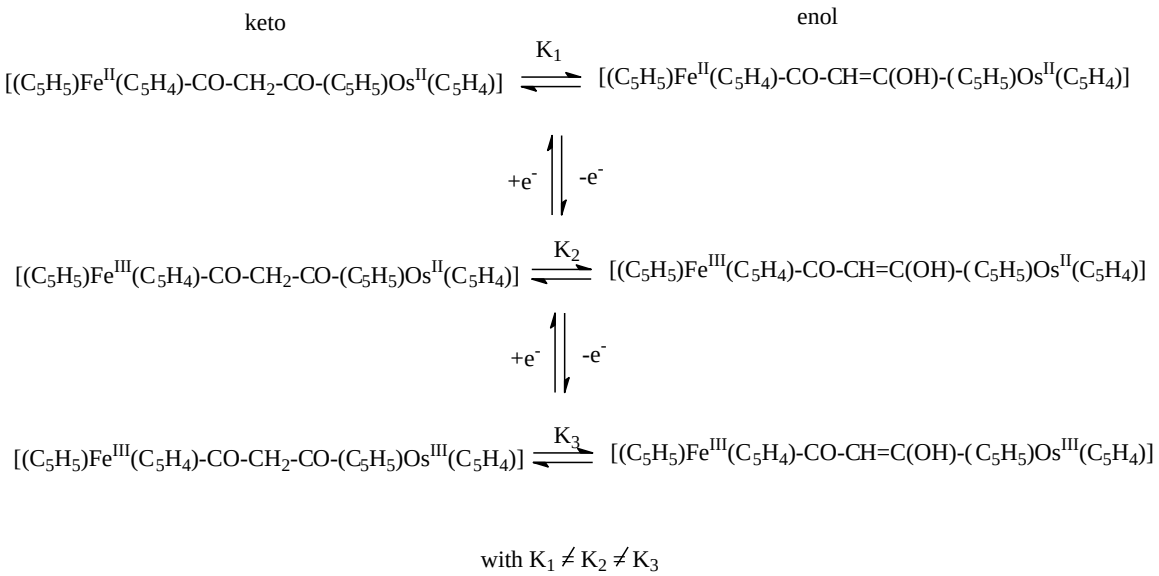

Figure 3.14 (Left) shows the cyclic voltammograms, SW and LSV of Hocrcm, **7**. This CV is fairly complex and involves both the keto and enol forms of **7** as well as an additional feature which involves the dimerisation of the ruthenocenium species, $(C_5H_5\text{-}Ru^{III}\text{-}C_5H_4)^+$.[7, 8] In principle one would expect two oxidation waves, 1 and 2, for the osmocenyl group, one for the keto and one for the enol isomer. One would also expect two oxidation waves, 3 and 4, for the ruthenium center, which are associated with the keto and enol isomers of Hocrcm, **7**. In practice, peaks 2 and 3 were found to overlap. Because dimerisation of the Rc^+ fragment to $[Rc\text{-}Rc]^{2+}$ occurs fast, reduction of the ruthenocenium fragment according to the reaction $Rc^+ \rightarrow Rc$ is either absent or only occurring in minute quantities for Hocrcm, **7**. The expected osmocenium cathodic reduction waves for peaks 1 and 2, here labeled 1_c and 2_c, were very weak, and are again considered the result of osmocenium, Oc^+, instability. The reduction peaks X (keto

isomer) and Y (enol isomer) are consistent with the reduction of a ruthenocenium dimer. The broadness of peaks X and Y is consistent with a mixture of many different isomers in solution. The $(C_5H_5)Ru^{III}(C_5H_4)$ center is a highly unstable species which is known to dimerise to form Ru^{III}-Ru^{III} bonds. Hocrcm, **7**, may dimerise according to the scheme shown in Figure 3.14 (below)[8]. An interesting observation from the fastest CV scan (Figure 3.14, Top left), is that no electrode deposition took place. It can be seen from the second oxidation cycle of this 500 mV s^{-1} scan that, apart from wave 1, cycle 2 overlaps almost exactly with the first cycle.

Figure 3.14 (Right) shows the comparative cyclic voltammograms of the osmocene-containing β-diketones at scan rate 200 mV s^{-1} and 25 ºC. The comparative electrochemical data resulting from these voltammograms are summarised in Table 3.6. A direct relationship was found between the E^{01} of the enol form of the Oc/Oc^+ couple and the $pKa^{/}$ of the β-diketone or group electronegativity of the R-group of the β-diketone (see Figure 3.15). The general trend between the E_{pa} of Oc/Oc^+ couple and group electronegativity of the R-group of the β-diketone is that $E^{o/}$ increases as the group electronegativity increases. This is consistent with groups having higher group electronegativities withdrawing more electron density from the osmocenyl group, making it more difficult to oxidise it to the osmocenium species, Oc^+. As for the $E^{o/+}$ - $pK_a^{/}$ plot, Fig 3.15 right, the best line was constructed through the $pK_a^{/}$ points for the CF_3, CH_3 and phenyl-containing betadiketones. When the pK_a of the β-diketone Fc-CO-CH_2-CO-Oc, (**7**) was superimposed onto this graph, it did not fit. This happened because when the osmocene fragment of (**7**) is oxidised, the ferrocenyl group has already been oxidised electrochemically to ferrocenium species. Consequently the electroactive species in solution when the osmocenyl species is oxidised is NOT Fc-CO-CH_2-CO-Oc, but rather

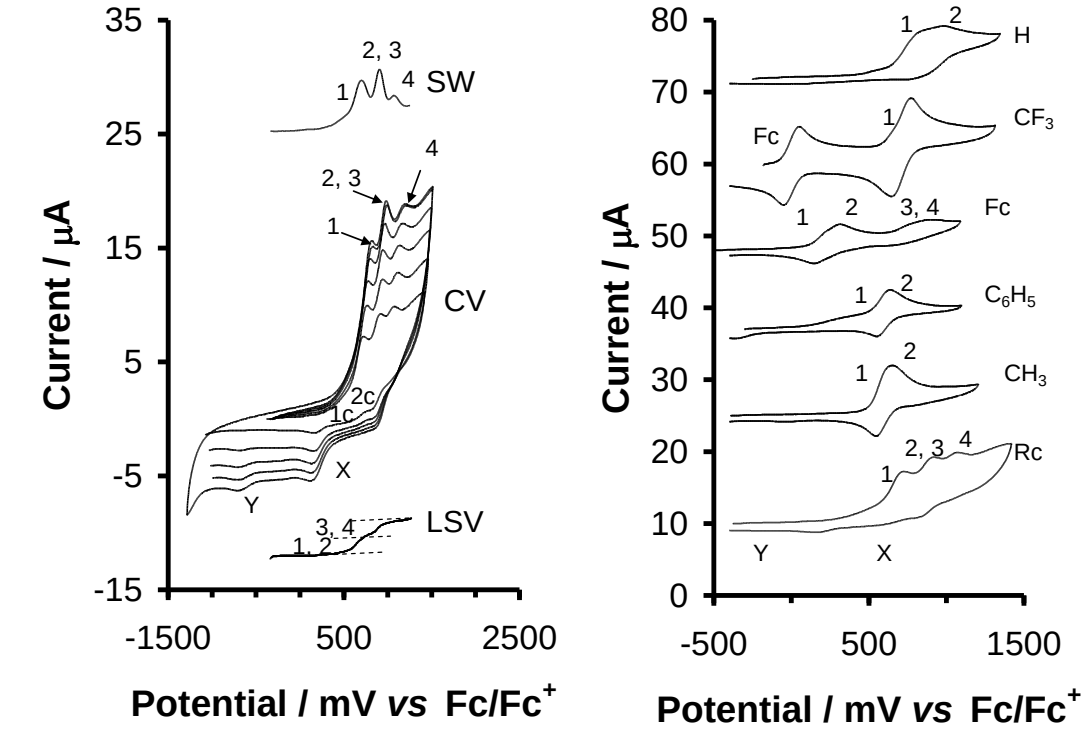

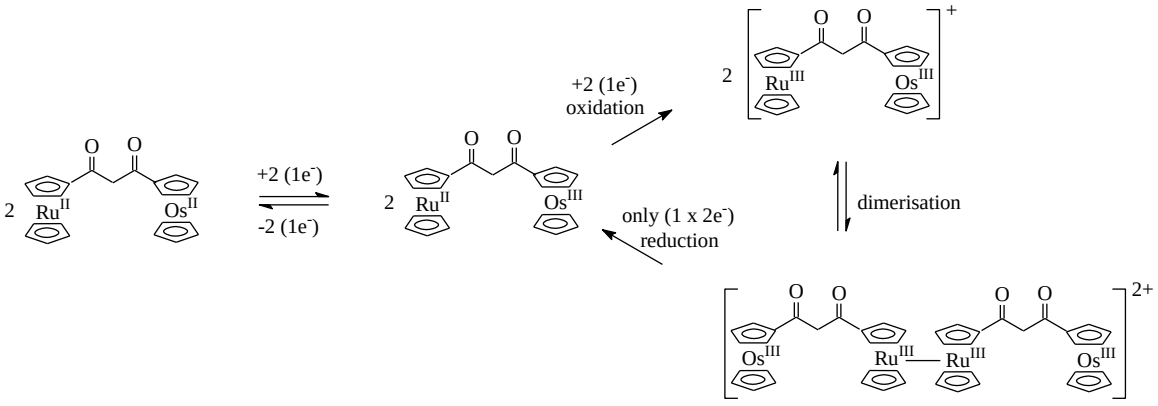

Figure 3.14. Top left: the cyclic voltammogram of a 2.0 mmol dm^{-3} Hocrcm (**7**) solution at scan rates 100, 200, 300, 400 and 500 mV s^{-1}. Top right: CV's of 3-8 at scan rate 500 mV s^{-1}. The supporting electrolyte is 0.1 mol dm^{-3} $[NBu_4][B(C_6H_3(CF_3)_2)_4]$ in dichloromethane utilizing a glassy carbon electrode. Bottom: Schematic representation of the oxidation and proposed dimerisation of the ruthenocene-containing β-diketone Hocrcm, **7**. Only the keto isomer is shown in this demonstration but many enol structures can also be drawn for this scheme.

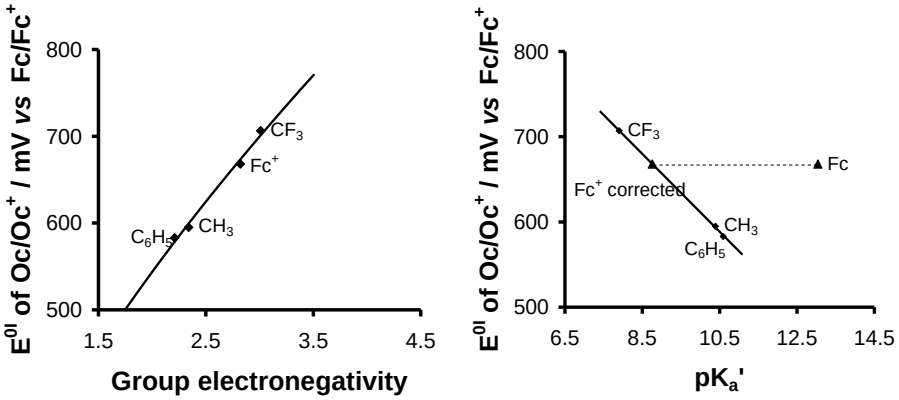

Figure 3.15. Left: The relationship peak anodic potentials between and group electronegativity (χ_R) for the first oxidation for the osmocene-containing β-diketones at scan rate 200 mV s^{-1}. Right: The relationship between peak anodic potentials and pK_a' for the first oxidation for the osmocene-containing β-diketones at scan rate 200 mV s^{-1}. The pK_a' of **6** was adjusted for the ferrocenium.

Fc^+-CO-CH_2-CO-Oc. By fitting the osmocene formal reduction potential for Fc-CO-CH_2-CO-Oc, **7**, to this graph, the pK_a' of Fc^+-CO-CH_2-CO-Oc may be estimated as 8.76.

Table 3.6. The cyclic voltammetric data obtained from the voltammograms (versus Fc/Fc^+) for the osmocene-containing β-diketone complexes at scan rate 200 mV s^{-1}. E_{pa} = peak anodic potentials, E_{pc} = peak cathodic potentials, E^{o1} = formal reduction potential, i_{pa} = peak anodic current and i_{pc} = peak cathodic current.

v / mV s^{-1}	E_{pa1} / mV	ΔE / mV	E^{01} / mV	i_{pa} / μA	i_{pa} / i_{pc}	E_{pa2} / mV	ΔE / mV	E^{01} / mV	i_{pa} / μA	i_{pa} / i_{pc}
Hoch, **8**, χ_H = 2.12										
100	840 [a]	-[b]	-	2.1	-	987	77 [b]	949	3.2	-
200	849 [a]	74 [b]	812	4.0	1.0	1006	111 [b]	951	4.2	0.8
300	921 [a]	79 [b]	882	5.9	0.9	1051	136 [b]	983	5.2	0.8
400	948 [a]	92 [b]	909	7.8	0.7	1068	138 [b]	999	6.2	0.7
500	956 [a]	92 [b]	910	9.8	0.5	1072	152 [b]	996	7.2	0.7

v / mV s^{-1}	E_{pa1} / mV	ΔE / mV	E^{01} / mV	i_{pa} / μA	i_{pa} / i_{pc}	$E_{paX\ or\ Y}$ / mV	i_{pc} / μA
Hoctfa, **3**, χ_{CF3} = 3.01							
100	773	149	699	2.5	0.7	-519	-
200	783	153	707	5.1	0.7	-608	0.2
300	789	170	704	7.7	0.7	-633	0.4
400	791	197	693	10.3	0.7	-633	0.6
500	795	218	686	13.0	0.7	-649	0.8

ν / mVs^{-1}	E_{pa1} / mV	ΔE / mV	E^{01} / mV	i_{pa} / µA	i_{pa} / i_{pc}	E_{pa2} / mV	i_{pa} / µA	E_{pa3} / mV	i_{pa} / i_{pc}	E_{pa4} / mV	i_{pc} / µA
Hocfcm, **6**, χ_{Fc+} = 2.82											
100	259 [a]	127	196	2.4	0.8	324[c]	1.6	751[c]	1.8	904[c]	1.8
200	261 [a]	131	196	3.2	0.8	331[c]	2.1	760[c]	2.5	916 [c]	2.6
300	263 [a]	144	191	4.0	0.8	334[c]	2.6	776[c]	3.1	933 [c]	3.0
400	265 [a]	146	192	4.8	0.8	344[c]	3.1	810[c]	3.7	953 [c]	3.6
500	268 [a]	154	191	5.9	0.8	346[c]	3.6	817[c]	4.2	965 [c]	4.3

ν / mV s^{-1}	E_{pa1} / mV	ΔE / mV	E^{01} / mV	i_{pa} / µA	i_{pa} / i_{pc}
Hoca, **4**, χ_{CH3} = 2.34					
100	618	75	581	6.5	0.4
200	633	76	595	8.2	0.5
300	635	80	595	9.9	0.6
400	635	85	592	11.6	0.7
500	642	90	597	13.4	0.8

ν / mV s^{-1}	$E_{pc1\ and\ 2}$ / mV	ΔE / mV	E^{01} / mV	i_{pa} / µA	i_{pa} / i_{pc}
Hbocm, **5**, χ_{C6H6} = 2.21					
100	630[d]	103	579	2.6	0.9
200	633 [d]	100	583	4.4	0.9
300	646 [d]	112	590	6.2	0.9
400	649 [d]	143	577	8.0	0.8
500	648 [d]	146	575	9.8	0.8

ν / mVs^{-1}	E_{pa1} / mV	i_{pa} / µA	$E_{pa2\ \&\ 3}$ / mV	i_{pa} / µA	E_{pa3} / mV	i_{pa} / i_{pc}	E_{paX} / mV	i_{pc} / µA	$E_{pa\ Y}$/ mV	i_{pc} / µA
Hocrcm, **7**, χ_{Rc} = 1.99										
100	729	2.6	926 [d]	4.8	1082	3.4	150	0.4	-740	0.2
200	730	3.9	950 [d]	5.3	1128	4.2	134	0.7	-718	0.4
300	775	5.2	951 [d]	5.8	1149	5.0	1171	1.1	-733	0.7
400	784	6.4	973 [d]	6.3	1184	5.8	109	1.5	-733	1.0
500	826	7.7	1000 [d]	6.7	1208	6.7	106	1.9	-732	1.3

[a] not exact value but estimate, due to overlapping peaks.

[b] ΔE was determined by estimation.

[c] E^{01} was not being determined due to overlapping of peaks.

[d] Peaks 1 and 2 (or 2 and 3) are overlapping to the extent that they cannot be separated; this is the most prominent peak potential.

3.6.3. Rhodium complexes

Analysis of the cyclic voltammetry data of the new [Rh(β-diketonato)(cod)] complexes in CH_2Cl_2/$[NBu_4][B(C_6F_5)_4]$ at -20 ºC were complex. All exhibit an irreversible anodic oxidation peak which corresponds to the oxidation of rhodium(I) according to $2Rh^I/[2Rh^{II} \rightleftharpoons (Rh^{II})_2]$ and a second oxidation peak that is consistent with the oxidation of the dimer according to $[2Rh^{II} \rightleftharpoons (Rh^{II})_2] \rightarrow 2Rh^{III}$. Two reversible to irreversible oxidation peaks of the Oc/Oc^+ couple could also be detected. The temperature of -20 ºC was chosen because CVs recorded at room temperature were much more complex to interpret.

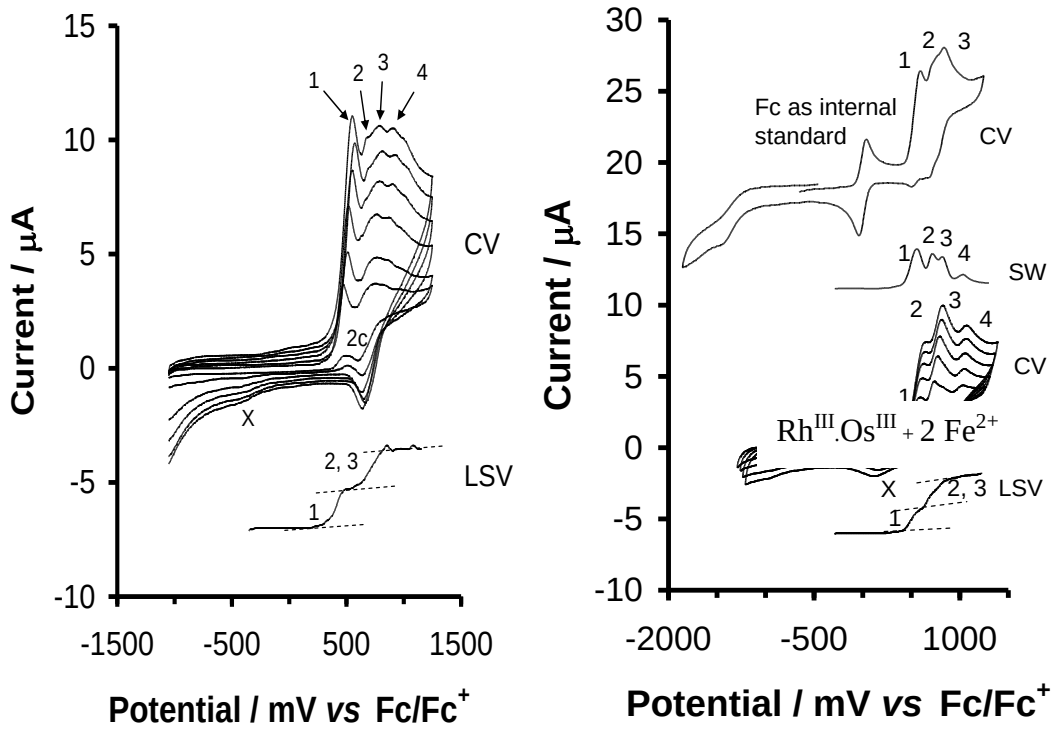

Figure 3.16. Left: The cyclic voltammogram of a 2.0 mmol dm^{-3} [Rh(oca)(cod)], **13**, solution at scan rates 50, 100, 200, 300, 400 and 500 mV s^{-1}. The supporting electrolyte is 0.1 mol dm^{-3} $[NBu_4][B(C_6H_3(CF_3)_2)_4]$ in dichloromethane utilizing a glassy carbon electrode at -20 ºC. Right: The cyclic voltammogram of a 2.0 mmol dm^{-3} [Rh(octfa)(cod)], **12**, solution at scans rates 50, 100, 200, 300, 400 and 500 mV s^{-1}. The SW

diagram was recorded at 10 Hz, while the LSV was recorded at 2 mV s^{-1}. The top CV has free ferrocene as internal standard in solution. Note the absence of peak 4.

Figure 3.16 shows the cyclic voltammograms of [Rh(OcCOCHCOCH$_3$)(cod)] (**13**) and [Rh(OcCOCHCOCF$_3$)(cod)] (**12**). The CV of **13** (Figure 3.16, Left) is rather complex and reveals four oxidation peaks. The peaks labeled 1 and 4 are assigned to the rhodium oxidation and the peaks labeled 2 and 3 are assigned to the osmocenyl moiety's oxidation. Peak 1 represents the oxidation of Rh^{I} to Rh^{II}. It is known that Rh^{II} is short-lived and often forms a diamagnetic dimer.[9] The existence for the two oxidation peaks for the osmocenyl moiety is consistent with the formation of rhodium dimeric species. Thus it is proposed that peak 1 represents oxidation of Rh^{I} according to $2Rh^{I}/[2Rh^{II} \rightleftharpoons (Rh^{II})_2]$. The formation of the Rh^{II}-Rh^{II} dimer is schematically shown in Scheme 3.11.

Due to the existence of the dimer, two osmocenyl moieties are contained in the dimer. Due to intramolecular electronic communication these two osmocenyl moieties do not oxidize at exactly the same potential, as shown by the existence of peaks 2 and 3 (Figure 3.16). The peak labeled 4 is assigned to the oxidation of Rh^{II} to Rh^{III}, this is thus the oxidation of the Rh^{II}-Rh^{II} dimer to two Rh^{III} monomers. Peak 2c is the only reduction peak, which is associated with the osmocenyl oxidation peak 2. This oxidation wave is electrochemically quasi-reversible to irreversible. The peak labeled X could possibly be assigned to the reduction of Rh^{III}; this was however not investigated, as it was considered outside the boundaries of this study. From the LSV (Figure 3.16, Left bottom) it can be seen that the rhodium oxidation and the osmocenyl oxidation transfer the same number of electrons.

For the osmocene group it is definitely one electron. This is further proof that peak 1 corresponds to a one-electron transfer process, implying Rh^{I} is oxidized to Rh^{II}.

Chapter 3
Results and discussion

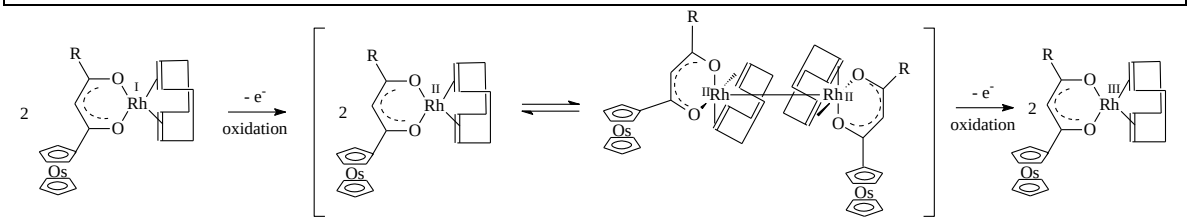

Scheme 3.11. The schematic representation of the formation of the rhodium(II) dimer *via* a Rh^{II}-Rh^{II} metal bond.

The CV of [Rh(octfa)(cod)] (**12**) displayed in Figure 3.16 (Right) is very similar to the CV of **13**. The peak labeled 1 is assigned to the oxidation of Rh^{I} to Rh^{II}, and is associated with the process $2Rh^{I}/[2Rh^{II} \rightleftharpoons (Rh^{II})_2]$. Peaks 2 and 3 are assigned to the electrochemically irreversible oxidation of osmocene and peak 4 is assigned to the oxidation of Rh^{II} to Rh^{III} according to the reaction $[2Rh^{II} \rightleftharpoons (Rh^{II})_2] \rightarrow Rh^{III}$. Lastly the peak labeled X could then be associated with the reduction of Rh^{III} but peak X was not investigated

Resolution of peaks 2 and 3 is improved by SW, which clearly shows that there are two osmocenyl peaks. The LSV showed that the Rh oxidation (peak 1) and the Oc oxidation (peaks 2 and 3 combined) transfer the same number of electrons.

An interesting observation from the CV with Fc as an internal standard (Figure 3.16, Right) is that peak 4 disappears. This observation is consistent with the argument that the ferrocene group is first oxidized to ferrocenium and the oxidized ferrocenium Fc^{+} reacts chemically with Rh^{II} to give Rh^{III}. A possible reaction scheme to explain this is as follows:

$$Fe^{2+} \xrightarrow{\text{electrochemically}} Fe^{3+}$$

$$Rh^{I}\text{-}Os^{II} \xrightarrow{\text{electrochemically}} Rh^{II}\text{-}Os^{II}$$

$$Rh^{II}\text{-}Os^{II} \xrightarrow{\text{dimerises}} Os^{II}\text{-}Rh^{II}\text{-}Rh^{II}\text{-}Os^{II}$$

$$Os^{II}\text{-}Rh^{II}\text{-}Rh^{II}\text{-}Os^{II} \xrightarrow{\text{electrochemically}} Os^{III}\text{-}Rh^{II}\text{-}Rh^{II}\text{-}Os^{II}$$

$$Os^{III}\text{-}Rh^{II}\text{-}Rh^{II}\text{-}Os^{II} \xrightarrow{\text{electrochemically}} Os^{III}\text{-}Rh^{II}\text{-}Rh^{II}\text{-}Os^{III}$$

$$Os^{III}\text{-}Rh^{II}\text{-}Rh^{II}\text{-}Os^{II} + 2\,Fe^{3+} \xrightarrow[\text{complete before the potential of peak 4 oxidation is reached}]{\text{slow chemical oxidation but fast enough to be}} 2\,Rh^{III}\text{-}Os^{II} + 2\,Fe^{2+}$$

If the above scheme is correct it could then be assumed that if an Rh complex contains a ferrocenyl fragment, the ferrocene could act as an oxidizing agent and oxidize the Rh^{II} to Rh^{III} chemically and no Rh^{II} oxidation peak would be observed. This was actually observed for [Rh(ocfcm)(cod)], **15**, (Figure 3.17, Left).

Complex **15** shows the chemically reversible and electrochemically irreversible oxidation wave of the ferrocenyl moiety (peak 1), the oxidation of Rh^{I} to the Rh^{II} dimer (peak 2) and the two oxidation peaks of the osmocenyl moieties from the dimer (peaks 3 and 4).

There is, however no peak 5 which could be associated with the oxidation of Rh^{II} to Rh^{III}. Results are therefore consistent with an interpretation that the oxidized intra-molecular ferrocenium moiety, Fc^{+}, oxidized Rh^{II} to Rh^{III} before the potential was reached at which Rh^{II} is oxidized to Rh^{III} electrochemically.

Cyclic voltammograms of [Rh(OcCOCHCOR)(cod)] complexes at a scan rate of 200 mV s^{-1} are stacked for comparative purposes on top of each other in Figure 3.17, Right). The electrochemical data of these [Rh(OcCOCHCOR)(cod)] complexes are summarized in Table 3.6.

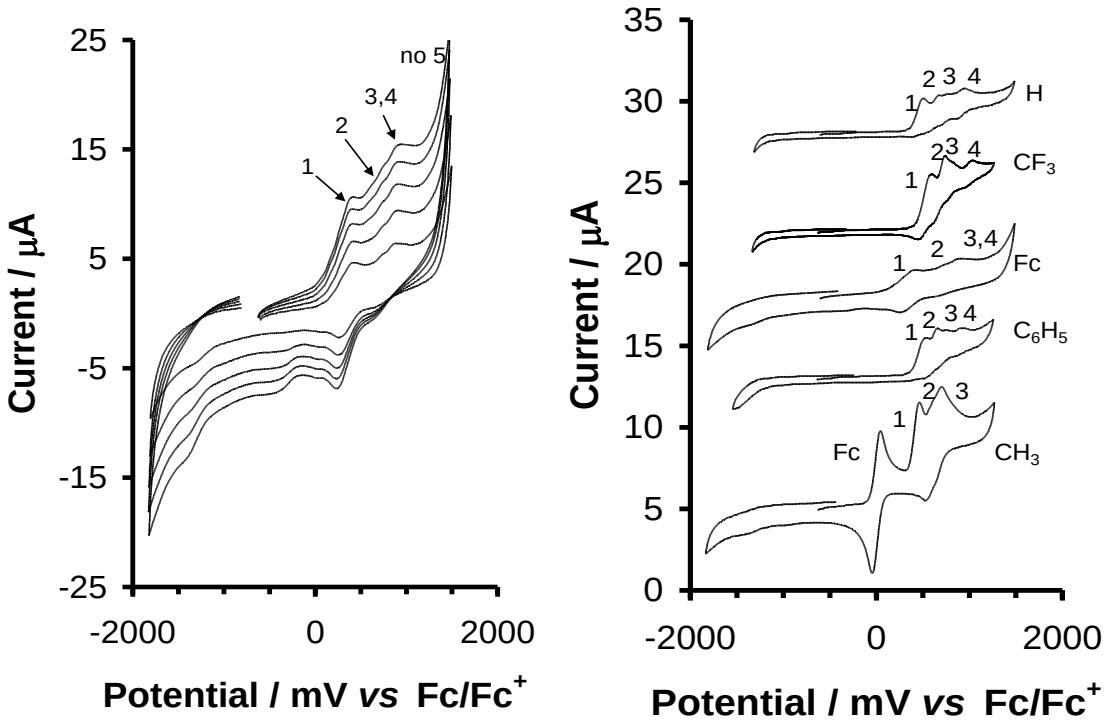

Figure 3.17. Left: The cyclic voltammogram of a 2.0 mmol dm^{-3} [Rh(ocfcm)(cod)], **15**, solution at scan rates 50, 100, 200, 300, 400 and 500 mV s^{-1}. The supporting electrolyte is 0.1 mol dm^{-3} $[NBu_4][B(C_6H_3(CF_3)_2)_4]$ in dichloromethane utilizing a glassy carbon electrode at -20 ºC. Right: The cyclic voltammograms (200 mV s^{-1}) of 2.0 mmol dm^{-3} solutions of [Rh(OcCOCHCOR)(cod)].

No direct relationship was found between the E_{pa} of the $2Rh^{I}/[2Rh^{II} \rightleftharpoons (Rh^{II})_2]$ couple and the pKa/ of the free β-diketone or group electronegativity of the R-group of the β-diketone (see Figure 3.18). However the general trend between the E_{pa} of the $2Rh^{I}/[2Rh^{II} \rightleftharpoons (Rh^{II})_2]$ couple and the group electronegativity of the R-group of the β-diketone was found to be as the group electronegativity of the R-group increases, the E_{pa} of the $2Rh^{I}/[2Rh^{II} \rightleftharpoons (Rh^{II})_2]$ couple increases. This is because as the group electronegativity increases the rhodium centre becomes more positive and thus more difficult to oxidize. The general trend between the E_{pa} of the $2Rh^{I}/[2Rh^{II} \rightleftharpoons (Rh^{II})_2]$ couple and the pKa/ of the β-diketone is as the pKa/ increases, the E_{pa} decreases.

Table 3.6. The cyclic voltammetric data obtained from the voltammograms (versus Fc/Fc^{+}) for [Rh(β-diketonato)(cod)] complexes the a scan rate 200 mV s^{-1}. E_{pa} = peak anodic potentials, E_{pc} = peak cathodic potentials, E^{o1} = formal reduction potential, i_{pa} = peak anodic current and i_{pc} = peak cathodic current.

ν / mV s^{-1}	E_{pa1} / mV	i_{pa} / μA	$E_{pa2,3}$ / mV	ΔE / mV	E^{01} / mV	i_{pa} / μA	i_{pa}/ i_{pc}	E_{pa4}/ mV	i_{pa} / μA	$E_{pcX\ or\ Y}$/ mV	i_{pc} / μA
[Rh(och)(cod)], **16,** χ_H = 2.12											
100	510	2.3	678 [a]	-	-	1.9	-	954	1.0	-	-
200	528	2.8	706 [a]	66	673	2.1	0.4	958	1.3	-	-
300	545	4.3	723 [a]	85	681	2.4	0.4	969	1.6	3	0.1
400	554	4.8	737 [a]	104	685	2.7	0.3	978	1.9	-26	0.1
500	568	5.3	756 [a]	123	695	3.0	0.3	988	2.2	-46	0.2

ν / mV s^{-1}	E_{pa1} / mV	i_{pa} / μA	$E_{pa2,3}$ / mV	i_{pa} / μA	E_{pa4} / mV	ΔE / mV	E^{01} / mV	i_{pa} / μA	i_{pa} / i_{pc}	$E_{pcX\ or\ Y}$/ mV	i_{pc} / μA
[Rh(octfa)(cod)], **12,** χ_{CF3} = 3.01, pK_a = 9.99											
100	596	3.1	749 [a]	2.1	1044	-	-	1.9	-	-	-
200	624	3.8	743 [a]	2.7	1053	-	-	2.2	-	-	-
300	636	4.7	802 [a]	3.4	1062	-	-	2.5	-	195	1.2
400	651	5.6	826 [a]	4.1	1072	448	848	2.8	0.4	140	1.6
500	664	6.4	832 [a]	4.7	1075	451	849	3.1	0.5	103	2.0

ν / mV s^{-1}	E_{pa1} / mV	ΔE / mV	E^{01} / mV	i_{pa} / μA	i_{pa} / i_{pc}	$E_{pa2,3}$ / mV	i_{pa} / μA	E_{pa4} / mV	i_{pa} / μA
[Rh(ocfcm)(cod)], **15,** χ_{Fc+} = 1.87, , pK_a (**15**) = 9.99, pK_a (**15**$^{+}$) = 8.76									
100	354[a]	264	222	3.6	1.0	612	2.3	844	2.7
200	352[a]	106	299	4.2	1.0	624	2.9	848	3.3
300	392[a]	89	348	4.9	1.0	670	3.6	880	4.0
400	386[a]	86	343	5.6	1.0	674	4.3	880	4.7
500	386[a]	90	341	6.3	1.0	686	4.9	887	5.4

ν / mV s^{-1}	E_{pa1} / mV	i_{pa} / μA	$E_{pa2,3}$ / mV	ΔE / mV	E^{01} / mV	i_{pa} / μA	i_{pa} / i_{pc}
[Rh(oca)(cod)], **13,** χ_{CH3} = 2.34, pK_a = 9.99							
100	465	4.9	703 [a]	180	612	5.7	0.6
200	481	6.7	715 [a]	174	628	6.9	0.6
300	495	8.5	725 [a]	182	634	8.1	0.7
400	505	10.3	737 [a]	198	638	9.3	0.7
500	516	12.2	744 [a]	204	642	10.6	0.7

ν / mV s^{-1}	E_{pa1} / mV	i_{pa} / μA	E_{pa2} / mV	i_{pa} / i_{pc}	E_{pa3} / mV	i_{pa} / μA	E_{pa4} / mV	i_{pa} / μA
[Rh(bocm)(cod)], **14,** χ_{C6H5} = 2.21, pK_a = 9.99								
100	543	1.9	663	1.5	755[b]	1.0	929	1.3
200	572	2.3	697	1.8	767[b]	1.1	938	1.4
300	596	2.7	712	2.1	775[b]	1.3	941	1.5
400	596	3.1	708	2.4	799[b]	1.5	926	1.6
500	609	3.5	727	2.7	810[b]	1.7	935	1.7

[a] Poorly resolved peaks, ΔE and E^{01} were determined with the most prominent peak.

[b] Very poorly resolved at high scan rates, not exact value but an estimate

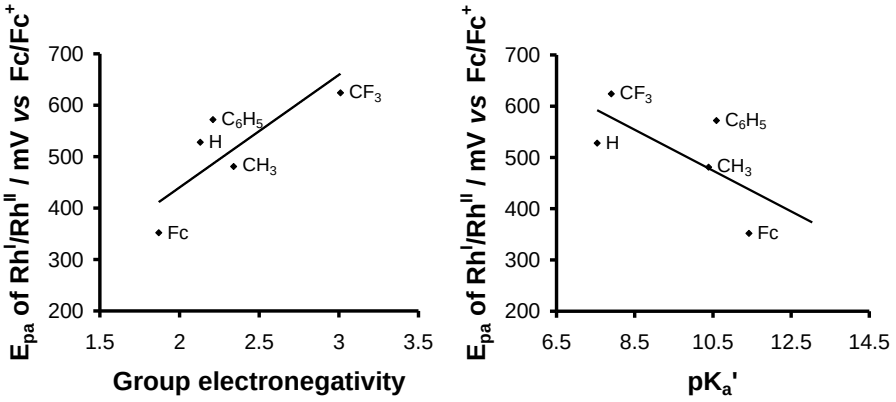

Figure 3.18. Left: The relationship between peak anodic potentials and group electronegativity (χ_R) for the first Rh oxidation for [Rh(OcCOCHCOR)(cod)] complexes at scan rate 200 mV s^{-1}. Right: The relationship between peak anodic potentials and $pK_a^{/}$ of the free β-diketone for the first Rh oxidation for the [Rh(OcCOCHCOR)(cod)] complexes at scan rate 200 mV s^{-1}.

References:

[1] P.J. Graham, R.V. Lindsay, G.W. Parshall, M.L. Peterson and G.M. Whitman, *J. Am. Chem. Soc*., 3416, **79** (1957).

[2] J. Chatt and L.M. Venanzi, *J. Am.Chem.Soc*., 4735, **79** (1957).

[3] W.C. du Plessis, W.L. Davies, S.J. Cronje and J.C. Swarts, *Inorg. Chim. Acta*, 97, **314** (2001).

[4] S.H. Maron and J.B. Lando, *Fundamentals of Physical Chemistry*, Macmillan Publishing Co. Inc., New York., p.326 (1974).

[5] J.H. Espenson, Chemical kinetics and reaction mechanism, McGraw-Hill, New York, p.46 (1995).

[5] J.C. Swarts, unpublished results.

[6] T.G. Vosloo, W.C. du Plessis and J.C. Swarts. *Inorg. Chim. Acta*., 188, **331** (2002).

[7] S. Trupia, A. Nafady and W.E. Geiger, *Inorg. Chem.*, 5480, **42**, (2003).

[8] E. Erasmus, Ph.D. *Study, Synthetic, kinetic and electrochemical aspects of ferrocene- and ruthenocene-containing titanium(IV) complexes with biomedical applications*, University of the Free State, R.S.A., 2005.

[9] E.B. Boyer and S.D. Robinson, *Coord. Chem. Rev.*, 109, **50**, (1983).

Chapter 3
Results and discussion

Chapter 4
Experimental

4.1. Introduction

In this chapter all experimental procedures, reaction conditions and techniques are described.

4.2. Materials

Solid reagents (Merck, Strem and Aldrich) employed in preparations were used without further purification. Liquid reagents were purchased from Aldrich and used without further purification. Solvents were distilled prior to use and water was double distilled. Organic solvents were dried according to published methods.[1]

4.3. Techniques and apparatus

4.3.1. Chromatography

Column chromatography was performed on Kieselgel 60 (Merck, grain size 0.063 - 0.2 mm, eluent ether:hexane = 1:1 by volume unless otherwise stated. Thin layer chromatography was used to monitor reaction progress, and to determine the retention factor (R_f) of the compound for the specific eluting solvents.

4.3.2. Melting point (m.p.) determination

Melting points (m.p.) were determined with a Reichert Thermopan microscope with a Koffler hot-stage and are uncorrected.

4.3.3. Proton Nuclear Magnetic Resonance (^{1}H NMR) spectroscopy

Proton nuclear magnetic resonance spectra (^{1}H NMR) measurements at 292 K were recorded on a Bruker Advance DPX 300 MHz NMR spectrometer. Chemical shifts are reported as δ-values (ppm) relative to tetramethylsilane (δ=0.00 ppm).

4.3.4. Infrared (IR) spectroscopy

Infrared spectra (wavenumber /cm^{-1}) were obtained with the use of a Digilab-Menlin 3.0 spectrometer with data processor. Both solid and liquid samples were recorded by placing a small amount of the material on the detecting plate of the machine. This machine does not need a liquid solvent or potassium bromide matrix to support samples when obtaining IR spectra.

UV-spectrophotometric measurements were made with a computer controlled Cary 50 UV-Visible spectrophotometer. Methanol was used as solvent unless otherwise indicated.

pH readings were obtained using an Orion model SA 720, equipped with a glass electrode. The pH meter was calibrated using buffers at pH 7.00 and 10.00. The temperature was controlled using a water bath to within 25.0 ^{o}C ± 0.1 ^{o}C.

4.3.5. Electrochemistry

Measurements on ca. 2.0 mmol dm^{-3} solutions of the complexes in dichloromethane containing 0.10 mmol dm^{-3} tetrabutylammonium tetrakis(pentafluorophenyl)borate as supporting electrolyte were conducted under a blanket of purified argon at 25 ˚C, -5 ˚C and -35 ˚C utilizing a BAS 100 B/W electrochemical workstation interfaced with a personal computer. A three-electrode cell, which utilized a Pt auxiliary electrode, a glassy carbon working electrode (surface area 0.0707 cm^2) and an in-house constructed Ag/AgCl reference electrode was employed. All temperatures were kept constant to within 0.5 ˚C. Successive experiments under the same experimental conditions showed that all formal reduction and oxidation potentials were reproducible within 5 mV. Experimentally potentials were referenced against an Ag/AgCl reference electrode, but results are presented referenced against ferrocene as an internal standard. To achieve this, each experiment were performed first in the absence of ferrocene and then repeated in the presence of < 1 mmol dm^{-3} ferrocene. Data were then manipulated on a Microsoft Excel worksheet to set the formal reduction potentials of the Fc/Fc^{+} couple at 0 V.

Chapter 4
Experimental

4.4. Synthesis

4.4.1. Synthesis of acetyl osmocene (Scheme 3.1.a)

Osmocene (0.3974 g; 1.24 mmol) was slowly added to a mixture containing acetic anhydride (40 cm^3) and 85% phosphoric acid (5 cm^3; 4.25 g; 4.34 mmol) under an argon atmosphere, while the reaction was kept cold on ice. Argon previously had been passed through the acetic anhydride and phosphoric acid for 20 minutes. The reaction mixture was then allowed to reflux for 4 hours at 80 ^oC. The mixture was cooled to room temperature, opened to the atmosphere and neutralized with aqueous sodium hydroxide for 2 hours. The reaction mixture was extracted into dichloromethane (DCM) and the layers separated. The organic layer was washed with water (3 x 100 cm^3) and dried with $MgSO_4$. (R_f =0.49). Yield: 0.3104 g (78.12 %); m.p. 131-133 ^oC; δ_H (300 MHz, $CDCl_3$) 2.24 (3H; s; CH_3), 4.81 (5H; s; C_5H_5), 4.96 (2H; t; C_5H_4) and 5.24 (2H; t; C_5H_4).

4.4.2. Synthesis of metallocene methyl esters (scheme 3.1.b)

4.4.2.1. Synthesis of methyl ferrocenoate

This compound was obtained in a three step synthesis *via* 2-chlorobenzoylferrocene and ferrocenecarboxylic acid.

(i) Synthesis of 2-chlorobenzoyl ferrocene

Ferrocene (37.2 g; 0.2 mol) and 2-chlorobenzoyl chloride (25.4 cm^3; 35 g; 0.2 mol) were dissolved in DCM (250 cm^3). The solution was stirred under nitrogen and placed in an ice bath. Over a period of 2 hours $AlCl_3$ (28 g; 0.2 mol) was added in small portions in order to keep the temperature below 5 ^oC. After addition, the reaction was kept cool for 15 minutes and then stirred at room temperature for 4 hours. The resulting mixture was cooled and H_2O (200 cm^3) was added carefully and the resulting mixture stirred for 30

minutes. The layers were separated and the H_2O layer was extracted with DCM (2 x 50 cm^3). All DCM layers where combined, washed with H_2O (100 cm^3), then with 10% NaOH (2 x 100 cm^3) and again with H_2O (100 cm^3). The organic layer was separated and dried over Na_2SO_4. This solution was then filtered and evaporated under reduced pressure to obtain 2-chlorobenzoyl ferrocene in 54.54 g (84.02 %) yield; m.p. 72-73 °C ; δ_H (300 MHz; $CDCl_3$) 4.25 (5H; s; C_5H_5), 4.58 (2H; t; C_5H_4), 4.72 (2H; t; C_5H_4), 7.3-7.5 (4H; m; C_6H_4Cl).

(ii) Synthesis of ferrocenecarboxylic acid

A 500 cm^3 three necked flask was charged with dimethoxyethane (200 cm^3) and potassium *t*-butoxide (100 g; 0.89 mol) under nitrogen and H_2O (4.4 cm^3; 0.24 mol) was added with stirring. 2-Chlorobenzoyl ferrocene (53.45 g; 0.16 mol) was added to the resulting mixture and the reaction mixture was refluxed and stirred for an hour. The reaction mixture was then cooled and added to H_2O (1 dm^3). The resulting aqueous solution was washed with ether (6 x 150 cm^3), and these ether portions were back extracted with 10% NaOH (4 x 50 cm^3). The newly obtained aqueous phases where combined and acidified with concentrated hydrochloric acid (HCl). The precipitate that formed was collected by filtration and air-dried. The product was dissolved in $CHCl_3$ and washed with H_2O (3 x 100 cm^3), dried over Na_2SO_4, filtered and the $CHCl_3$ evaporated under reduced pressure to obtain ferrocenecarboxylic acid in 26.98 g (71.21%) yield; m.p. 171 ºC; δ_H (300 MHz; $CDCl_3$) 4.28 (5H; s; C_5H_5), 4.49 (2H; t; C_5H_4), 4.88 (2H; t; C_5H_4).

(iii) Synthesis of methyl ferrocenoate

Ferrocenecarboxylic acid (13.68 g; 0.06 mol) was refluxed in methanol (600 cm^3) in the presence of concentrated H_2SO_4 (0.5 cm^3) under a N_2 atmosphere for 48 hours. The resulting solution was poured over ice (500 g) and extracted with ether (3 x 350 cm^3). The combined ether extractions were washed with H_2O (4 x 200 cm^3), 0.5 mol dm^{-3} NaOH (3 x 100 cm^3) and again with H_2O (3 x 200 cm^3). The resulting solution was then dried over Na_2SO_4, filtered and the organic layer was evaporated to obtain

methylferrocenoate in 12.44 g (85.63 %) yield; m.p. 69 ºC; δ_H (300 MHz; $CDCl_3$) 3.82 (3H; s; OCH_3), 4.22 (5H; s; C_5H_5), 4.41 (2H; t; C_5H_4), 4.82 (2H; t; C_5H_4) ; IR (KBr cm^{-1}) 1704 (C=O).

4.4.2.2. Synthesis of methyl ruthenocenoate

This compound was obtained in a three-step synthesis *via* 2-chlorobenzoylferrocene and ferrcenecarboxylic acid.

(i) Synthesis of 2-chlorobenzoyl ruthenocene

Ruthenocene (5.49 g; 0.024 mol) and 2-chlorobenzoyl chloride (4.15 g; 3.00 cm^3; 0,024 mol) were dissolved in DCM (250 cm^3). The solution was stirred and placed in an ice bath. Over a period of 2 hours $AlCl_3$ (4.74 g; 0.036 mol) was added in small portions in order to keep the temperature at 5 ºC while being kept under nitrogen. After addition, the reaction was kept at 0 ºC for 15 minutes and then stirred at room temperature for 4 hours. The resulting mixture was cooled, and water (200 cm^3) was carefully added and the resulting mixture stirred for 30 minutes. The layers were separated and the H_2O layer was extracted with DCM (2 x 50 cm^3). All DCM layers were combined, washed with H_2O (100 cm^3), then with 10% NaOH (2 x 100 cm^3) and again with H_2O (100 cm^3). The organic layer was separated and dried over Na_2SO_4. This solution was filtered and evaporated under reduced pressure to obtain 5.91 g (67.41 %) 2-chlorobenzoylruthenocene. M.p. 88-90 °C; δ_H (300 MHz; $CDCl_3$) 4.64 (5H; s; C_5H_5), 4.84 (2H; t; C_5H_4), 5.03 (2H; t; C_5H_4), 7.3-7.5 (4H; m; C_6H_4Cl).

(ii) Synthesis of ruthenocenoic acid

A 500 cm^3 three necked flask was charged with dimethoxyethane (50 cm^3) and potassium *t*-butoxide (30.54 g) under nitrogen and H_2O (1.5 cm^3) was added with stirring. 2-chlorobenzoyl ruthenocene (2.51 g; 6.79 mmol) was added to the resulting mixture and this mixture was refluxed and stirred overnight. The reaction mixture was then cooled and poured into H_2O (200 cm^3). The resulting aqueous solution was washed with ether (6 x 50 cm^3), and these ether portions were back-extracted with 10% NaOH (2 x 100 cm^3).

The NaOH aqueous phases were combined and acidified with concentrated HCl. The precipitate that formed was collected by filtration, washed with H_2O and then air-dried. The product was dissolved in $CHCl_3$ and washed with H_2O (3 x 100 cm^3), dried over Na_2SO_4, filtered and the $CHCl_3$ evaporated under reduced pressure to obtain ruthenocenoic acid in 0.84 g (45.22 %) yield; m.p. 167-168 ºC ; δ_H (300 MHz; $CDCl_3$) 4.65(5H; s; C_5H_5), 4.77 (2H; t; C_5H_4), 5.19 (2H; t; C_5H_4).

(iii) Synthesis of methyl ruthenocenoate

Ruthenocenecarboxylic acid (0.84 g; 2.44 mmol) was refluxed in methanol (600 cm^3) in the presence of concentrated H_2SO_4 (0.5 cm^3) under a N_2 atmosphere for 48 hours. The resulting solution was poured over ice (500 g) and extracted with ether (3 x 350 cm^3). The combined ether extractions were washed with H_2O (4 x 200 cm^3), 0.5 mol dm^{-3} NaOH (3 x 100 cm^3) and again with H_2O (3 x 200 cm^3). The resulting ether solution was then dried over Na_2SO_4, filtered and the organic layer was evaporated under reduced pressure to obtain methylruthenocenoate. Yield: 0.85 g (95.00 %), m.p. 89-91 ºC; δ_H (300 MHz; $CDCl_3$) 3.75 (3H; s; OCH_3); 4.62 (5H; s; C_5H_5), 4.72 (2H; t; C_5H_4), 5.15 (2H; t; C_5H_4) ; IR(KBr cm^{-1}) 1707 (C=O).

4.4.3. Synthesis of β-diketones

4.4.3.1. Synthesis of 1-osmocenyl-4,4,4-trifluorobutan-1,3-dione (Hoctfa)

(Scheme 3.2)

The reaction vessel was degassed for one hour and filled with argon. The argon atmosphere was maintained through the entire duration of the experiment. Acetyl osmocene (0.1 g; 0.275 mmol) was dissolved in dry THF (5 cm^3) and lithium diisopropylamide (0.153 cm^3 of a 2.0 mol dm^{-3} solution; 0.275 mmol) was added to the solution while the reaction mixture was kept cooled on an ice bath. The reaction mixture was stirred for 20 minutes. Ethyltrifluoroacetate (0.0327 cm^3; 0.275 mmol) was added to the ice cold reaction mixture and stirred overnight. Ether (40 cm^3) was then added and a salt precipitated. The salt was filtered off and hydrolyzed by stirring it for 20 minutes in

HCl (20 cm^3, 1mol dm^{-3}) covered with a layer of ether (30 cm^3). The layers were separated and the organic layer of the reaction mixture was washed with water (4 x 100 cm^3) to remove the THF. All organic layers were than combined, dried over Na_2SO_4 and filtered. Hoctfa was obtained after ether removal. After recrystallization (hexane:ether; 2:1) a yield of 85.95 mg (68 %) was obtained. M.p. 121-123 ^oC; δ_H (300 MHz, $CDCl_3$), 2.88 (2H; s; COC<u>H</u>$_2$CO), 4.83 (5H; s; C_5H_5), 4.86 (5H; s; C_5H_5), 5.00 (2H; t; C_5H_4) 5.10 (2H; t; C_5H_4), 5.25 (2H; t; C_5H_4), 5.35 (2H; t; C_5H_4) and 5.95 (1H; s; COC<u>H</u>COH).

4.4.3.2. Synthesis of 1-osmocenyl-3-phenylpropano-1,3-dione (Hbocm)

(Scheme 3.2.)

The reaction vessel was evacuated, flame dried and filled with a nitrogen atmosphere that was maintained through the entire duration of the experiment. Acetyl osmocene (100 mg; 0.275 mmol) was dissolved in dry THF (5 cm^3) and lithium diisopropylamide (0.153 cm^3 of a 2.0 mol dm^{-3} solution; 0.275 mmol) was added while the reaction mixture was kept on an ice bath. The ice cold reaction mixture was stirred for 20 minutes. Methyl benzoate (0.034 cm^3; 0.275 mmol) was added and the reaction mixture was stirred overnight. Ether (40 cm^3) was added and a salt precipitated. The salt was filtered off and hydrolyzed by stirring it for 20 minutes in HCl (20 cm^3, 1mol dm^{-3}) covered with a layer of ether (30 cm^3). The layers were separated and the organic layer of the reaction mixture was washed with water (4 x 100 cm^3) to remove the THF. The combined organic layers were dried over Na_2SO_4 and filtered. Hbocm was separated form the reagents by column chromatography (R_f = 0.63) to give 23.15 mg (18 %). M.p.: 122 ^oC; δ_H (300 MHz; $CDCl_3$) only an enol isomer was detected, 4.83 (5H; s; C_5H_5), 5.04 (2H; t; C_5H_4), 5.38 (2H; t; C_5H_4), 6.22 (1H; s; COC<u>H</u>COH), 7.49 (3H; C_6H_5) and 7.88 (2H; C_6H_5).

After allowing the solid sample to remain in the solid state, it converted qualitatively to the enol isomer. A $CDCl_3$ solution that was allowed to age for three days had the equilibrium statistics of keto isomer (16.17 %) and enol isomer (83.83 %), implying K_c = 5.18.

4.4.3.3. Synthesis of 1-osmocenylbutane-1,3-dione (Hoca) (Scheme 3.2.)

In a previously argon degassed reaction vessel, acetyl osmocene (100 mg; 0.275 mmol) was dissolved in dry THF (5 cm^3). Lithium diisopropylamide (0.153 cm^3 of a 2.0 mol dm^{-3} solution; 0.275 mmol) was added while the reaction mixture was kept on ice. The ice-cold reaction mixture was stirred for 20 minutes. Freshly dried ethyl acetate (0.027 cm^3; 0.275 mmol) was added and the reaction mixture stirred overnight. Ether (40 cm^3) was added in a normal atmosphere and a salt precipitated. The salt was filtered off and hydrolyzed by stirring it for 20 minutes in HCl (20 cm^3, 1mol dm^{-3}) covered with a layer of ether (30 cm^3). The layers were separated and the organic layer of the reaction mixture was washed with water (4 x 100 cm^3) to remove the THF. The combined organic layers were dried over Na_2SO_4 and filtered. Hoca was purified by crystallization (hexane:ether; 2:1) (R_f =0.59) to yield 18.96 mg (17 %) pure Hoca. M.p.: 121 ^oC; δ_H (300 MHz; $CDCl_3$); enol isomer: 2.01 (3H; s; CH_3), 4.78 (5H; s; C_5H_5), 4.95 (2H; t; C_5H_4), and 5.55 (1H; d; COC<u>H</u>COH); keto isomer: 2.29 (3H, s, CH_3), 3.62 (2H, s, COC<u>H_2</u>CO), 4.85 (5H; s; C_5H_5), 5.02 (2H; t; C_5H_4) and 5.23 (2H; t; C_5H_4).

After allowing the solid sample to remain in the solid state, it converted qualitatively to the enol isomer. A $CDCl_3$ solution that was allowed to age for three days had the equilibrium statistics of keto isomer (39.50%) and enol isomer (60.50%), implying K_c = 1.49.

4.4.3.4. Synthesis of 1-ferrocenyl-3-osmocenylpropane-1,3-dione (Hocfcm) (Scheme 3.2.)

Acetyl osmocene (100 mg; 0.275 mmol) was dissolved in dry THF (5 cm^3) in a previously argon degassed reaction vessel. Lithium diisopropylamide (0.153 cm^3 of a 2.0 mol dm^{-3} solution; 0.275 mmol) was added while the reaction mixture was kept cold. The reaction mixture was stirred for 20 minutes. Freshly dried methyl ferrocenoate (158 mg; 0.275 mmol) was dissolved in dry THF (5 cm^3). The resulting solution was added to

the reaction mixture with cooling and the reaction mixture was stirred overnight. Ether (40 cm^3) was added and a salt precipitated. The salt was filtered off and hydrolyzed by stirring it for 20 minutes in HCl (20 cm^3, 1mol dm^{-3}) covered with a layer of ether (30 cm^3). The layers were separated and the organic layer of the reaction mixture was washed with water (4 x 100 cm^3) to remove the THF. The combined organic layers were dried over Na_2SO_4 and filtered. Hocfcm was purified by column chromatography (R_f = 0.62) to yield 41.23 mg (26 %). M.p.:194 ^oC; δ_H (300 MHz; $CDCl_3$) enol isomer: 4.20 (5H; s; C_5H_5; Fc), 4.50 (2H; t; C_5H_4; Fc), 4.73 (5H; s; C_5H_5; Oc), 4.93 (2H; t; C_5H_4; Fc), 5.00 (2H; t; C_5H_4; Oc), 5.39 (2H; t; C_5H_4; Oc), 5.83 (1H; s; COC<u>H</u>CO); keto isomer: 3.89 (2H; s; COC<u>H</u>$_2$CO; Oc), 4.22 (5H; s; C_5H_5; Fc), 4.59 (2H; t; C_5H_4; Fc), 4.84 (5H; s; C_5H_5; Oc), 4.96 (2H; t; C_5H_4; Fc), 5.00 (2H; t; C_5H_4; Oc), 5.37 (2H; t; C_5H_4; Oc).

After allowing the solid sample to remain in the solid state, it converted qualitatively to the enol isomer. A $CDCl_3$ solution that was allowed to age for three days had the equilibrium statistics of keto (55.50%) and enol (44.50%), implying K_c = 0.80.

4.4.3.5. Synthesis of 1-osmocenyl-3-ruthenocenylpropane-1,3-dione (Hocrcm) (Scheme 3.2.)

Acetyl osmocene (100 mg; 0.275 mmol) was dissolved in dry THF (5 cm^3) in a previously argon degassed reaction vessel. Lithium diisopropylamide (0.153 cm^3 of a 2.0 mol dm^{-3} solution; 0.275 mmol) was added while the reaction mixture was kept cold. The reaction mixture was stirred for 20 minutes. Methyl ruthenocenoate (170 mg; 0.275 mmol) was added in the solid form by way of Schlenck apparatus with cooling, the resulting solution was stirred overnight. Ether (40 cm^3) was added and a salt precipitated. The salt was filtered off and hydrolyzed by stirring it for 20 minutes in HCl (20 cm^3, 1mol dm^{-3}) covered with a layer of ether (30 cm^3). The layers were separated and the organic layer of the reaction mixture was washed with water (4 x 100 cm^3) to remove the THF. The combined organic layers were dried over Na_2SO_4 and filtered. Hocrcm was purified by column chromatography to (R_f = 0.58), yield 15.34 mg (9%) pure Hocrcm. M.p. 189 ^oC; δ_H (300 MHz; $CDCl_3$) enol isomer: 4.56 (5H; s; C_5H_4; Rc), 4.85 (2H; t; C_5H_4; Rc), 4.97 (5H; s; C_5H_4; Oc), 5.30 (2H; t; C_5H_4; Oc), 5.53 (2H; t; C_5H_4; Oc),

5.75(1H; s; COC<u>H</u>CO); keto isomer: 3.75 (2H; s; COC<u>H</u>$_2$CO), 4.46 (5H; s; C_5H_5; Rc), 4.52 (5H; s; C_5H_5; Rc); 4.85 (2H; t; C_5H_4; Rc), 5.08 (2H; t; C_5H_4; Rc), 5.19 (5H; s; C_5H_5; Oc), 5.41 (2H; t; C_5H_4; Oc), 5.65 (2H; t; C_5H_4; Oc).

After allowing the solid sample to remain in the solid state, it converted qualitatively to the enol isomer. A $CDCl_3$ solution that was allowed to age for three days had the equilibrium statistics of keto (73.70%) and enol (26.30%), implying a $K_c = 0.36$.

4.4.3.6. Synthesis of 1-osmocenyl-1,3-propanedione (Hoch) (Scheme 3.2.)

Acetyl osmocene (100 mg; 0.275 mmol) was dissolved in dry THF (5 cm^3) in a previously argon degassed reaction vessel. Lithium diisopropylamide (0.153 cm^3 of a 2.0 mol dm^{-3} solution; 0.275 mmol) was added while the reaction mixture was kept cold. The reaction mixture was stirred for 20 minutes. Methyl formate (16.5 mg; 0.275 mmol) was added in the solid form by way of Schlenk apparatus with cooling, the resulting solution was stirred overnight. Ether (40 cm^3) was added and a salt precipitated. The salt was filtered off and hydrolyzed by stirring it for 20 minutes in HCl (20 cm^3, 1mol dm^{-3}) covered with a layer of ether (30 cm^3). The layers were separated and the organic layer of the reaction mixture was washed with water (4 x 100 cm^3) to remove the THF. The combined organic layers were dried over Na_2SO_4 and filtered. Hoch was obtained after ether removal to (R_f = 0.63) yield 25.77 mg (24 %); m.p. 128 °C; δ_H (300 MHz; $CDCl_3$) 3,56 (2H; s; COC<u>H</u>$_2$CO), 4.80 (5H, s, C_5H_5), 4.83 (5H, s, C_5H_4), 4,99 (2H; t; C_5H_4), 5.04 (2H; t; C_5H_4), 5,22 (2H; t; C_5H_4), 5,27 (2H; t; C_5H_4), 5,55 (1H; s; COC<u>H</u>COH), 7.48 (1H, t, C(OH)<u>H</u>) and 9.70 (1H, t, C(OH)H).

Chapter 4
Experimental

4.4.4. Synthesis of rhodium complexes

4.4.4.1. Synthesis of di-μ-chloro-bis[(1,2,5,6-η)1,5-cyclooctadiene]rhodium

(Scheme 3.3.)

$RhCl_3.3H_2O$ (1.0 g: 4.89 mmol) was dissolved in 20 drops (about $1cm^3$) of H_2O at room temperature after which ethanol (24 cm^3) was added with stirring. 1,5-cyclooctadiene (7 cm^3) was slowly added to the mixture and the resulting mixture was refluxed at 78 °C for 2½ hours. The mixture was cooled in an ice bath, the precipitate of di-μ-chloro-bis[(1,2,5,6-η)1,5-cyclooctadiene]rhodium was filtered and washed with cold methanol and air-dried in the dark to yield 1.88 g (78 %) of the desired product. This product was clean enough for follow up reactions. M.p. 243°C; δ_H (300 MHz, $CDCl_3$), 1.78(4H, m, ½ of $4CH_2$), 2.5(4H, m, ½ of $4CH_2$), 4.25 (4H, m, 4CH).

4.4.4.2. Synthesis of [Rh(octfa)(cod)] **(Scheme 3.4.)**

$[Rh_2Cl_2(cod)_2]$ (105 mg; 0.207 mmol) was dissolved in dimethylformamide (6 cm^3) and Hoctfa (190 mg; 0.414 mmol) was added. After 3 hours of stirring the product was precipitated by the *slow* addition of ice water. The product was filtered off, washed with water and dissolved in ether. The organic layer was washed with water (3 x 100 cm^3) and dried over sodium sulfate. The organic layer was filtered and [Rh(octfa)(cod)] was obtained after ether removal and purification by column chromatography to (R_f = 0.94) yield 142 mg (51.23 %). M.p. 165 ^oC; δ_H (300 MHz; $CDCl_3$) 1.84 (4H; m; ½ aliphatic protons of C_8H_{12}), 2.47 (4H; m; ½ aliphatic protons of C_8H_{12}), 4.10 (4H; m; olefinic protons of C_8H_{12}), 4.77 (5H; s; C_5H_5), 4.93 (2H; t; C_5H_4), 5.15 (2H; t; C_5H_4) and 5.78 (1H; s; COCHCO).

4.4.4.3. Synthesis of [Rh(oca)(cod)] (Scheme 3.4.)

$[Rh_2Cl_2(cod)_2]$ (110 mg; 0.224 mmol) was dissolved in dimethylformamide (6 cm^3) and Hoca (181 mg; 0.448 mmol) was added. After 5 hours of stirring the product was precipitated by the *slow* addition of ice water. The product was filtered off and dissolved in ether. The organic layer was washed with water (3 x 100 cm^3) and dried over anhydrous sodium sulfate. The organic layer was filtered and [Rh(oca)(cod)] was obtained after ether removal and purification by column chromatography to (R_f = 0.87) yield 136 mg (49.31 %). M.p. 146 °C; δ_H (300 MHz; $CDCl_3$) 1.95 (4H; m; ½ aliphatic protons of C_8H_{12}), 2.50 (4H; m; ½ aliphatic protons of C_8H_{12}), 4.05 (4H; m; olefinic protons of C_8H_{12}), 4.75 (5H; s; C_5H_5), 4.85 (2H; t; C_5H_4), 5.15 (2H; t; C_5H_4) and 5.54 (1H; d; COC<u>H</u>CO).

4.4.4.4. Synthesis of [Rh(bocm)(cod)] (Scheme 3.4.)

$[Rh_2Cl_2(cod)_2]$ (90 mg; 0.18 mmol) was dissolved in dimethylformamide (6 cm^3) and Hbocm (168 mg; 0.36 mmol) was added. After 3 hours of stirring the product was precipitated by the *slow* addition of ice water. The product was filtered off and dissolved in ether. The organic layer was washed with water (3 x 100 cm^3) and dried over sodium sulfate. The organic layer was filtered and [Rh(bocm)(cod)] was obtained after ether removal and purification by column chromatography to (R_f = 0.86) yield 114 mg (46.73 %). M.p. 172 °C; δ_H (300 MHz; $CDCl_3$) 1.89 (4H; m; aliphatic protons of C_8H_{12}), 2.53 (4H; m; aliphatic protons of C_8H_{12}), 4.22 (4H; m; olefinic protons of C_8H_{12}), 4.75 (5H; s; C_5H_5), 4.95 (2H; t; C_5H_4), 5.23 (2H; t; C_5H_4), 6.14 (1H; s; COC<u>H</u>CO), 7.39 (3H; m; C_6H_5) and 7.75 (2H; m; C_6H_5).

4.4.4.5. Synthesis of [Rh(ocfcm)(cod)] (Scheme 3.4.)

$[Rh_2Cl_2(cod)_2]$ (60 mg; 0.117 mmol) was dissolved in dimethylformamide (6 cm^3) and Hocfcm (134 mg; 0.234 mmol) was added. After 30 minutes of stirring the product was precipitated by the *slow* addition of ice water. The product was filtered off and dissolved in ether. The organic layer was washed with water (3 x 100 cm^3) and dried over sodium sulfate. The organic layer was filtered and [Rh(ocfcm)(cod)] was obtained after ether removal and purification by column chromatography to (R_f = 0.90) yield 67 mg (36.39 %). m.p. 183 °C; δ_H (300MHz; $CDCl_3$) 1.87 (4H; m; aliphatic protons of C_8H_{12}), 2.54 (4H; m; aliphatic protons of C_8H_{12}), 4.00 (4H; m; olefinic protons of C_8H_{12}), 4.13 (5H; s; C_5H_5 Fc), 4.45 (2H; t; C_5H_4 Fc), 4.59 (2H; t; C_5H_4 Fc), 4.79 (5H; s; C_5H_5 Oc), 5.00 (2H; t; C_5H_4 Oc), 5.20 (2H; t; C_5H_4 Oc) and 5.80 (1H; s; COC<u>H</u>CO).

4.4.4.6. Synthesis of [Rh(och)(cod)] (Scheme 3.4.)

$[Rh_2Cl_2(cod)_2]$ (50 mg; 0.109 mmol) was dissolved in dimethylformamide (6 cm^3) and Hoch (85 mg; 0.217 mmol) was added. After 30 minutes of stirring the product was precipitated by the *slow* addition of ice water. The product was filtered off and dissolved in ether. The organic layer was washed with water (3 x 100 cm^3) and dried over sodium sulfate. The organic layer was filtered and [Rh(och)(cod)] was obtained after ether removal and purification by column chromatography to (R_f = 0.83) yield 60 mg (46.28 %). M.p. 168 ^oC; δ_H (300 MHz; $CDCl_3$) 1.84 (4H; m; aliphatic protons of C_8H_{12}), 2.47 (4H; m; aliphatic protons of C_8H_{12}), 4.08 (4H; m; olefinic protons of C_8H_{12}), 4.76 (5H; s; C_5H_5), 4.87 (2H; t; C_5H_4), 5.17 (2H; t; C_5H_4), 5.42 (1H; d; COC<u>H</u>CO) and 7.83 (1H; d, C(O-Rh-)<u>H</u>).

4.4.5. Electrolyte synthesis

Lithium tetrakis[pentafluorophenyl]borate (25g, 0.046 mol) was dissolved in 20 cm^3 methanol (AR). Tetrabutylammonium bromide (12.75g, 0.039 mmol) dissolved in 10 cm^3 methanol (AR) was added dropwise at room temperature over 15 minutes to the lithium solution. The solution (closed with a septum) was left at 0 ^oC for 30 minutes. It was then

left overnight at -25 ^{o}C. An off-white precipitate from a brown liquid was obtained by filtration and washed with 10 cm^3 cold methanol. The solid was dissolved in excess (30 cm^3) dry dichloromethane (DCM). A few spatulas of $MgSO_4$ was added and covered with a septum, and the mixture were stirred for 2 hours at room temperature. The $MgSO_4$ was filtered off and washed with DCM. The DCM was evaporated and a crude white solid was obtained. Further recrystallisation was achieved by dissolving 0.01 mol in 11 cm^3 DCM and adding 55 cm^3 ether over 20 minutes, while stirring. The covered solution was cooled at 0 ^{o}C for 1 hour and then overnight at -25 ^{o}C. The precipitate was filtered off and washed with 30 cm^3 hexane. The solid was air-dried for 2 hours and recrystillization was repeated for a second time. Yield 58% (20.7g). M.p.: 159-161 ^{o}C. δ_H (300 MHz; $CDCl_3$) 0.98 (12H; t; 4 x CH_3); 1.36 (8H; q; 4 x CH_2); 1.56 (8H;q; 4 x CH_2); 3.03 (8H;t; 4 x CH_2).

4.5. Observed acid dissociation constant, $pK_a^{/}$, determination

The $pK_a^{/}$ values were obtained by measuring the absorbance at different pH during an acid-base titration in water-acetonitrile-tetrahydrofuran 90:9:1 by volume, μ = 0.100 mol dm^{-3} (sodium perchlorate monohydrate, $NaClO_4$) at 25(1) ^{o}C with β-diketone concentrations ± 0.04 mol dm^{-3} in 90% water. A 90:9:1 water:CH_3CN:THF solvent system was used since the β-diketones were insoluble in 10:90 =CH_3CN: water ratio.

UV-spectra of the free (0.2 mmol dm^{-3} β-diketone at pH = 2) and the deprotonated β-diketonato forms (0.2 mmol dm^{-3} β-diketone at pH = 12) of the β-diketones were obtained from these dissolved analyte systems. From these data an analytical wavelength was chosen at which the $pK_a^{/}$ could be determined (Hoctfa, 310 nm; Hoca, 320 nm; Hbocm, 380 nm; Hocfcm, 305 nm; Hocrcm, 395 nm and Hoch, 390 nm). The analytical wavelength was chosen where the difference in absorbance between the protonated and unprotonated forms was the greatest, or sufficiently large to monitor conversion.

The titrations of the solutions were done with 0.1 mol dm^{-3} and 1 mol dm^{-3} NaOH or with 0.1 mol dm^{-3} and 1 mol dm^{-3} $HClO_4$ depending whether an acidic or a basic titration was

performed. An effort was made to ensure that the increase in volume during the titration was no more than 5%.

A linear response by the pH meter (Orion model SA 720), fitted with a glass electrode, was ensured by calibration with buffers at pH = -log α_H = 7.00 and 10.00 respectively, α_H = activity of H^+. A test $pK_a^/$ determination were performed by titrating Hfca, which was previously characterized.[2] The titrations were performed with $HClO_4$ from high pH, adjusted with NaOH to low pH. The least squares fit of the obtained UV absorbance/pH data for this titration using equation,

$$A_T = \frac{A_{HA}10^{-pH} + A_A10^{-pKa^/}}{10^{-pH} + 10^{-pK_a^/}}$$

Equation 4.1.

utilizing the fitting program MINSQ,[3] resulted in $pK_a^/$ of 10.06 ± 0.03. This was within experimental error of the published $pK_a^/$ of 10.01 ± 0.02. It was therefore concluded that the electrode system was calibrated to measure hydrogen ion activity under the conditions used.

The $pK_a^/$ values of the β-diketones under investigation where obtained by insertion of the absorption/pH data obtained into Equation 3.1.

4.6. Isomerization kinetics study

4.6.1. Monitoring of the conversion of enol- to keto-isomer

The solvent for this ^1H NMR kinetic study, $CDCl_3$, was dried and made acid-free by running it through a small column of basic alumina just prior to use. NMR spectra of the compounds Hoca, Hbocm, Hocfcm and Hocrcm were obtained from $CDCl_3$ solutions with β-diketone concentrations about 5.5 mg sample per cm^3 $CDCl_3$. In the solid state, after enough time had elapsed, the equilibrium:

$$OcCOCH_2COR \rightleftharpoons OcCOCH{=}C(OH)R$$

is driven completely to the enol isomer.[4] Therefore, upon dissolving aged samples of the β-diketones in $CDCl_3$, the formation of keto-isomers until the solution equilibrium position was reached could be monitored with time. For Hoctfa, the observed rate constant could only be followed by monitoring the conversion of keto to enol isomer, as the % of keto isomer in the equilibrium position was *ca*. 7%. This value is too small to allow accurate ^1H NMR measurements. For Hoca, Hocfcm, Hbocm and Hocrcm the isomerization could be followed from both the keto and enol isomer sides of the equilibrium. The experiments were repeated in dried acetonitrile for Hoca, Hbocm, Hocfcm and Hocrcm.

4.6.2. Monitoring of the conversion of keto to enol isomer

An acetonitrile/ether mixture (ca 1:1 by volume) (50 mg β-diketone in 10 cm^3) of Hoca was prepared. An aqueous solution of 0.1 mol dm^{-3} NaOH solution was prepared, and the β-diketone in the organic layer was extracted into the aqueous layer to convert the Oc-COCH=C(OH)-CH_3 to [Oc-COCHCO-CH_3]$^-$. The organic layer was then discarded and 2.5 cm^3 of $CDCl_3$ was added to the aqueous layer. Acidification with HCl-generated Oc-CO-CH_2-CO-CH_3 as the keto isomer and it was immediately extracted into the $CDCl_3$ layer. The aqueous layer was discarded and the $CDCl_3$ layer was quickly washed with water. From this organic layer the NMR analysis was performed. At different times the percentage keto isomer was determined and from these data the observed first-order rate constant, k_{obs} was determined. The individual rate constants, k_1 and $k_{-1,}$ were obtained by simultaneously solving the equations $k = k_1 + k_{-1}$ and $K = {}^{k1}/_{k-1}$.

The equilibrium constant K for this equilibrium was found from the ^1H NMR data after the solution had stood long enough (2-3 days) for the equilibrium to set in. Detailed methods of calculations can be found in Chapter 3).

Chapter 4
Experimental

4.7. Substitution kinetics

Due to the fact that the substitution kinetics proceeded very quickly, a computer-controlled Applied PHOTOPHYSICS SX.18MV Stopped Flow Instrument was used to collect kinetic data. The rate constants were determined using the associated Applied Photophysics software. The temperature was controlled using a water bath to within 0.1 ^{o}C.

The UV spectra of [Rh(β-diketonato)(cod)] and product of the substitution reaction between the [Rh(β-diketonato)(cod)] complexes and 1,10-phenanthroline (phen), *viz.* [Rh(phen)(cod)]$^{+}$, in methanol at 25 ^{o}C where determined for [Rh(octfa)(cod)], [Rh(bocm)(cod)], [Rh(ocfcm)(cod)], [Rh(oca)(cod)] and [Rh(och)(cod)]. From these spectra the wavelength where the reaction was followed kinetically was determined. The appropriate wavelengths can be found in chapter 3.

The Beer-Lambert law ($A = \varepsilon cl$, with ε = molar absorptivity and l = path length = 1 cm) were found to be valid for all complexes under investigation, at the wavelengths at which the kinetics where performed.

All substitution reactions were performed in freshly distilled methanol under pseudo first-order conditions, where the 1,10-phenanthroline concentrations were 10-100 times in excess over the rhodium complex concentrations (*ca*. 4 x 10^{-4} mol dm^{-3}). The reactions were also conducted at five different temperatures between 15 ^{o}C and 40 ^{o}C with an appropriate excess concentration of the 1,10-phenanthroline (10-100 fold). The temperatures used can be found in chapter 3.

References:

[1] J.R. Boyles, M.C. Baird, B.G. Campling and N.Jain, *J. Inorg. Biochem*., 159, **84** (2001).

[2] W.C. Du Plessis, T.G. Vosloo and J.C. Swarts, *J. Chem. Soc., Dalton Trans*., 2507, (1998).

[3] L. Helm, MINSQ. Non-linear parameters estimation and model development, least squares parameters optimization V3.12, MicroMath Scientific Software, Salt Lake City, UT, 1990.

[4] W.C. du Plessis, W.L. Davies, S.J. Cronje and J.C. Swarts, *Inorg. Chim. Acta*, 97, **314** (2001).

Chapter 4
Experimental

Chapter 5
Summary and future perspectives

5.1. Summary

The Claisen condensation of an appropriate ester with acetyl osmocene under the influence of lithium diisopropylamide yielded the six new osmocene-containing β-diketones, 1-osmocenyl-4,4,4-trifluorobutan-1,3-dione (Hoctfa), **3**, 1-osmocenylbutane-1,3-dione (Hoca), **4**, 1-osmocenyl-3-phenylpropane-1,3-dione (Hbocm), **5**, 3-ferrocenyl-1-osmocenylpropane-1,3-dione (Hocfcm), **6**, 1-osmocenyl-3-ruthenocenylpropane-1,3-dione (Hocrcm), **7**, and 1-osmocenyl-1,3-propanedione (Hoch), **8**. The Rh-complexes [Rh(octfa)(cod)], **12**, [Rh(oca)(cod)], **13**, [Rh(bocm)(cod)], **14**, [Rh(ocfcm)(cod)], **15**, and [Rh(och)(cod)], **16**, were prepared form the reactions between $[Rh_2Cl_2(cod)_2]$ and the osmocene-containing β-diketones .

The pK_a' values for the compounds Hoctfa (7.90(2)), Hoca (10.39(3)), Hbocm (10.59(2)), Hocfcm (13.04(1)), Hocrcm (11.42(1)) and Hoch (7.54(3)), were obtained by measuring the absorbances at different pH during an acid-base titration in water-acetonitrile-tetrahydrofuran, 90:9:1 by volume.

Substitution kinetics of the β-diketonato ligand from the complexes [Rh(octfa)(cod)], **12**, [Rh(oca)(cod)], **13**, [Rh(bocm)(cod)], **14**, [Rh(ocfcm)(cod)], **15**, and [Rh(och)(cod)], **16**, by 1,10-phenanthroline was studied with stopped flow UV spectroscopy. The electronic influence of the various β-diketonato R- side groups on the substitution rate results in an increase in the substitution rate according to the series (values in brackets are second order substitution rate constants in units $mol^{-1}dm^3s^{-1}$) R = CF_3(524.1)>> C_6H_5(24.35)>CH_3(20.94)>H(16.23)>Fc(9.12). The relatively large negative entropy values are indicative of an associative mechanism.

The isomerization kinetics of the β-diketones Hoctfa, **3**, Hoca, **4**, Hbocm, **5**, Hocfcm, **6**, and Hocrcm, **7**, enol-keto conversion, were studied by NMR spectroscopy. It was shown that the rate of enol-keto isomerization is effected by the electronic influence of the various β-diketone side groups, the isomerization rate was shown to increase according to

the series CF_3> C_6H_5 > CH_3 > Fc >Rc The isomerization kinetics of the β-diketone, Hoca, **4**, keto-enol conversion, was studied by NMR spectroscopy

Cyclic voltammetry was conducted on the β-diketones Hoctfa, Hoca, Horcm, Hocfcm, Hoch and Hocrcm as well as their associated [Rh(β-diketonato)(cod)] complexes with the exception of [Rh(ocrcm)(cod)]. Evidence for Rh^{II}-Rh^{II} metal-bonded dimers was found. The Rh^{II} dimer was intramolecular by oxidized by ferrocenium groups to a Rh^{III} species. Most osmocenyl redox processes were slow resulting in electrochemical quazi to fully irreversible osmocenyl electrochemical processes.

5.2. Future perspectives

Future studies in this field could concern synthesizing a wider range of osmocene-containing β-diketones to determine if there are relations between the different R groups electronegativities and the different physical properties (*viz*: $pK_a^{/}$, E_{pa}, isomerization, etc.) of the compounds. Data from the present study are not enough to draw clear conclusions in this regard.

High pressure stopped flow kinetics should be conducted to determine activation volumes. This will independently confirm whether the mechanism for the substitution reaction between the [Rh(β-diketonato)(cod)] complexes and 1,10-phenanthroline is associative in nature. The present series of compounds can also be extended to include complexes of the types [Rh(OcCOCHCOR)$(CO)_2$], {Rh[OcCOCHCOR][$P(OPh)]_2$**}** and [Rh(OcCOCHCOR)(CO)(PPh_3)]. The latter complex may prove to be an efficient catalyst in the Monsanto type of chemistry, where methanol is converted to acetic acid *via* oxidative addition and reductive elimination reactions.

Further electrochemical analysis must be done to determine the formal reduction potentials of the Oc moiety in the various β-diketone compounds, as well as for the complexes [Rh(β-diketonato)(cod)]. Especially studies at low temperature and in non-coordinating solvents utilizing non-coordinating supporting electrolytes may be

beneficial. Isolation of oxidized products will also greatly enhance the present understanding of the electrochemical behavior of osmocene derivatives.

The present study also laid the foundations for expanding metallocene chemistry to include other metallocenes such as cobaltocene and nickelocene.

Appendix A

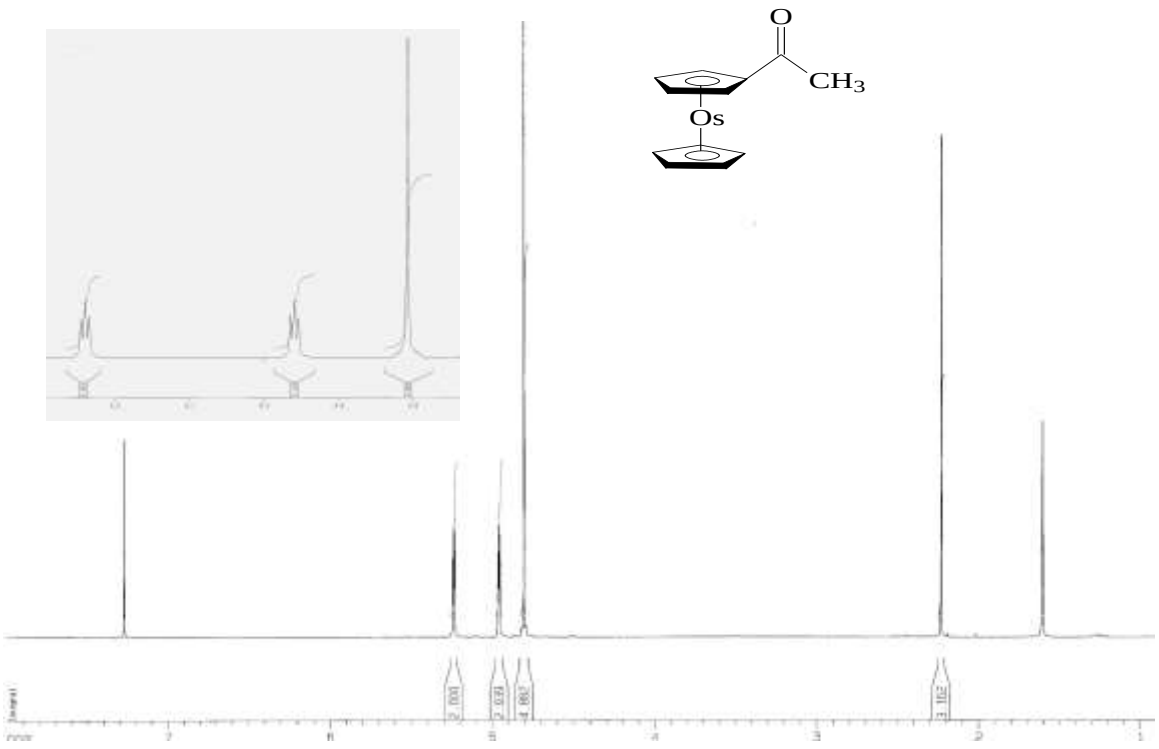

Spectrum A.1. **^{1}H NMR-spectrum of OcCOCH$_3$**

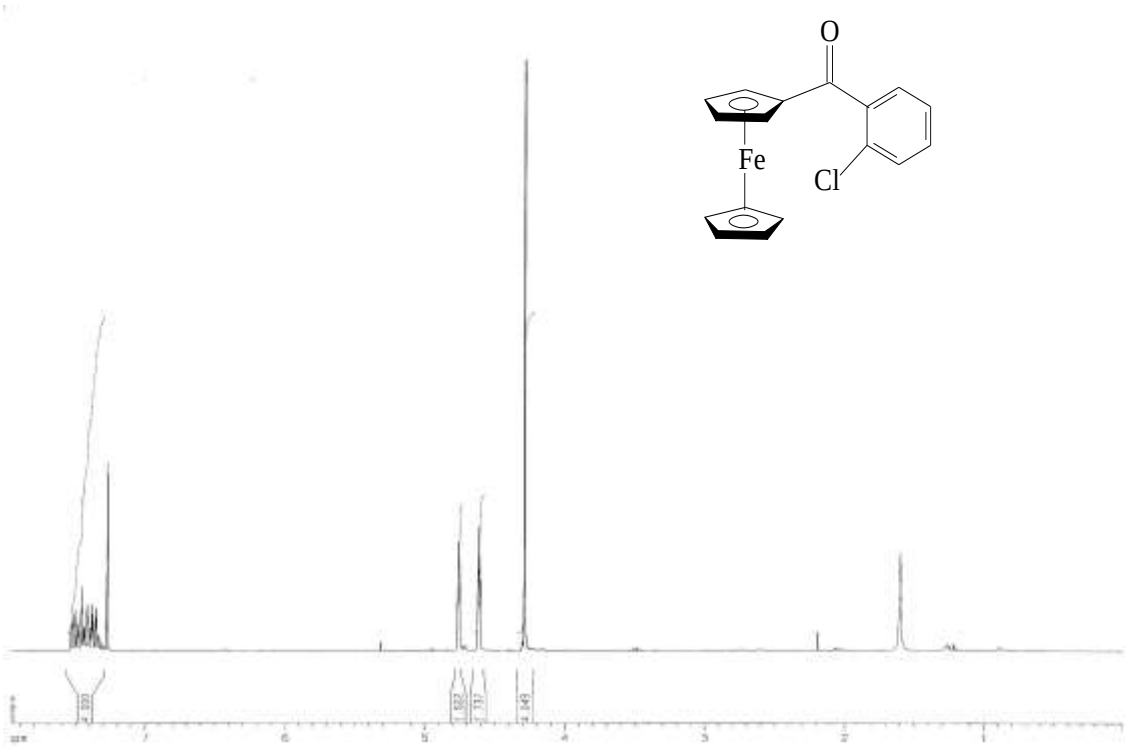

Spectrum A.2. **^{1}H NMR-spectrum of FcCOPhCl**

Appendix A

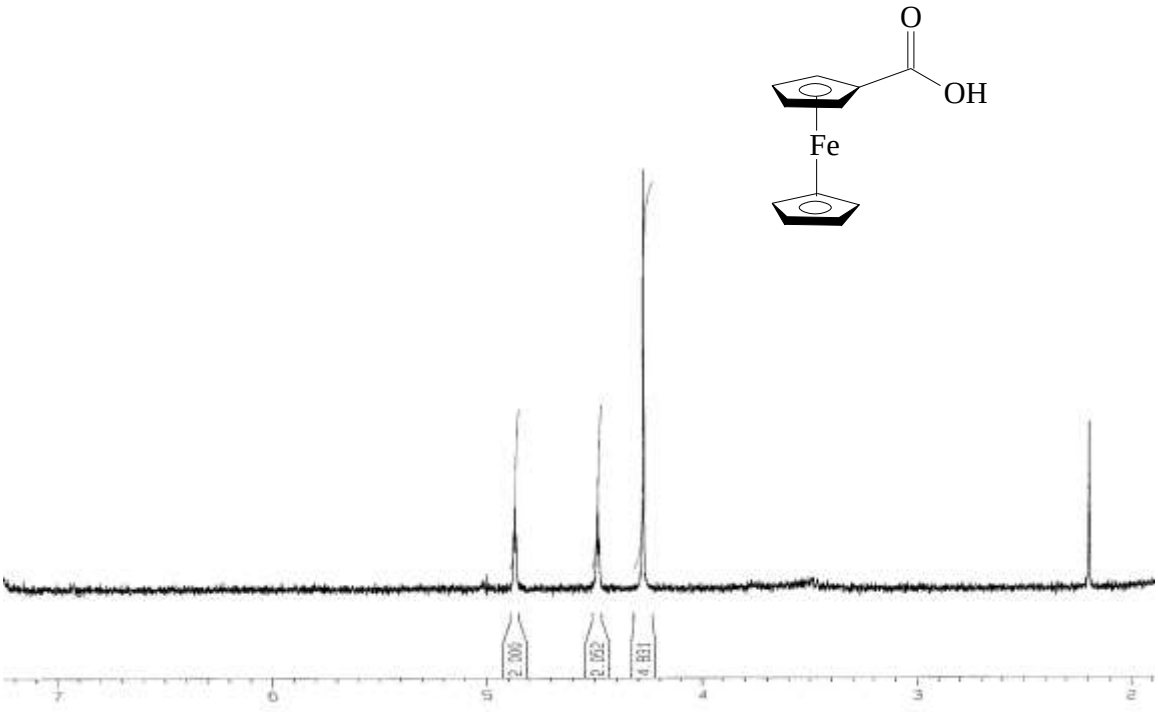

Spectrum A.3. **^{1}H NMR-spectrum of FcCOOH**

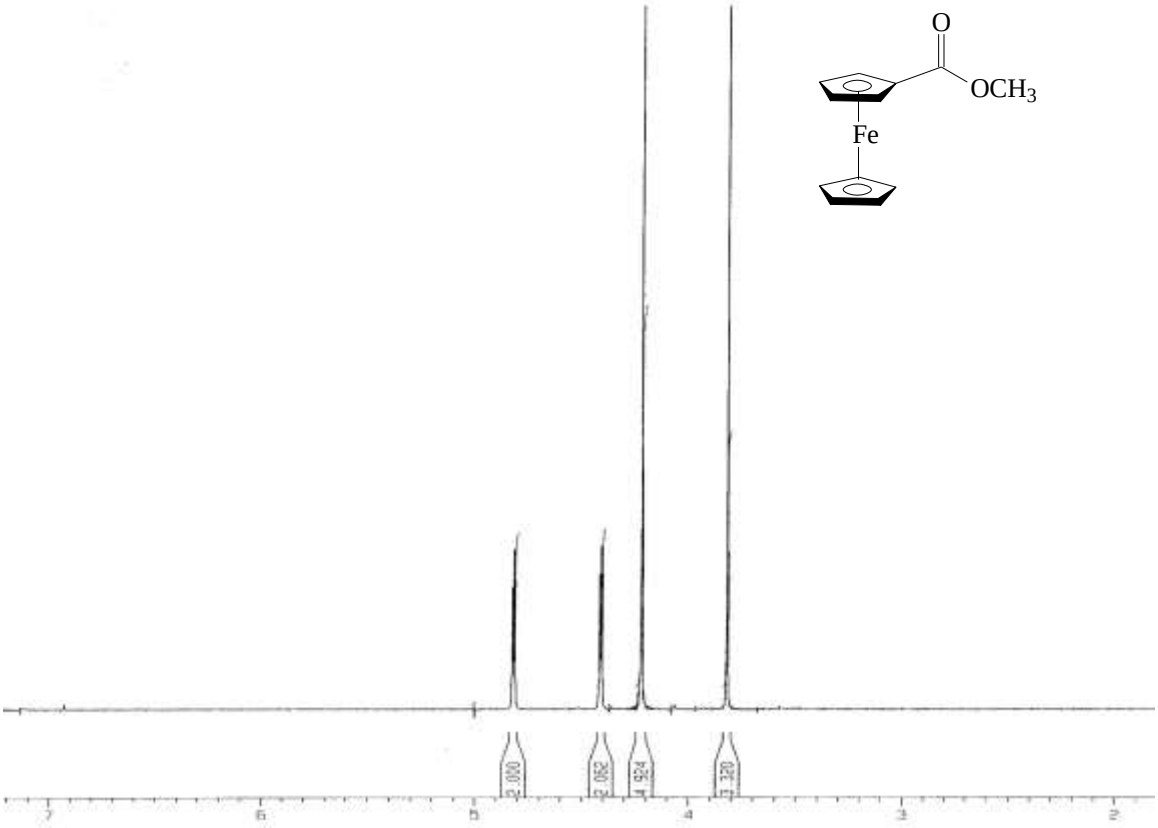

Spectrum A.4. **^{1}H NMR-Spectrum of FcCOOCH$_3$**

Appendix A

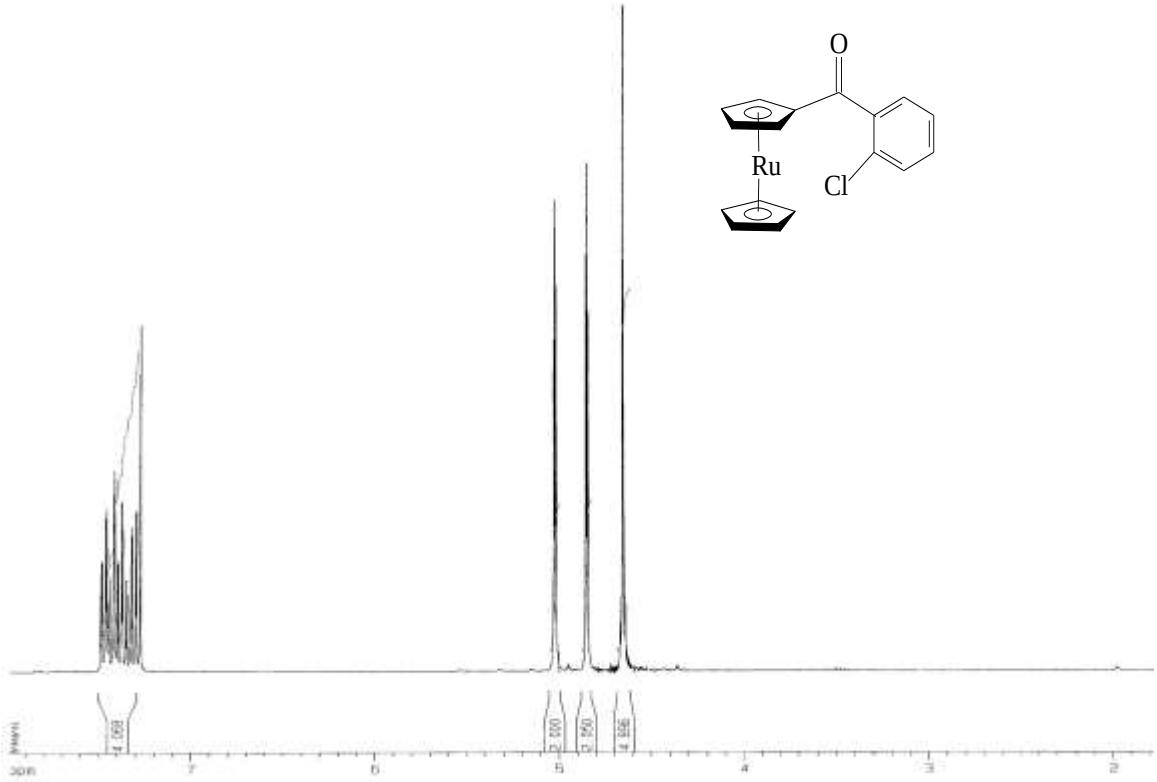

Spectrum A.5. **^{1}H NMR-spectrum of RcCOPhCl**

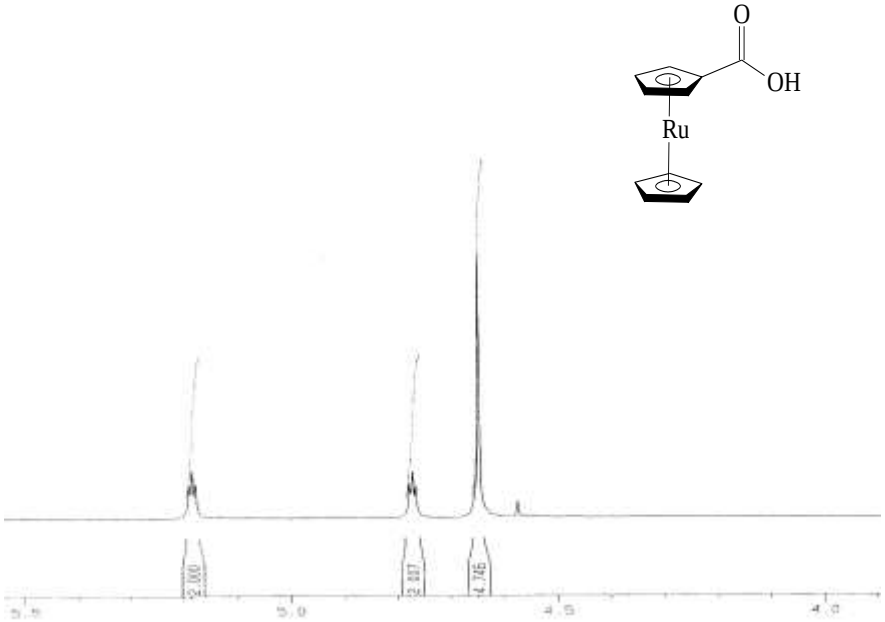

Spectrum A.6. **^{1}H NMR-spectrum of RcCOOH**

Appendix A

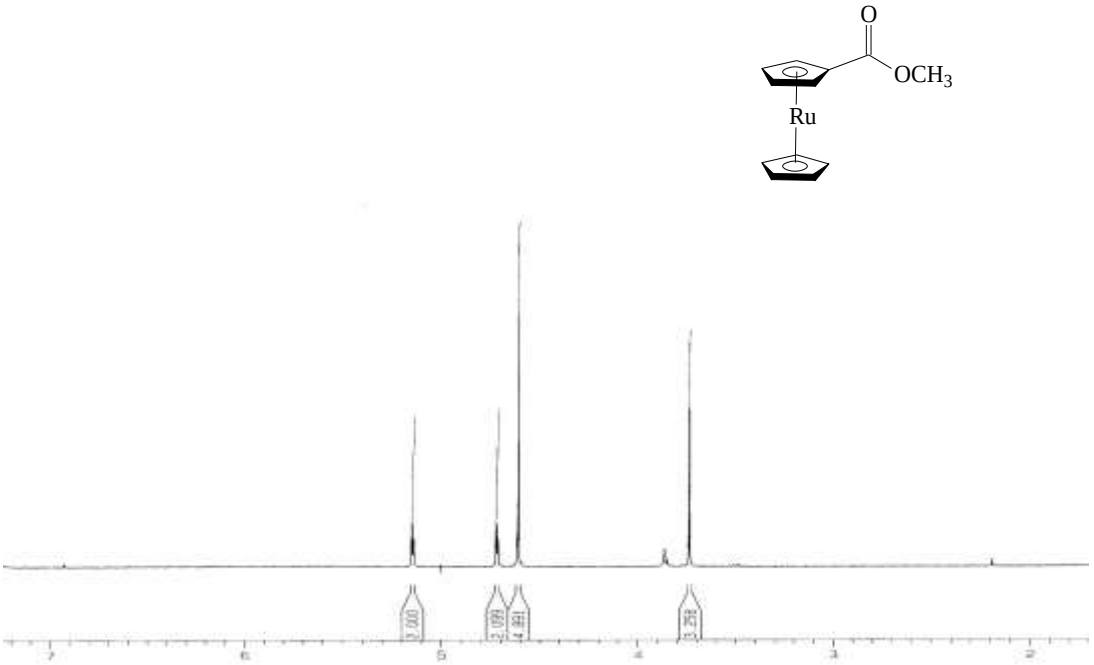

Spectrum A.7. ^{1}H NMR-Spectrum of RcCOOCH$_3$

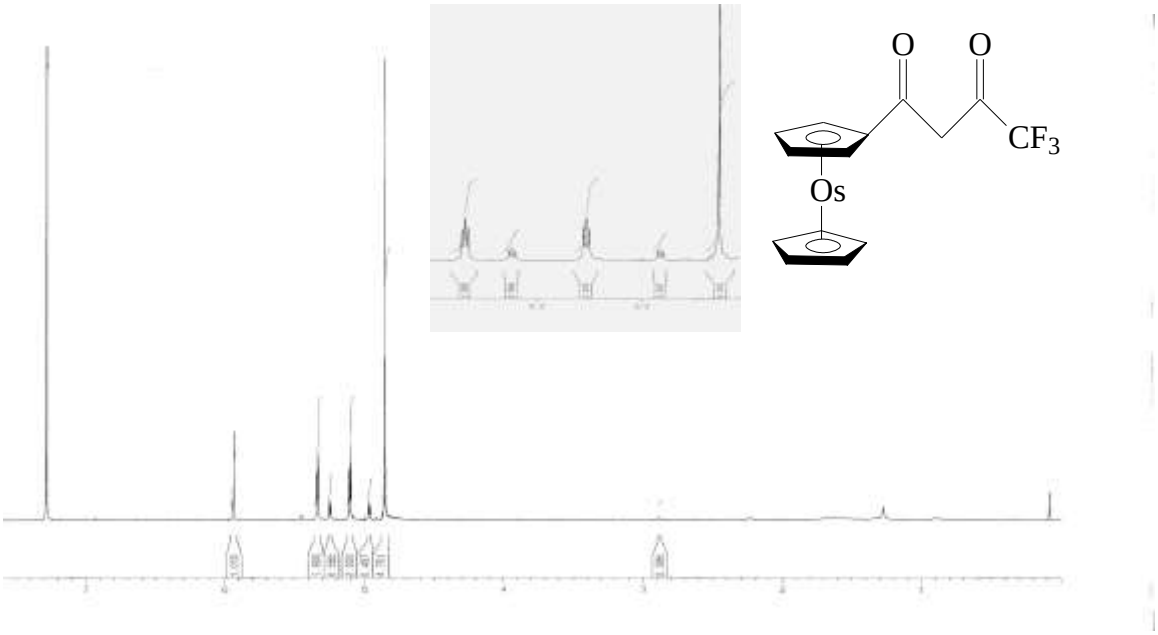

<u>Spectrum A.8.</u>^{1}H NMR spectrum of OcCOCH$_2$COCF$_3$

Appendix A

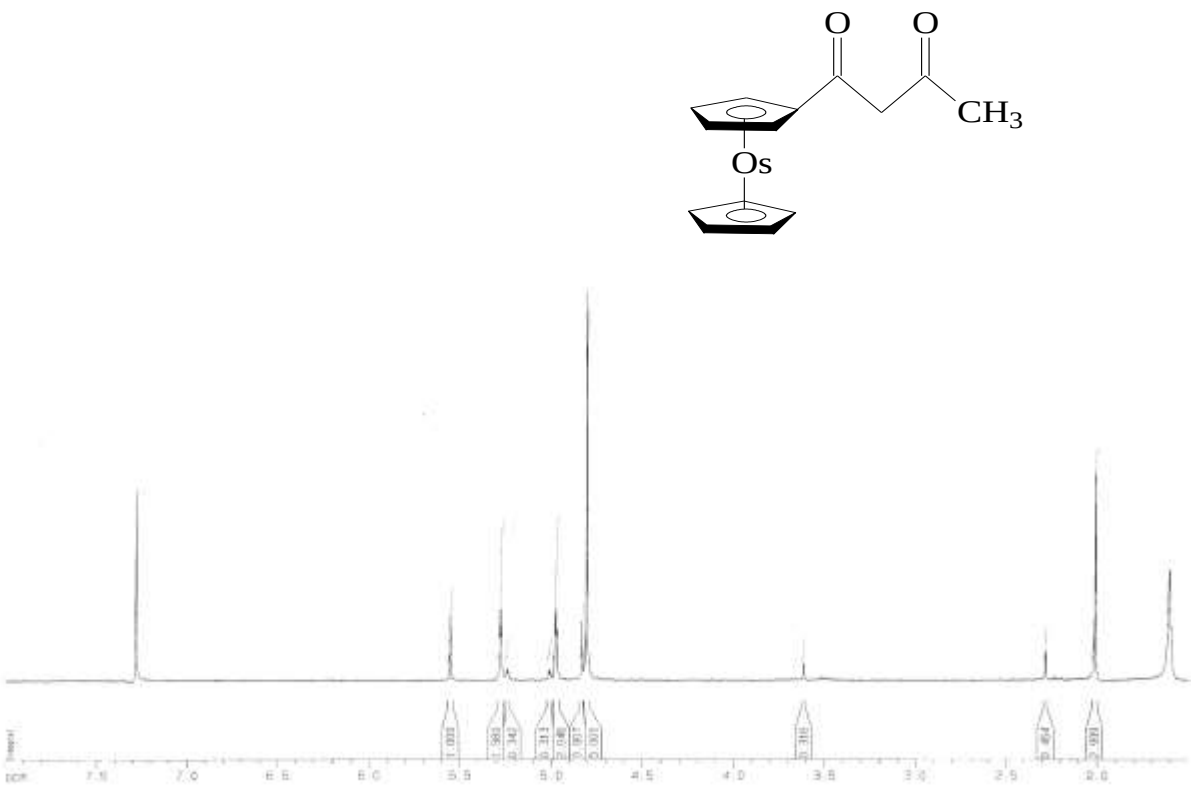

Spectrum A.9. ^{1}**H NMR-spectrum of OcCOCH$_2$COCH$_3$**

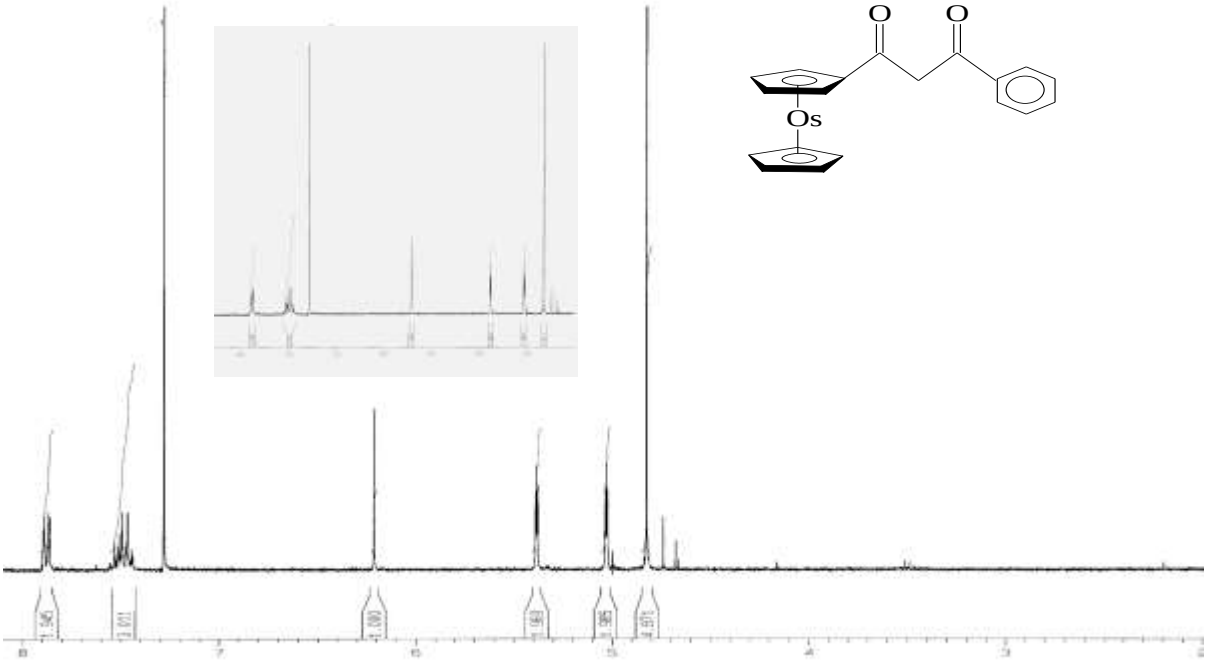

Spectrum A.10. ^{1}**H NMR-spectrum of OcCOCH$_2$COPh**

Appendix A

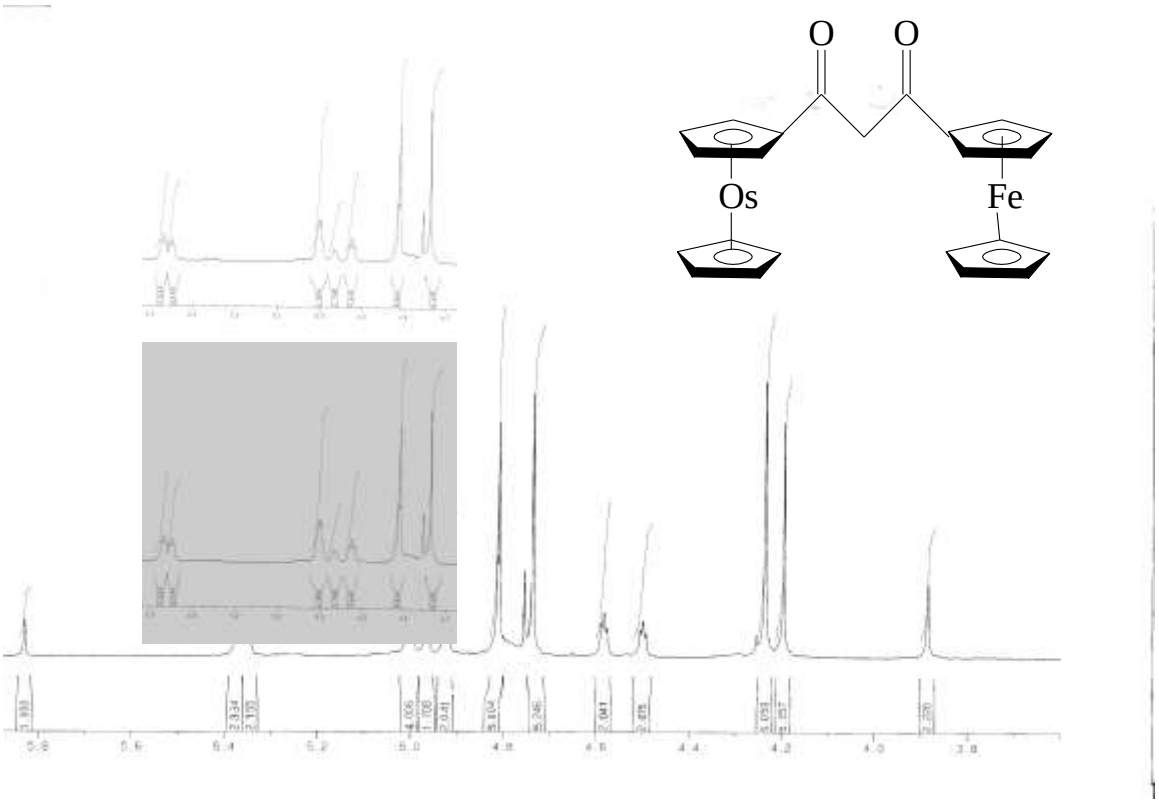

Spectrum A.11. **^{1}H NMR-spectrum of OcCOCH$_2$COFc**

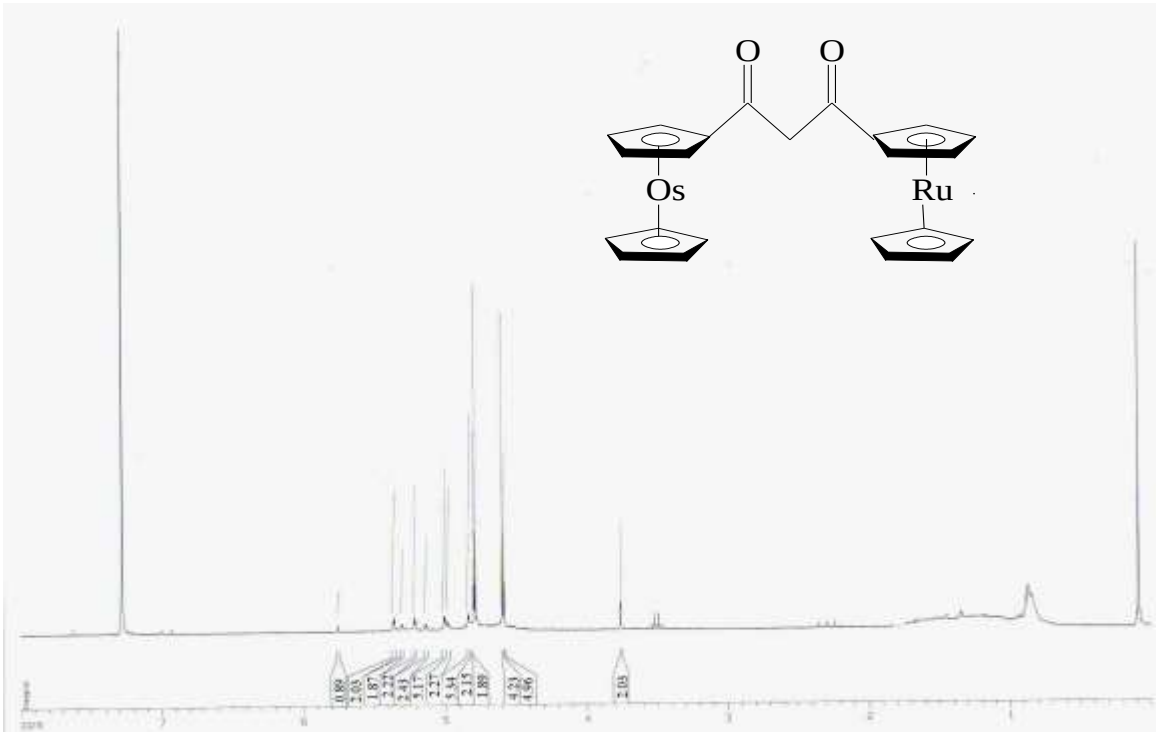

Spectrum A.12. **^{1}H NMR-spectrum of OcCOCH$_2$CORc**

Appendix A

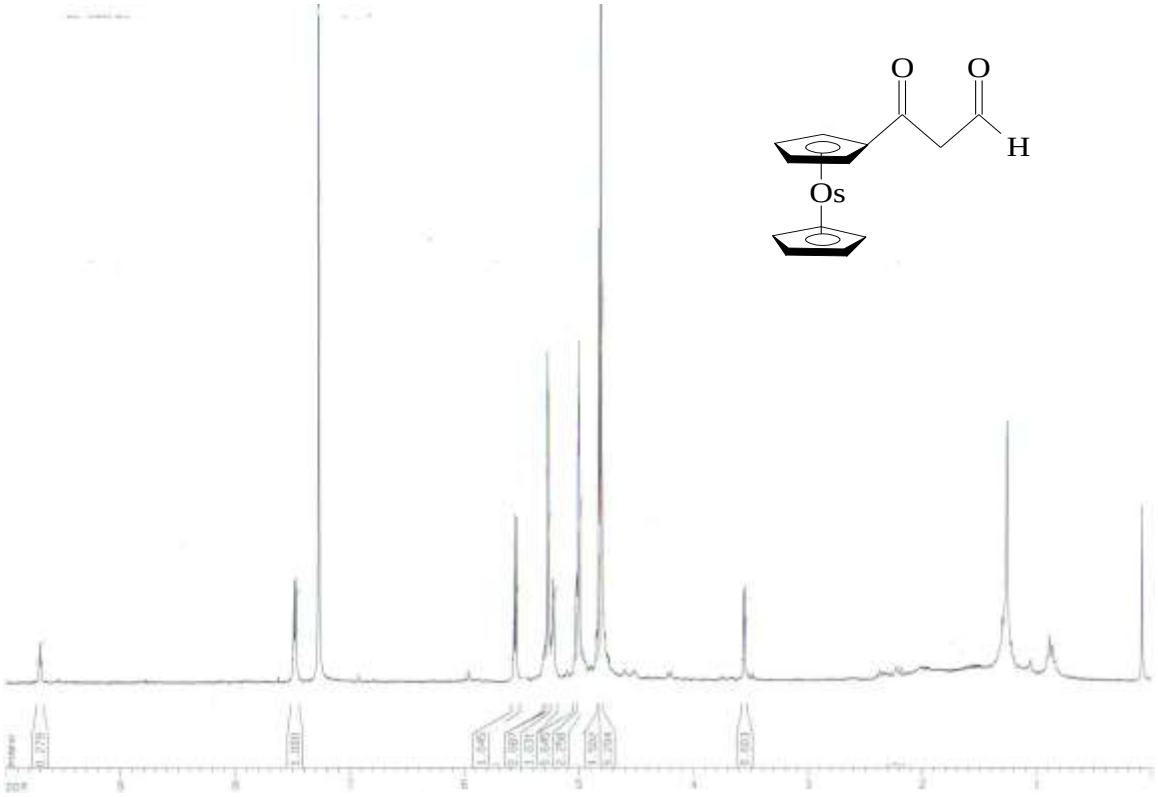

Spectrum A.13. **^{1}H NMR-spectrum of OcCOCH$_2$CHO**

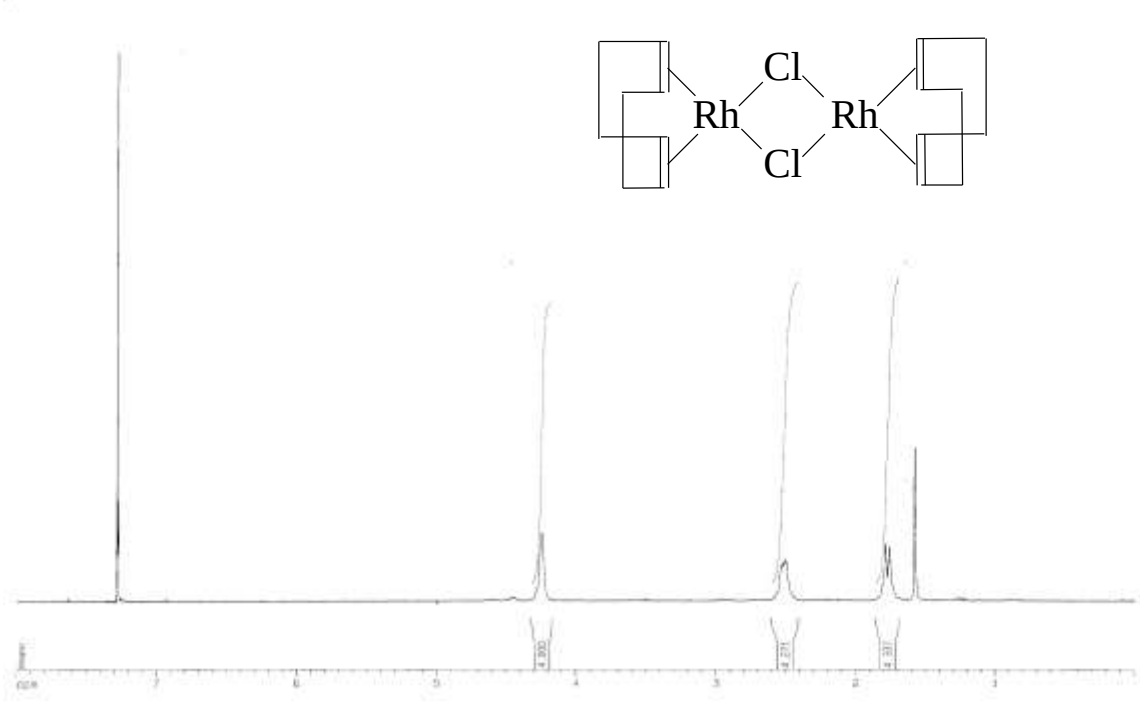

Spectrum A.14. **^{1}H NMR-spectrum of [Rh(Cl)(cod)]$_2$**

Appendix A

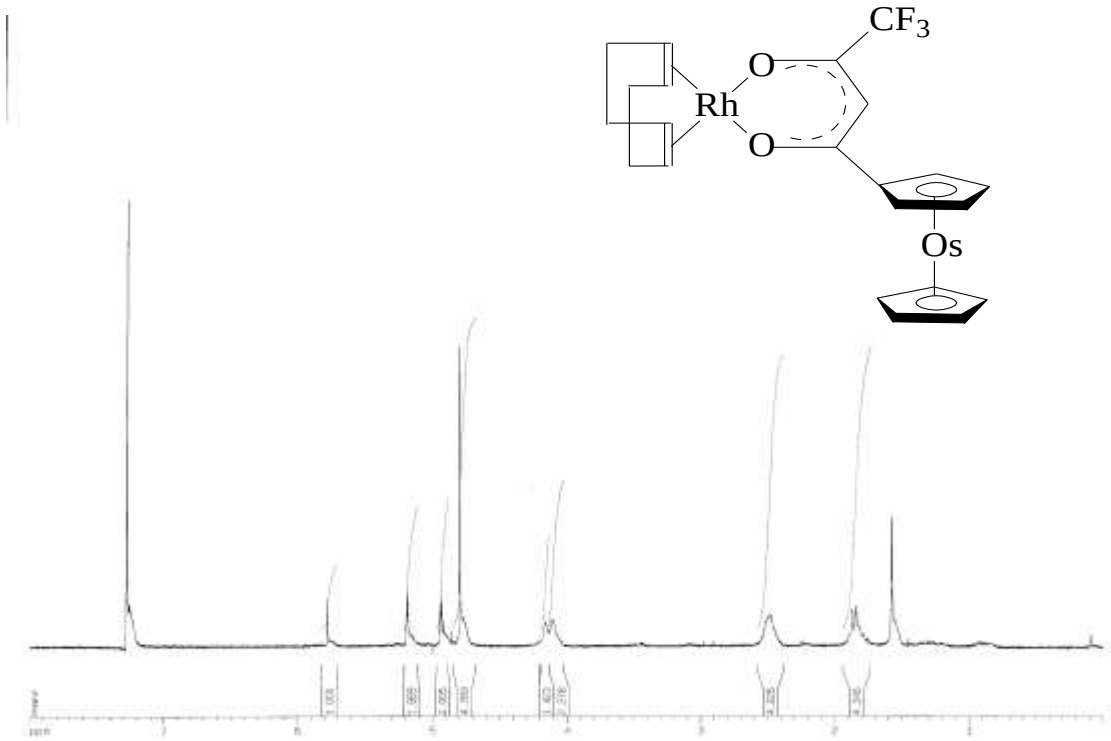

Spectrum A.15. **^{1}H NMR-spectrum of [Rh(octfa)(cod)]**

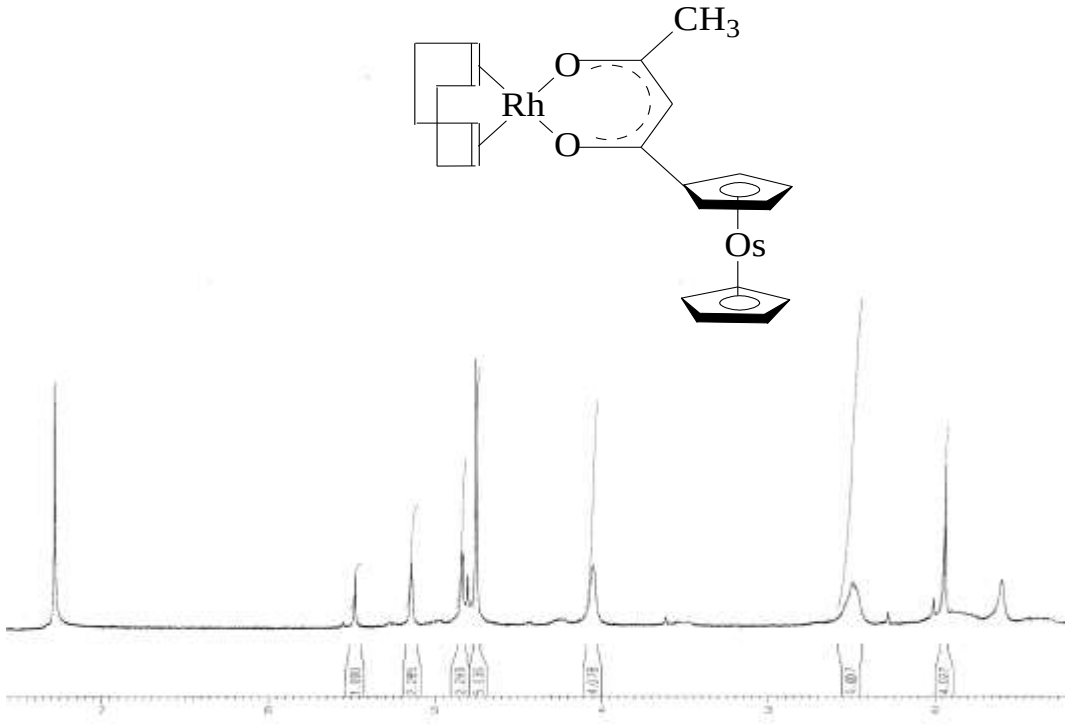

Spectrum A.16. **^{1}H NMR-spectrum of [Rh(oca)(cod)]**

Appendix A

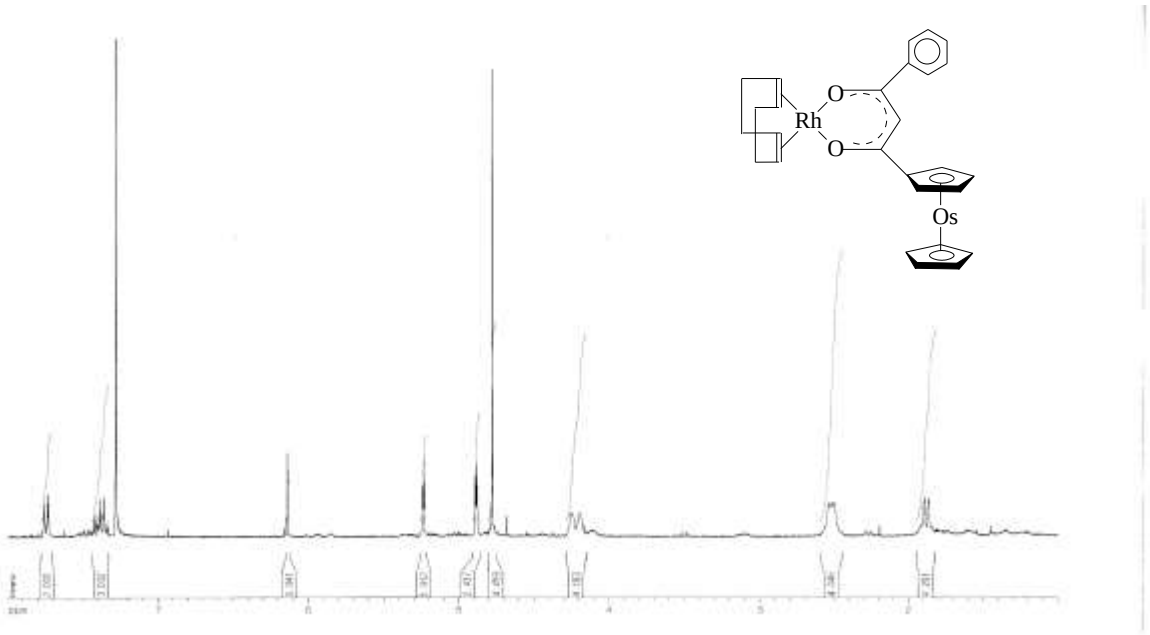

Spectrum A.17. **^{1}H NMR-spectrum of [Rh(bocm)(cod)]**

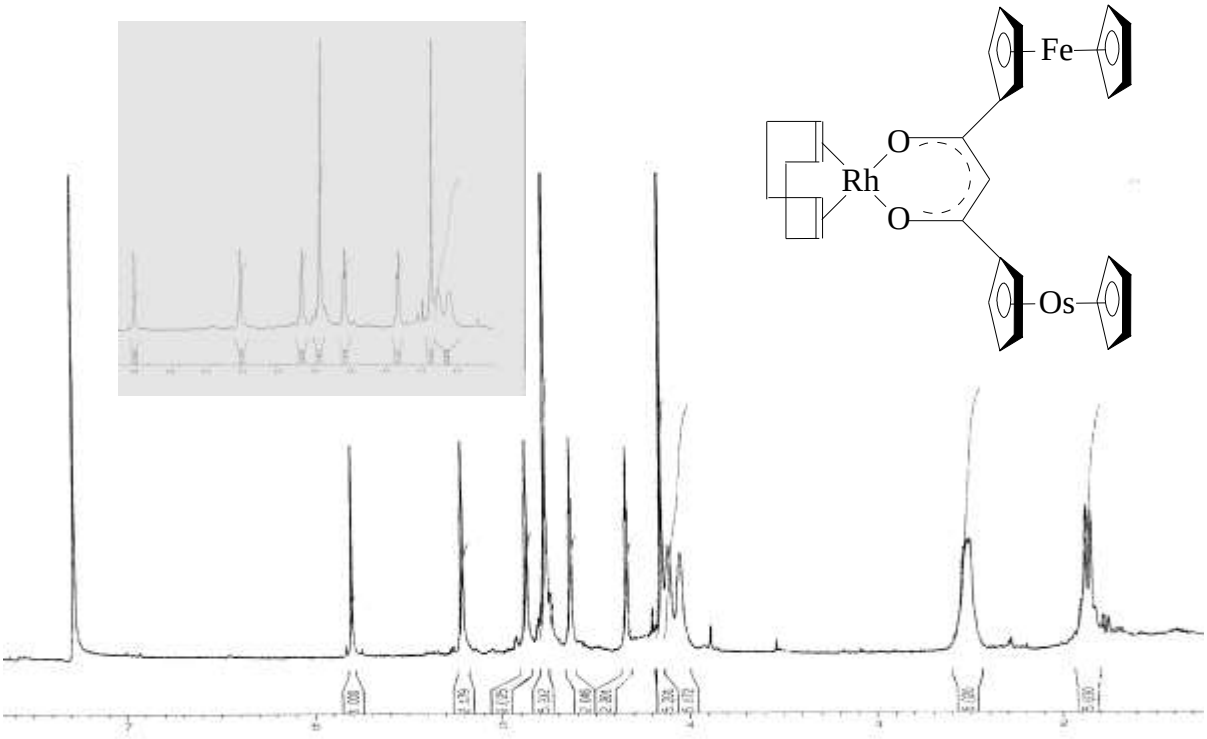

Spectrum A.18. **^{1}H NMR-spectrum of [Rh(ocfc)(cod)]**

Appendix A

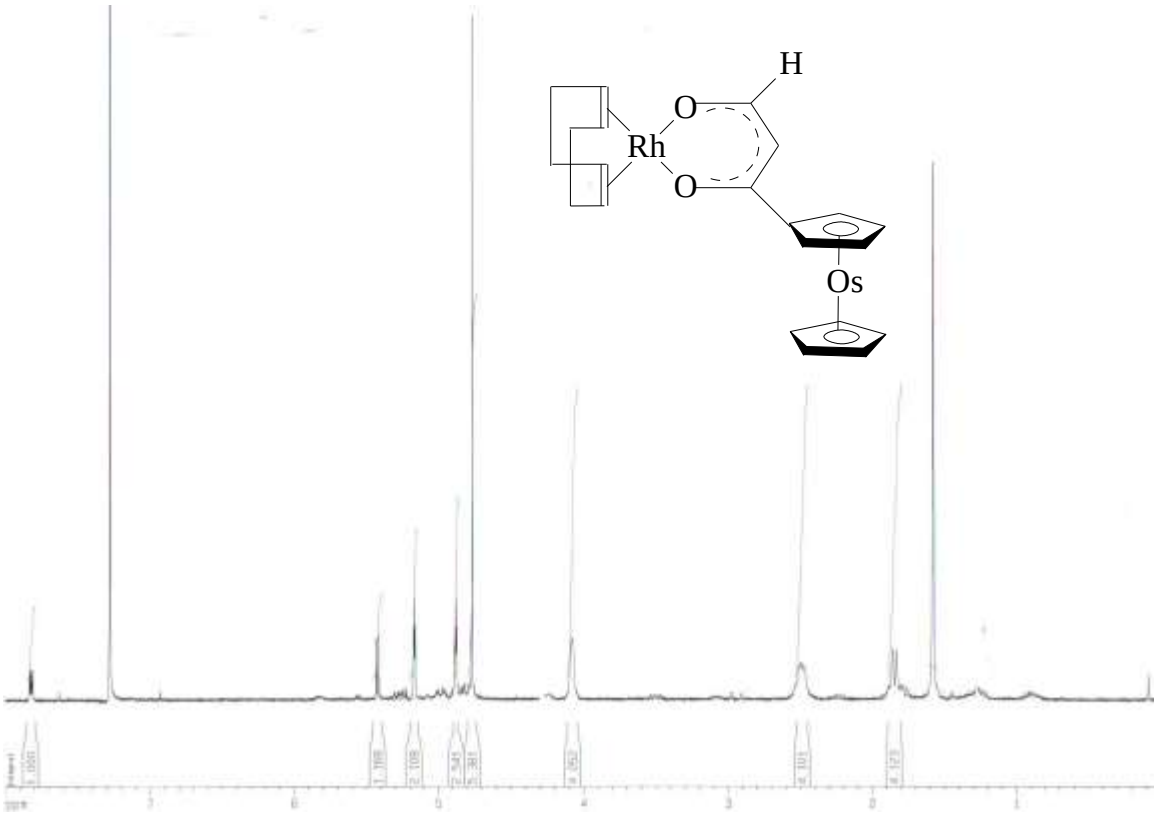

Spectrum A.19. **^{1}H NMR-spectrum of [Rh(och)(cod)]**

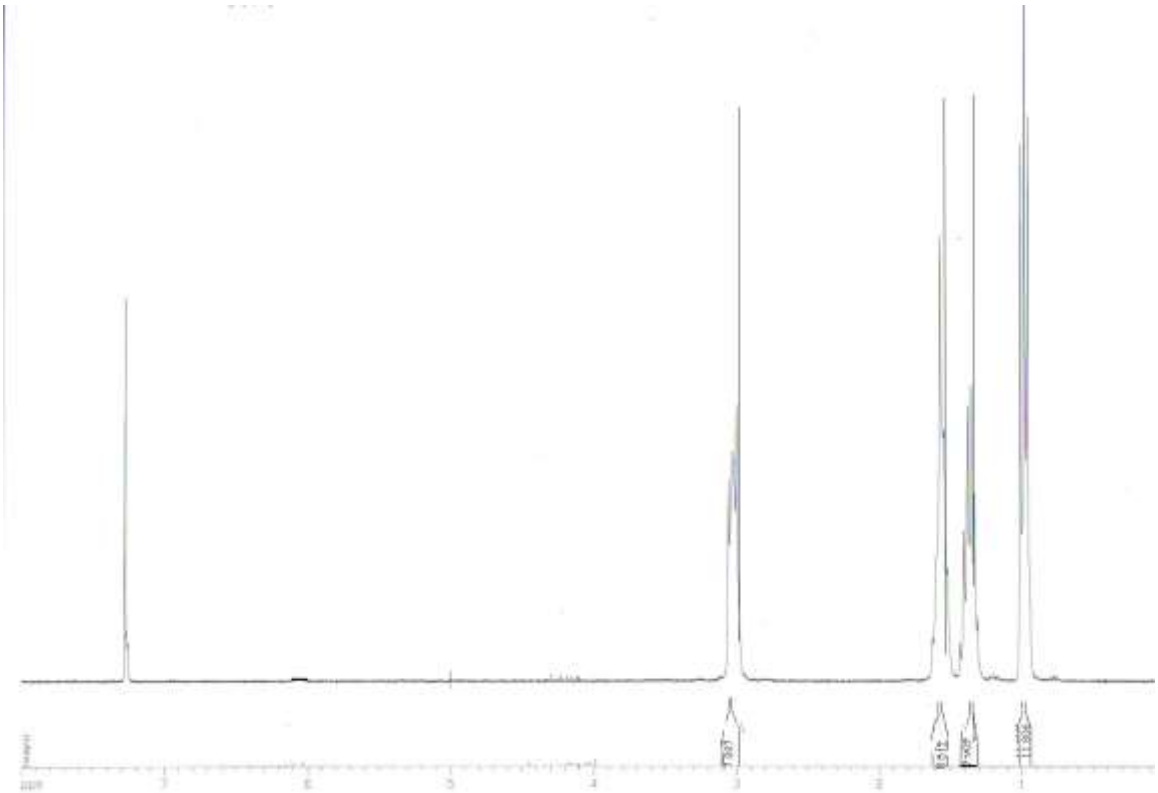

Spectrum A.20. **^{1}H NMR-spectrum of lithium tetrakis[pentafluorophenyl]borate**

Opsomming

Nuwe osmoseen-bevattende β-diketone, 1-osmocenyl-4,4,4-trifluorobutan-1,3-dione [Hoctfa, $pK_a^{/}$ = 7.90(2)], **3**, 1-osmocenylbutane-1,3-dione [Hoca, $pK_a^{/}$ = 10.39(3)], **4**, 1-osmocenyl-3-phenylpropane-1,3-dione [Hbocm, $pK_a^{/}$ = 10.59(2)],), **5**, 3-ferrocenyl-1-osmocenylpropane-1,3-dione [Hocfcm, $pK_a^{/}$ =13.04(1)], **6**, 1-osmocenyl-3-ruthenocenylpropane-1,3-dione [Hocrcm, $pK_a^{/}$ =11.42(1)], **7** en 1-osmocenyl-1,3-propanedione [Hoch, $pK_a^{/}$ =7.54(3)], **8**, is berei deur die Claisen kondensasie van asetielosmoseen en die toepaslike ester onder die invloed van litiumdiisopropielamied.

Waar moontlik is resultate vergelyk met die toepaslike R-groep elektronegatiwitiet van die onderskeie komplekse bestudeer in die studie.

Die [Rh(β-diketonato)(cod)]-komplekse, [Rh(octfa)(cod)], **12**, [Rh(oca)(cod)], **13**, [Rh(bocm)(cod)], **14**, [Rh(ocfcm)(cod)], **15**, en [Rh(och)(cod)],**16**, is berei vanaf die reaksie tussen die toepaslike osmocene β-diketone en $[Rh_2(cod)_2Cl_2]$.

'n Kinetiese studie van enol-keto isomerisasie vir die β-diketone Hoctfa, **3**, Hoca, **4**, Hbocm, **5**, Hocfcm, **6**, en Hocrcm, **7** , is met behulp van ^1H KMR spektroskopie bestudeer. Dit was gevind dat die snelheid van enol-keto isomerisasie elektronies deur die β-diketoon sy-groepe beinvloed word. Dit word aangetoon dat die isomerisasie kinetika versnel volgens die reeks $CF_3 > C_6H_5 > CH_3 > Fc > Rc$. Die isomerisasie kinetika vir keto-enol omskakeling vir die β-diketoon Hoca, **4**, is ook met behulp van ^1H KMR spektroskopies bestudeer.

Kinetiese resultate vir die substitusie van die β-diketonato ligand van die Rh(β-diketonato)(cod)] komplekse [Rh(octfa)(cod)], [Rh(oca)(cod)], [Rh(bocm)(cod)], [Rh(ocfcm)(cod)] en [Rh(och)(cod)]) met 1,10-fenantrolien in metanol word ook aangebied. Die groot negatiewe entropie waardes wat verkry is, dui op 'n assosiatiewe substitusie meganisme.

Opsomming

Oksidasiepotensiale (E_{pa} waardes *vs*. Ag/Ag^{+}) van die osmium kern in die vry β-diketone (Hoctfa, Hoca, Hbocm, Hocfcm, Hocrcm en Hoch), en in die [Rh(β-diketonato)(cod)] komplekse, ([Rh(octfa)(cod)], [Rh(oca)(cod)], [Rh(bocm)(cod)], [Rh(ocfcm)(cod)] en [Rh(och)(cod)]) is bepaal. Die piek oksidasiepotensiale (E_{pa} waardes *vs*. Ag/Ag^{+}) vir die oksidasie van die rhodium(I) kern is ook bepaal.

Kernwoorde: Osmoseen, β-diketone, rhodium, groepelektronegatiwiteit, sikliese voltametrie, substitusie kinetika, isomeriasaie kinetika.

2 Junie 2006

Ek,…… verklaar dat die proefskrif/ verhandeling wat hierby vir hierdie graad, Synthesis, electrochemical, kinetic and thermodynamic studies of new osmocene-containing betadiketones rhodium(I) complexes with biomedical application aan die Universiteit van die Vrystaat deur my ingedien word my, selfstandige werk is en nie voorheen deur my vir 'n graad aan 'n universitiet/ fakulteit ingedien is nie. Ek doen voorsts afstand van outeursreg in die proefskrif/ verhandeling ten gunste van die Universiteit van die Vrystaat.

---------- **……**

Handtekening **Datum**